

APR 8 1974
JUL 15 1974

AEDC-TR-73-172

cy.2



**COMPONENT PERFORMANCE AND STABILITY
CHARACTERISTICS OF AN ENGINE PROPULSION SIMULATOR
WITH UNIFORM AND DISTORTED INLET PRESSURE PROFILES
AT REYNOLDS NUMBER INDICES OF 0.39, 0.78, AND 0.91**

**C. R. Darlington, R. M. Brooksbank, and J. O. Brooks
ARO, Inc.**

March 1974

Approved for public release; distribution unlimited.

**ENGINE TEST FACILITY
ARNOLD ENGINEERING DEVELOPMENT CENTER
AIR FORCE SYSTEMS COMMAND
ARNOLD AIR FORCE STATION, TENNESSEE**

Property of U. S. Air Force
AEDC LIBRARY
F40600-74-C-0001

NOTICES

When U. S. Government drawings specifications, or other data are used for any purpose other than a definitely related Government procurement operation, the Government thereby incurs no responsibility nor any obligation whatsoever, and the fact that the Government may have formulated, furnished, or in any way supplied the said drawings, specifications, or other data, is not to be regarded by implication or otherwise, or in any manner licensing the holder or any other person or corporation, or conveying any rights or permission to manufacture, use, or sell any patented invention that may in any way be related thereto.

Qualified users may obtain copies of this report from the Defense Documentation Center.

References to named commercial products in this report are not to be considered in any sense as an endorsement of the product by the United States Air Force or the Government.

**COMPONENT PERFORMANCE AND STABILITY
CHARACTERISTICS OF AN ENGINE PROPULSION SIMULATOR
WITH UNIFORM AND DISTORTED INLET PRESSURE PROFILES
AT REYNOLDS NUMBER INDICES OF 0.39, 0.78, AND 0.91**

**C. R. Darlington, R. M. Brooksbank, and J. O. Brooks
ARO, Inc.**

Approved for public release; distribution unlimited.

FOREWORD

The test program reported herein was conducted at the Arnold Engineering Development Center (AEDC), Air Force Systems Command (AFSC), under the sponsorship of Aero-Propulsion Laboratory (AFAPL), AFSC, Wright-Patterson AFB, Ohio, under Program Element 63202F. The propulsion simulator was furnished by the General Electric Company, Cincinnati.

The results of the test were obtained by ARO, Inc. (a subsidiary of Sverdrup and Parcel and Associates, Inc.), AEDC, AFSC, Arnold Air Force Station, Tennessee. The test was conducted in the Propulsion Research Area (R-2C-4) of the Engine Test Facility (ETF) during the period from June 5, 1972, to February 10, 1973, under ARO Project number RA168. The manuscript was submitted for publication on August 8, 1973.

This technical report has been reviewed and is approved.

CHAUNCEY D. SMITH, JR.

Lt Colonel, USAF

Chief Air Force Test Director, ETF
Directorate of Test

FRANK J. PASSARELLO

Colonel, USAF

Director of Test

ABSTRACT

An investigation was conducted on an engine propulsion simulator (S/N 001/02) to determine sea-level-static component performance and to determine the compressor performance and stability characteristics with uniform and distorted inlet pressure profiles at Reynolds number indices of 0.39 and 0.78. Steady-state component performance data are presented and are compared with predicted data. The effect of Reynolds number indices and the effect of circumferential inlet distortion on the compressor performance are shown.

CONTENTS

	<u>Page</u>
ABSTRACT	iii
NOMENCLATURE	vi
I. INTRODUCTION	1
II. APPARATUS	2
III. PROCEDURE	7
IV. RESULTS AND DISCUSSION	9
V. SUMMARY OF RESULTS	14
REFERENCES	16

APPENDIXES

I. ILLUSTRATIONS

Figures

1. Engine Propulsion Simulator	21
2. Lube Oil System	26
3. Compressor Mapping Nozzle	28
4. Propulsion Simulator Test Installation in Propulsion Research Area (R-2C-4)	29
5. Schematic of Turbine Drive Air System	31
6. Compressor Loading System	32
7. One/Rev Distortion Screen Assembly	33
8. Inlet Duct and Test Chamber Instrumentation	34
9. Propulsion Simulator Instrumentation	36
10. Typical Transient Pressures during Incipient Compressor Surge	40
11. Typical Compressor Uniform Inlet Total Pressure Profile and Distortion at $Re_1 = 0.39$ ($P_1 = 6$ psia, $T_2 = 80^\circ F$)	41
12. Typical Compressor Uniform Inlet Total Pressure Profiles and Distortion at $Re_1 = 0.78$ ($P_2 = 12$ psia, $T_2 = 80^\circ F$)	42
13. Typical Compressor Inlet Circumferential Total Pressure Profiles and Distortion for the One/Rev Screen ($P_2 = 6$ psia, $T_2 = 80^\circ F$)	43
14. Compressor Performance at Sea-Level-Static Condition ($A_8 = 2.612$ in. ² , Uniform Inlet)	45
15. Turbine Performance and Operating Parameters at Sea-Level-Static Conditions ($A_8 = 2.612$ in. ² , Uniform Inlet)	48
16. Effect of Reynolds Number Index on Compressor Performance ($A_8 = 2.80$ in. ² , Uniform Inlet)	50
17. Compressor Stability Map with Uniform Inlet ($Re_1 = 0.39$, $P_2 = 6$ psia, $T_2 = 80^\circ F$, $A_8 = 2.80$ in. ²)	53
18. Effect of Reynolds Number Index on Compressor Operating Map, ($A_8 = 2.80$ in. ² , Uniform Inlet)	54

<u>Figure</u>	<u>Page</u>
19. Effect of Circumferential Inlet Distortion on Compressor Performance ($A_g = 2.80 \text{ in.}^2$, $Re_l = 0.39$, $P_2 = 6 \text{ psia}$, $T_2 = 80^\circ\text{F}$)	55
20. Effect of Circumferential Inlet Distortion on Compressor Operating Map ($A_g = 2.80 \text{ in.}^2$, $Re_l = 0.39$, $P_2 = 6 \text{ psia}$, $T_2 = 80^\circ\text{F}$)	58
21. Typical Compressor Discharge Pressure Profiles ($Re_l = 0.39$, $A_g = 2.80 \text{ in.}^2$, $P_2 = 6 \text{ psia}$, $T_2 = 80^\circ\text{F}$)	59
22. Compressor Stability Map with Circumferential Inlet Distortion, ($A_g = 2.80 \text{ in.}^2$, $Re_l = 0.39$, $P_2 = 6 \text{ psia}$, $T_2 = 80^\circ\text{F}$)	60
 II. TABLE	
I. Steady-State Measurement Uncertainty	61
 III. METHODS OF CALCULATION	

NOMENCLATURE

A	Area, in. ²
C	Critical flow factor
C_d	Discharge coefficient
C_F	Flow coefficient
C_P	Specific heat of air at constant pressure
C_{S V}	$1.18 \times 10^4 P_{V1}/14.969 + 0.6845$
C_T	Thermal expansion factor
C_{TE}	Thermal expansion coefficient for mild steel
D	Diameter, in.
DP	Delta pressure, psia
H	Enthalpy, Btu/lbm
M	Mach number
N	Rotor speed, rpm

P	Total pressure, psia
PS	Static pressure, psia
R	Gas constant, ft-lbf/lbm - °R
Re _I	Reynolds number index
T	Total temperature, °F or °R
W	Airflow Rate, lbm/sec
W _A	Airflow rate, lbm/sec
W _{A_c}	Bearing cooling airflow rate, lbm/sec
β	Ratio of orifice diameter to line diameter
γ	Ratio of specific heats
δ	Ratio of measured pressure to standard sea-level pressure (14.696 psia)
η	Efficiency, percent
θ	Ratio of total temperature to standard sea-level temperature (518.67°F)
φ	Ratio of absolute viscosity to absolute viscosity at standard sea level

SUBSCRIPTS

0,0,1,1N,
2 through 8 Instrumentation stations
etc.

BM	Bellmouth
BO	Bleed orifice
C	Compressor
DV	Turbine drive venturi
MDO	Mapping downstream orifice
MO	Mapping orifice

MUO	Mapping upstream orifice
OU	Upstream bleed orifice
R	Corrected to standard sea-level conditions
R2	Station 2 conditions corrected to sea-level conditions
T	Turbine
VI	Turbine drive venturi inlet
VT	Turbine drive venturi throat

SECTION I INTRODUCTION

The primary purpose of the engine propulsion simulator is to provide simultaneous simulation of inlet and exhaust flow fields in a full-span, multimission aircraft model, thereby allowing direct determination of aircraft/propulsion system performance at angle-of attack and/or yaw for a wide range of flight conditions. When combined with an aircraft scale model in a wind tunnel test, the engine propulsion simulator can also be used as a tool for identification of system performance improvements prior to and during flight operations (Ref. 1).

A test program was conducted in the Propulsion Research Area (R-2C-4) of the Engine Test Facility to determine the simulator component performance with both uniform and distorted inlet pressure profiles as a function of Reynolds number index. Specific objectives were to compare the measured sea-level-static compressor and turbine performance with predicted performance and to determine the effects of circumferential inlet distortion and Reynolds number index on the compressor performance and stability characteristics.

The steady-state component performance and stability characteristics of the Engine Propulsion Simulator (S/N 001/2) are reported herein. The test program was conducted with uniform compressor inlet pressure profiles at sea-level-static conditions and at Reynolds number indices (Re_I) of 0.39 and 0.78. Testing was also accomplished with circumferential (one/rev screen) distorted inlet pressure profiles at an Re_I of 0.39.

Engine propulsion simulator stability characteristics were determined by inbleeding air into the exhaust nozzle to load the compressor while maintaining a constant corrected compressor rotor speed. High response compressor inlet and compressor discharge instrumentation was used to indicate incipient compressor surge. When incipient compressor surge was indicated, the back pressure was decreased slightly, and steady-state data were recorded near the indicated compressor surge line. The compressor was not taken into the fully stalled condition because of the possibility of destructive rotor overspeed upon removal of the compressor load.

The results of this test program are presented herein. Simulator component performance at sea-level-static test conditions and the effects of Reynolds number index and circumferential inlet distortion on the compressor performance are presented and discussed. In addition, operational difficulties encountered during the program are discussed.

SECTION II APPARATUS

2.1 TEST ARTICLE

The multimission engine propulsion simulator (Fig. 1, Appendix I) is a 0.085-scale version of a mixed-flow augmented turbofan engine planned for use on a multimission supersonic aircraft. The simulator inlet is 3.0 in. in diameter, and total simulator length (with dry nozzle) is 11 in. The nominal weight of the simulator assembly is 27 lb. The major components of the simulator, the compressor, turbine, and exhaust nozzle are described in detail in the following sections.

2.1.1 Compressor

The four-stage, single-rotor axial compressor has an overall design pressure ratio of 2.82 and a design corrected airflow of 1.554 lb/sec at a corrected (100 percent rated) rotor speed of 75,185 rpm. The compressor airflow is ducted directly from the compressor discharge station to the exhaust nozzle, thereby bypassing the turbine (Fig. 1c).

2.1.2 Turbine

The single-stage, turbine is driven by an external high-pressure air source. Nominal design turbine efficiency is 0.72. The single compressor/turbine rotor (Fig. 1e) is supported by forward and aft bidirectional bearings which are lubricated by an external capillary oil flow system (Fig. 2). To aid bearing seating and improve rotor stability, a preset aft load of 40 lbf is applied to the rotor during installation. To maintain this negative loading during all operating conditions, the cavity aft of the turbine is partially vented by the rotor thrust trim orifice in the solid mixer. Phenolic rub strips form the interface between the compressor tip/case wall and turbine tip/case wall (Fig. 1c).

The high-pressure turbine drive air enters an annular manifold at a forward plane of the simulator through a 0.66-in.-diam port perpendicular to the simulator centerline (Figs. 1a and c). From the manifold, the air flows axially aft along the periphery of the simulator through five 0.25-in.-diam channels, then enters five sets of two radial holes (0.25- and 0.16-in.-diam) in each of five struts leading to the turbine drive air plenum just upstream of the turbine nozzles (Fig. 1c). After passing axially through the turbine, the air turns outward 90 deg through two elliptical holes (0.28- by 0.125-in. wide) in the five struts to an annular manifold and then flows axially forward through five pairs of similar channels around the simulator periphery to a forward manifold which bleeds the air perpendicular to the simulator centerline through a 1.66-in.-diam port (Figs. 1b and c). A small amount (nominally 1 percent) of the turbine discharge airflow is bled into the mixer (Fig. 1c) to provide rotor thrust balance pressure. This air was discharged axially through an orifice on the mixer centerline into the compressor discharge airflow in the nozzle.

2.1.3 Mixers and Nozzles

A mixer assembly was located downstream of the turbine (Figs. 1c and d). The mixer was designed to permit turbine drive air to bleed and mix with the compressor air to obtain a desired simulation of full-scale nozzle flow function. The mixer designs utilize radial and/or axial injection of air through choked orifices from a conical afterbody. For the test reported herein, only the solid mixer configuration was employed (G. E. Part No. 4013097-341), which incorporated a single axial orifice (Figs. 1c and d).

Two nozzle configurations were utilized for this test program. A "dry" nozzle (G. E. P/N 401206-83P01) (Fig. 1c) of throat area 2.612 in.² was used during all sea-level static tests. A compressor mapping nozzle (Fig. 3), designed and fabricated at the AEDC, of throat area 2.80 in.² having provisions for inbleeding air to back pressure the compressor for determination of the compressor surge line was used during the performance tests at 6 and 12 psia inlet pressure (Re_l of 0.39 and 0.78, respectively).

2.2 INSTALLATION

2.2.1 Engine Propulsion Simulator

The simulator, with the associated bellmouth/inlet duct assembly, was secured to a support stand suspended from the top of the test chamber located in the Propulsion Research Test Area (R-2C-4). The engine propulsion simulator installation is shown in Fig. 4.

The simulator inlet duct consists of a bellmouth with a 3:2 ratio elliptical inlet. Forward of the bellmouth is a 10-in.-diam by 58-in.-long duct which incorporates a flow-straightening screen. A 24-ft³ plenum, with controllable inlet valve for setting the desired inlet pressure, was installed upstream of the 10-in.-diam duct. A critical-flow airflow-measuring venturi was installed between the inlet plenum and 10-in. duct and located approximately 23 engine inlet diameters upstream of the engine compressor face. The venturi was used only during testing at 6-psia inlet pressure and was replaced with a 4-in.-diam spoolpiece for testing at 12-psia inlet pressure. With the venturi removed, airflow was calculated from measurements at the exit plane of the simulator inlet bellmouth (Fig. 4b). An inflatable rubber seal (Fig. 4b) between the bellmouth and the inlet duct prevented flow leakage.

Air from the simulator exhaust nozzle was discharged into the exhaust ducting through a 6-in.-diam duct. A steam ejector located in the exhaust ducting maintained a test chamber pressure equivalent to the compressor inlet pressure, thereby maintaining essentially zero differential pressure across the bellmouth seal.

2.2.2 Turbine Drive Air System

The facility high-pressure turbine drive air system is shown schematically in Fig. 5. The system was capable of supplying conditioned airflow up to 4 lbm/sec at the required turbine inlet pressure and temperature. Supply air temperature control was provided by a steam-air heat exchanger which maintained the desired turbine inlet air temperature at $200 \pm 3^{\circ}\text{F}$. A critical-flow airflow-measuring venturi was used to measure turbine drive inlet airflow and an ASME sharp-edged orifice was used to measure turbine drive bleed airflow. Two spring-loaded quick release valves were included in the turbine drive air system (Fig. 5) to automatically shut off air to the turbine and simultaneously vent air from the turbine inlet manifold in the event certain operational parameters exceeded prescribed levels (see Section 2.2.3).

2.2.3 Emergency Shutdown System

The emergency shutdown system was designed to unload the simulator as rapidly as possible by shutting off the turbine drive air and venting the turbine drive inlet manifold to ambient pressure (Fig. 5). The emergency shutdown system is comprised of two 1-in. Jamesbury® valves with spring-loaded handles that are actuated by a pull-type plunger solenoid. (The valves and solenoids were supplied by General Electric.) The valves are automatically operated when a preset rotor-speed level, bearing temperature level, or an acceleration "g" level is exceeded. General Electric provided bearing temperature controllers equipped with contacts which close and activate the valve solenoids when a preset bearing temperature level is exceeded. The overspeed system was designed and fabricated by ARO, Inc., personnel. The speed shutdown system converts a frequency signal from the General Electric-supplied speed pickup to an analog signal used to activate the emergency shutoff valve solenoids. The acceleration shutdown system is activated by a contact contained within the accelerometer amplifier which closes when a preset "g" level is exceeded. In addition to the automatic simulator shutdown systems, four manual shutdown switches were available in the control room to initiate shutdown when it was deemed advisable from visual observations.

When the emergency shutdown system was activated, the following valves were operated:

1. The turbine drive air emergency shutoff valve is closed.
2. The turbine drive air emergency dump valve is opened.
3. The compressor inlet control valve (Fig. 4a) is opened.
4. The compressor loading control valve (Fig. 6) is closed.
5. The turbine drive bypass valve is opened.

The turbine drive air safety valves operated full travel (open to closed or closed to open) in 60 to 65 msec from application of the shutoff signal to the valve solenoid. Compressor rotor speed and turbine inlet pressure decayed to ambient conditions in approximately 0.5 sec when the valves were activated at rated speed of 75,185 rpm and at a turbine inlet pressure of 725 psia.

2.2.4 Compressor Loading System

Loading of the compressor during compressor stability testing was accomplished by metering air from the facility high-pressure air system to the compressor mapping nozzle (Fig. 3). A schematic of the compressor loading system is shown in Fig. 6.

2.2.5 Distortion Screen Assembly

The screen used to distort the compressor inlet pressure profiles was located approximately 5 in. forward of the compressor face (Fig. 4b). Testing was conducted using a one-per-revolution, 180-deg circumferential distortion screen. Details of the distortion screen configuration used during this investigation are shown in Fig. 7.

2.3 INSTRUMENTATION

Instrumentation was provided to measure aerodynamic pressures and temperatures, rotor speed, and other simulator and test cell system parameters as required for proper and safe operation of the engine simulator. Aerodynamic pressure and temperature sensors for the inlet ducting and test chamber were located at the stations shown in Fig. 8a. Diagrams showing the number and type of instrumentation installed at each station are shown in Fig. 8b. Internal simulator instrumentation was located at the stations shown in Fig. 9.

Steady-state aerodynamic pressures were measured with strain-gage-type transducers; temperatures were measured with Chromel®-Alumel® (CA) or Iron-Constantan (IC) thermocouples. The millivolt outputs of the transducers were recorded on magnetic tape using a high-speed analog-to-digital data acquisition system and converted to engineering units and calculated performance parameters by a high-speed digital computer. Selected channels of pressure, temperature, acceleration, and vibration were displayed in the control room for monitoring and manual recording.

Engine rotor speed was measured with a variable reluctance magnetic pickup whose output signals were converted from a frequency signal-to-analog signal and then recorded on an analog-to-digital data acquisition system. Speed was also displayed in the control room on variable-time-base electronic counters.

Magnetic tape in the frequency modulation mode was used to document transient engine simulator performance. Transient aerodynamic pressures were measured throughout the engine with close-coupled strain-gage-type transducers.

High-response, static pressure instrumentation consisted of four piezoelectric pressure transducers, two each located at the compressor inlet (station 2) and discharge (station 23) to detect high-frequency pressure fluctuations occurring during compressor surge conditions. These data were recorded in the frequency modulation mode on magnetic tape and visually displayed on oscilloscopes in the control room.

Turbine drive air and compressor loading system instrumentation are shown in Figs. 5 and 6, respectively. The quick-release safety shutoff valves on the turbine drive air system were independently activated by any of six control monitors: (1) forward bearing temperature, (2) aft-bearing temperature, (3) forward, horizontal acceleration, (4) rotor speed, (5) forward bearing temperature rate of rise, and (6) aft-bearing temperature rate of rise. The first four monitors were automatically activated when the affected parameters reached a preset limit. The bearing temperature rate of rise was calculated as a part of the performance program and was indicated via color-coded lights on the General Electric monitor console. The shutoff valves were actuated manually when a temperature rise rate of 3.0°F/sec was reached on either the forward or aft bearing.

The instrumentation ranges, measurement and recording methods, and an estimate of the steady-state measurement uncertainties are presented in Table I (Appendix II).

2.4 CALIBRATION

All transducer and system calibrations performed during this test are traceable to the National Bureau of Standards (NBS). Each link in the traceability chain to the NBS is maintained and documented by the AEDC Standards Laboratory (Ref. 2).

The aerodynamic pressure measurement transducers utilized in the Automatic Multiple Pressure Scanning (AMPS) System (Table I) as well as all other pressure transducers were pretest calibrated in the Standards Laboratory. Before and after each test period, these transducer systems were calibrated by an electrical, four-step calibration, using precision resistors in the transducer circuits to simulate selected pressure levels.

Calibration data for the piezoelectric pressure transducers were provided by the manufacturer.

Lubrication oil flow rate was indicated by flow rate meters and was volumetrically measured using two graduated cylinders, one each for the forward and aft bearings.

The temperature transducers (thermocouples) were fabricated from wire conforming to Instrument Society of America Specifications. Before and after each test period, known millivolt levels were applied to each temperature recording system, and the corresponding temperature equivalents were obtained from 150°F reference tables based on the NBS temperature versus millivolt tables. Nonlinearity in the thermocouple characteristics was accounted for in the data reduction program.

The vibration transducers were calibrated in the standards laboratory to establish their displacement versus voltage output relationship. Before and after each test period, the vibration recording systems were calibrated by applying known voltage input levels measured with a calibrated voltmeter.

The rotor speed measuring system transducer (variable reluctance magnetic pickup) characteristics of rotational speed versus frequency were supplied by General Electric. Before and after each test period, the speed recording systems were calibrated by applying known frequency input levels from a calibrated frequency generator.

SECTION III PROCEDURE

3.1 TEST CONDITIONS

Simulator component performance was conducted at atmospheric inlet conditions with uniform compressor inlet pressure profiles. Air was supplied to the compressor inlet at a nominal total pressure and temperature of 14.2 psia and 80°F, respectively (Reynolds number index of 0.91).

Compressor mapping tests were conducted with uniform inlet pressure profiles at compressor inlet total pressures of 6 and 12 psia (Reynolds number indices of 0.39 and 0.78). Compressor mapping tests were also conducted with imposed circumferential inlet distorted pressure profiles at a compressor inlet pressure of 6 psia ($Re_1 = 0.39$). All compressor mapping tests were conducted at a nominal compressor inlet temperature of 80°F.

Test chamber pressure was maintained at a pressure equivalent to the compressor inlet pressure.

Turbine drive air was supplied to the turbine drive manifold at a pressure required to set the desired rotor speed. The drive air temperature was controlled to $200 \pm 3^{\circ}\text{F}$ by a steam-air heat exchanger.

The air temperature was maintained constant over the entire drive airflow range (0.35 to 4.0 lb/sec) by an automatic control system. The turbine drive air, heat exchanger, and control systems were designed and fabricated by ARO, Inc., personnel.

3.2 SIMULATOR OPERATING LIMITS

Simulator operating limits were established by the General Electric Company (Ref. 3). An emergency shutdown system (Section 2.2.3) was activated when prescribed limits were exceeded.

Maximum simulator operating limits are as follows:

Compressor Inlet Pressure	16 psia
Compressor Inlet Temperature	180°F
Turbine Inlet Pressure	1000 psia
Turbine Inlet Temperature	250°F
Forward Bearing Temperature	250°F
Aft Bearing Temperature	225°F
Bearing Temperature Rate of Rise	3.0°F/sec
Acceleration	6 g
Speed	86,000 rpm

The bearing temperature rate of rise limit was the only limit exceeded during simulator operation, as discussed in Section 4.6.

3.3 LUBE OIL

A continuous flow of MIL-L-7808F oil was supplied to the simulator front and rear bearings by a capillary oil flow system (Fig. 2) provided by G. E. The capillary tube for each system was fed by a bladder-type reservoir which held approximately 1000 cc of oil. In order to force the oil from the bladder through the capillary tube and into the simulator, the bladder was pressurized by gaseous nitrogen. Four oil systems were required: front and rear main oil systems and front and rear dampener oil systems. Flow rates for the front and rear bearing systems were identical: the main oil systems flow rates ranged from 40 to 55 cc/hr; the dampener oil systems flow rates ranged from 20 to 25 cc/hr.

3.4 TEST PROCEDURE

For the sea-level-static simulator component performance tests, the 10-in.-diam inlet ducting section was removed (Fig. 4), and an inlet screen was installed upstream of the simulator. Simulator inlet total pressure and temperature were nominally 14.2 psia and 80°F, respectively. The turbine inlet air was conditioned to a nominal temperature of $200 \pm 3^{\circ}\text{F}$ at a pressure of approximately 2000 psia upstream of the turbine drive inlet control valve. The turbine bleed valve was fully opened, then the turbine inlet control valve was manually opened to set the desired rotor speed. Air was exhausted to atmospheric conditions via the exhaust duct.

For the 6-psia compressor mapping tests, the following facility changes were made: Inlet ducting and an airflow metering venturi were added upstream of the simulator (Fig. 4). Upstream of the inlet venturi, a plenum and an inlet control valve were added. A steam ejector was added downstream of the test chamber to set the desired exhaust pressure of 6 psia. The G.E.-supplied dry nozzle was replaced by the mapping nozzle (Fig. 3).

The procedure for testing at an inlet pressure of 6 psia is described as follows: Conditioned turbine drive air at $200 \pm 3^{\circ}\text{F}$ and 2000 psia was supplied at the turbine drive inlet control valve. The turbine bleed valve was opened completely. The turbine drive inlet control valve was opened until rotor speed reached a nominal value of 20,000 rpm. The steam ejector was started and the test chamber pressure was lowered to 6 psia. The compressor inlet control valve was manually closed until the simulator inlet pressure was lowered to approximately 6 psia. The compressor inlet control system was switched to automatic mode, and inlet pressure was maintained at 6 ± 0.1 psia. The turbine drive inlet control valve was manually opened until the desired rotor speed was obtained.

The procedure used to obtain the simulator compressor maps was to obtain steady-state data on the operating line at various rotor speeds and then to back pressure the compressor, while maintaining constant corrected compressor rotor speeds, by a controlled inbleed of air into the mapping nozzle (Fig. 3). Steady-state data were obtained at several points while loading the compressor to its surge line. Incipient compressor surge was determined by monitoring the compressor inlet (PS_2) and compressor discharge (PS_{23}) dynamic static pressure instrumentation (Kulite transducers signals on oscilloscopes) for a rapid increase in dynamic pressure flucuations, as typically shown in Fig. 10. When incipient compressor surge was indicated, the compressor back pressure was decreased slightly, and a steady-state data point was recorded near the indicated incipient compressor surge line. The compressor was not taken into the fully stalled condition because of the possibility of destructive rotor overspeed upon removal of the compressor load.

For the 12-psia compressor mapping tests, the inlet venturi was replaced with a 4-in.-diam spool piece, and the compressor inlet control valve size was increased (3-in. valve to 4-in. valve). All other hardware and the test procedure were identical to that used in the 6-psia compressor mapping tests.

3.5 CALCULATIONS

The methods used to calculate steady-state performance parameters are presented in Appendix III.

SECTION IV RESULTS AND DISCUSSION

An investigation was conducted to determine the steady-state component performance and stability characteristics of an engine propulsion simulator. Testing was accomplished with uniform inlet total pressure profiles at sea-level-static conditions and at Reynolds number indices of 0.39 and 0.78. Testing was also accomplished with a distorted inlet total pressure profile at a Reynolds number index of 0.39. Inlet total temperature for all tests was nominally 80°F . The simulator was operated at corrected compressor rotor speeds ranging from approximately 34,000 to 82,500 rpm.

Surge limits of the simulator were determined by inbleeding air into the mapping nozzle to load the compressor while maintaining a constant corrected compressor rotor speed. High response compressor inlet and compressor discharge instrumentation was used to indicate the onset of compressor surge.

Engine propulsion simulator component performance at sea-level-static conditions are presented and compared with predicted data (Ref. 3). Also presented are the effects of Reynolds number index (0.39 and 0.78) and circumferential inlet distortion on the compressor performance and stability characteristics.

4.1 SIMULATOR INLET FLOW QUALITY

Simulator compressor performance testing was conducted at Reynolds number indices of 0.39 and 0.78 with a uniform (low distortion) total pressure profile, and at a Re_I of 0.39 with a distorted (one/rev screen) total pressure profile. Inlet temperature for all testing was nominally 80°F.

Typical compressor inlet uniform face profiles and inlet distortion [$(P_{2_{\max}} - P_{2_{\min}})/P_{2_{avg}} \times 100$] as a function of corrected airflow are shown in Figs. 11 and 12 for Re_I of 0.39 and 0.78, respectively. Compressor inlet distortions were 3.5 and 3.0 percent for Re_I of 0.39 and 0.78, respectively, at an airflow of 1.65 lbm/sec.

Typical compressor inlet circumferential total pressure profiles and distortion for the one/rev screen at an Re_I of 0.39 are presented in Figs. 13a and b. The total pressure distortion ranged from approximately 4 to 21 percent over an airflow range from 0.7 to 1.6 lbm/sec. Typical compressor inlet face pressure profile maps are shown in Fig. 13c.

4.2 SEA-LEVEL-STATIC PERFORMANCE

Engine propulsion simulator S/N 001/02 was initially tested at sea-level-static conditions ($P_2 = 14.2$ psia, $T_2 = 80^\circ\text{F}$) to compare the simulator component performance with predicted data (Ref. 3). Testing at sea-level-static conditions was conducted with the dry nozzle (G. E. P/N 401364-836P01) and solid mixer (G. E. P/N 4013097-341) configuration.

4.2.1 Compressor Performance

Corrected compressor inlet airflow at rated rotor speed (75.185 rpm) was 1.61 lbm/sec, or approximately 4.0 percent higher than the predicted value of 1.548 lbm/sec (Fig. 14a). The compressor pressure ratio at rated airflow was approximately 5.4 percent lower than the predicted value of 2.358 (Fig. 14b). Compressor efficiency peaked at 78 percent at an airflow of approximately 1.41 lbm/sec (equivalent to approximately 87 percent of rated speed) and decreased to 74 percent at rated airflow of 1.548 lbm/sec.

Peak compressor efficiency was approximately 12 percentage points greater than predicted (Fig. 14b). For a compressor temperature ratio of 1.43, the compressor pressure ratio was approximately 3 percent higher than the predicted value of 2.358.

4.2.2 Turbine Performance

During initial testing at sea-level-static conditions, a turbine rub strip was utilized to seal airflow leakage around the turbine blade tips. After 8 hr and 18 min of operation, the rub strip failed and was replaced for subsequent testing with a metal sleeve for the turbine blade tip seal (see Section 4.6).

4.2.2.1 Rub Strip Installed for Turbine Blade Tip Seal

Turbine performance and operating parameters as a function of corrected compressor rotor speed are compared with the predicted data in Fig. 15a. With the turbine rub strip installed, the turbine efficiency ranged from 2 to 9 percentage points higher than predicted. At rated rotor speed (75,185 rpm), the turbine efficiency was 74 percent, or 2 percentage points higher than the predicted value. A turbine drive airflow of 2.95 lbm/sec at an inlet pressure of 725 psia was required, as predicted, to drive the rotor at rated speed.

4.2.2.2 Metal Sleeve Installed for Turbine Blade Tip Seal

With the metal sleeve installed for the turbine blade tip seal, the turbine performance and operating parameters are shown (Fig. 15b) and compared with the measured data obtained with the turbine rub strip. With the metal sleeve installed, the turbine efficiency at rated rotor speed (75,185 rpm) was 65 percent, or 9 percentage points lower than the value obtained with the rub strip. The decrease in turbine efficiency is attributed to an increase in turbine blade tip seal leakage flow as further evidenced by the increase in turbine drive airflow and turbine inlet manifold pressure required to drive the rotor. At rated speed (75,185 rpm), an increase in turbine drive airflow and turbine inlet pressure of approximately 8 percent was required to drive the rotor at rated speed.

4.3 EFFECT OF REYNOLDS NUMBER INDEX ON COMPRESSOR PERFORMANCE (UNIFORM INLET)

The effects of Reynolds number index on corrected compressor inlet airflow, corrected compressor rotor speed, compressor pressure ratio, compressor temperature ratio, and compressor efficiency are shown in Fig. 16 for Re_l of 0.39 and 0.78.

As Re_l was decreased from 0.78 to 0.39, corrected compressor inlet airflow decreased by approximately 12 percent at 35,000 rpm and by approximately 2.6 percent at 67,500 rpm (Fig. 16a). However, at rated rotor speed (75,185 rpm), compressor airflow was approximately 1.6 lbm/sec for both an Re_l of 0.39 and 0.78.

Compressor pressure ratio and compressor efficiency are presented in Fig. 16b as a function of corrected compressor airflow. As Re_I was decreased from 0.78 to 0.39, pressure ratio increased by approximately 4.5 percent at an airflow of 0.8 lbm/sec and by approximately 1.4 percent at rated airflow of 1.548 lbm/sec. Peak compressor efficiency occurred at a corrected airflow of approximately 1.42 lbm/sec and increased 3 percentage points (to 78 percent) as Re_I decreased from 0.78 to 0.39.

Compressor pressure ratio as a function of compressor temperature ratio is presented in Fig. 16c. No effect of Re_I was observed at temperature ratios below 1.1. However, at a temperature ratio above 1.1, the compressor pressure ratio increased as Re_I was decreased from 0.78 to 0.39. At a temperature ratio of 1.4, the pressure ratio increased by approximately 2.8 percent for a decrease in Re_I from 0.78 to 0.39.

4.4 COMPRESSOR STABILITY, UNIFORM INLET

Compressor mapping tests were conducted with uniform inlet pressure profiles Figs. 11 and 12) at Reynolds number indices of 0.39 and 0.78 per the procedure described in Section 3.5. All mapping tests were conducted at an inlet temperature of nominally 80°F and with the solid mixer (G. E. P/N 4013097-341) and mapping nozzle (Fig. 3) configuration.

Initial compressor mapping tests were performed at a Reynolds number index of 0.39 ($P_2 = 6$ psia, $T_2 = 80^\circ\text{F}$) to reduce the loads on the compressor and increase the margin of safety during compressor surge. The compressor was not taken to the fully stalled condition because of the possibility of destructive rotor overspeed upon removal of the compressor load.

4.4.1 Compressor Operating Map at $Re_I = 0.39$

The uniform inlet compressor operating map is presented in Fig. 17a for an Re_I of 0.39. For a constant corrected compressor airflow of 1.60 lbm/sec, the compressor pressure ratio increased from 2.31 at the normal operating line to approximately 3.3 at the indicated incipient surge line, resulting in a stability margin of approximately 42.9 percent.

4.4.2 Effect of Reynolds Number Index on Compressor Operating Map

The uniform inlet compressor operating map at an Re_I of 0.78 is shown in Fig. 18. At a constant corrected airflow of 1.60 lbm/sec, the compressor pressure ratio increased from 2.30 at the normal operating line to approximately 3.34 at the estimated surge line resulting in a stability margin of approximately 45.2 percent. The uniform inlet operating map at an Re_I of 0.39 is also shown in Fig. 18 for comparison purposes. There was no significant effect of Re_I on the compressor operating map.

Operation of the simulator at an Re_I of 0.78 near the surge line at 80, 90, and 100 percent of rated rotor speed resulted in forward bearing temperature rate of rise exceeding established safety limits (see Section 4.6).

4.5 EFFECT OF CIRCUMFERENTIAL INLET DISTORTION ON COMPRESSOR PERFORMANCE AND STABILITY

The effects of circumferential inlet distortion on the corrected compressor inlet airflow, compressor pressure ratio, corrected compressor rotor speed, compressor temperature ratio, and compressor efficiency are shown in Fig. 19.

4.5.1 Compressor Performance

Corrected compressor inlet airflow as a function of corrected compressor rotor speed is presented in Fig. 19a. Corrected airflow was approximately 1 to 2 percent lower with circumferential inlet distortion than with a uniform inlet. At rated speed of 75,185 rpm, corrected airflow decreased 1.6 percent from approximately 1.60 lbm/sec to 1.575 lbm/sec with circumferential distortion of 21 percent.

Compressor pressure ratio and compressor efficiency as a function of corrected compressor inlet airflow are presented in Fig. 19b. Compressor pressure ratio with circumferential distortion was generally within ± 2 percent of the uniform inlet at corrected airflows greater than 1.1 lbm/sec. With inlet distortion, the compressor pressure ratio increased from 2.31 to 2.36 at a corrected airflow of 1.60 lbm/sec.

The compressor efficiency with a distorted inlet was approximately 3 to 8 percent lower than the compressor efficiency with a uniform inlet. Compressor efficiency decreased from a peak value of approximately 78 percent with a uniform inlet to the value of approximately 75 percent with a distorted inlet at a corrected airflow of 1.42 lbm/sec.

Compressor pressure ratio as a function of compressor temperature ratio is presented in Fig. 19c. With a distorted inlet, the compressor pressure ratio was approximately 1 to 2 percent lower than the compressor pressure ratio with a uniform inlet. The compressor pressure ratio decreased from approximately 2.38 with a uniform inlet to 2.36 with a distorted inlet at a temperature ratio of 1.4.

4.5.2 Compressor Stability (Distorted Inlet)

The effect of circumferential inlet distortion on the compressor operating map is shown in Fig. 20 for an Re_l of 0.39. At a constant corrected compressor inlet airflow of 1.60 lbm/sec, the compressor pressure ratio ranged from 2.36 at the normal operating line to 3.34 at the indicated surge line resulting in a stability margin of 41.5 percent. The uniform inlet map is also shown in Fig. 20 for comparison purposes. There was no significant effect of distortion on the compressor operating map. It was noted during analysis of the test data that the compressor discharge distortion parameter [$(P_{23 \text{ max}} - P_{23 \text{ min}})/P_{23 \text{ avg}} \times 100$] decreased as the compressor was loaded from the normal operating line towards the surge line at constant corrected rotor speed. For example, at 100-percent rated speed, the compressor discharge distortion decreased from approximately 16 percent on the normal operating line to approximately 6 percent near the surge line.

The compressor discharge distortion level appeared to be a function only of compressor rotor speed and operating point on the compressor operating map and was essentially independent of the distortion imposed at the compressor inlet as shown in Fig. 21. It was further noted that an increase in compressor efficiency occurred as the compressor approached surge as shown in Fig. 22.

4.6 OPERATIONAL EXPERIENCES

Approximately 39 hr and 9 min of powered time was accumulated on the simulator during the test program.

After 8 hr and 18 min of powered time on the simulator, the turbine rub strip failed while the simulator was operating at 101-percent rated speed (76,000 rpm). A manual shutdown was initiated and no other apparent damage was incurred by the simulator as a result of the rub strip failure. The rub strip was replaced with a metal sleeve for subsequent testing by Tech Development Company under contract to General Electric.

Operation of the simulator near the surge line at 80, 90, and 100 percent of rated rotor speed at an Re_l of 0.78 (compressor inlet pressure of 12 psia) resulted in forward bearing temperature rate of rise of nominally 3°F/sec , barely exceeding the established safety limit. Manual shutdowns of the simulator were initiated when the rate of rise exceeded 3.0°F/sec .

The bearing temperature rate of rise in excess of 3.0°F/sec was apparently caused by an increased load imposed on the bearing at the aforementioned test condition. This phenomenon did not appear to damage the simulator in any way or hinder operation of the simulator during subsequent testing.

SECTION V SUMMARY OF RESULTS

A test program was conducted to determine the sea-level-static component performance of an engine propulsion simulator and to determine the effects of Reynolds number index ($Re_l = 0.39$ and 0.78) and circumferential inlet distortion on the compressor performance and stability. The test results are summarized as follows:

Sea-Level-Static Performance

1. Corrected compressor inlet airflow of 1.61 lbm/sec at a corrected compressor rated rotor speed of 75,185 rpm was approximately 4.0 percent higher than the predicted value of 1.548 lbm/sec.
2. Compressor efficiency peaked at 78 percent at an airflow of 1.41 lbm/sec (equivalent to approximately 87 percent rated speed) and decreased to 74 percent at rated airflow of 1.548 lbm/sec. Peak compressor efficiency was approximately 12 percentage points greater than predicted.

3. Compressor pressure ratio at rated airflow of 1.548 lbm/sec was approximately 5.4 percent lower than the predicted pressure ratio of 2.358.
4. With the turbine rub strip installed, turbine efficiency was approximately 2 to 9 percentage points higher than predicted and was 74 percent at rated rotor speed. When the turbine rub strip was replaced with a metal sleeve, the turbine efficiency at rated speed decreased 9 percentage points.
5. A turbine drive airflow of approximately 3.2 lbm/sec at a turbine inlet manifold pressure of approximately 790 psia was required to drive the rotor at rated speed when the metal sleeve was used as the turbine blade tip seal. The turbine drive airflow and turbine inlet manifold pressure at rated speed were approximately 8 percent higher than predicted values or the values required to drive the rotor prior to the turbine rub strip failure.

Effect of Circumferential Inlet Distortion and Reynolds Number Index on Compressor Performance and Stability

1. Corrected compressor airflow decreased, approximately 12 percent at 35,000 rpm and approximately 2.6 percent at 67,500 rpm as Re_l decreased from 0.78 to 0.39. At rated rotor speed (75,185 rpm), compressor airflow was 1.60 lbm/sec at rated speed for both an Re_l of 0.78 and 0.39.
2. Compressor pressure ratio and efficiency increased as the Re_l decreased from 0.78 to 0.39. At rated airflow of 1.548 lbm/sec as Re_l decreased, the compressor pressure ratio increased 1.4 percent from 2.17 to 2.20. Peak compressor efficiency increased 3 percentage point, 75 to 78 percent, as Re_l decreased from 0.78 to 0.39.
3. There was no significant effect of Re_l (0.78 and 0.39) on the compressor operating map. At an Re_l of 0.78 and at a constant corrected airflow of 1.60 lbm/sec, the compressor pressure ratio increased from 2.30 at the normal operating line to 3.34 at the indicated surge line resulting in a stability margin of 45.2 percent.
4. Corrected compressor airflow as a function of corrected compressor rotor speed was approximately 1 to 2 percent lower with circumferential inlet distortion than with a uniform inlet at $Re_l = 0.39$. At rated speed of 75,185 rpm, the corrected compressor airflow decreased 1.6 percent from 1.60 lbm/sec to 1.575 lbm/sec with circumferential inlet distortion of 21 percent.
5. Compressor efficiency with a distorted inlet was approximately 3 to 8 percent lower than with a uniform inlet. Compressor efficiency decreased from a peak value of 78 percent with a uniform inlet to 75 percent with a distorted inlet.

6. There was no significant effect of distortion on the compressor operating map. With a distorted compressor inlet and at a constant corrected airflow of 1.60 lbm/sec, the compressor pressure ratio increased from 2.36 on the normal operating line to 3.34 at the indicated surge line resulting in stability margin (compressor surge margin) of 41.5 percent.
7. During compressor mapping tests with both a uniform and a distorted inlet pressure profile at an Re_1 of 0.39 and at a rated speed of 75,185 rpm, the compressor discharge distortion level decreased from approximately 16 percent on the normal operating line to approximately 6 percent near the surge line. The compressor distortion level appeared to be a function only of compressor rotor speed and operating point on the compressor stability map, and was essentially independent of the distortion imposed at the compressor inlet. It was further noted that the compressor efficiency increased as the compressor approached the surge line.
8. The turbine rub strip failed after 8 hr and 18 min of powered simulator time while the simulator was operating at 101 percent rated speed (76,000 rpm).
9. When operating the simulator with a uniform inlet at an Re_1 of 0.78 ($P_2 = 12$ psia) and at rated speeds greater than 70 percent, established bearing temperature rate of rise limit of 3.0°F/sec was exceeded when the compressor approached the surge line, resulting in manual shutdowns of the simulator with no apparent damage.
10. Approximately 39 hr and 9 min of powered time was accumulated on the simulator during this test program.

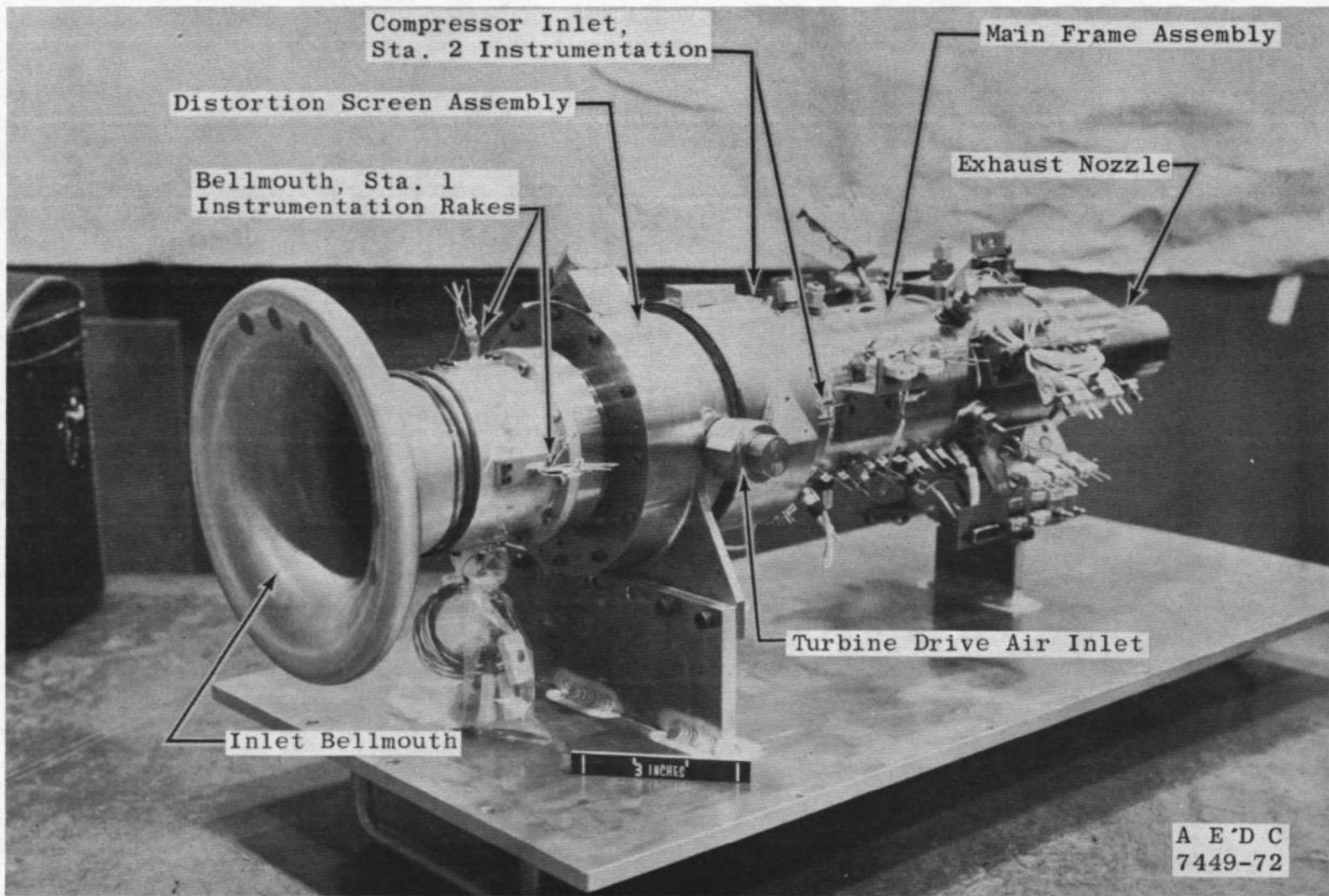
REFERENCES

1. Anderson, R. M., Laich, M. S., and Eigenmann, M. F. "Multimission Turbine Engine Propulsion Simulator Application Study." AFAPL-TR-72-107, November 1972.
2. Owens, C. L. "Capabilities of the ESF Instrument Branch." AEDC-TR-67-18 (AD648707), March 1967.
3. Delaney, B. R. "Pretest Report for Propulsion Simulator." General Electric Technical Memorandum No. 72-187, March 1972.
4. Smith, Robert E., Jr. and Matz, Roy J. "Verification of a Theoretical Method of Determining Discharge Coefficients for Venturis Operating at Critical Flow Conditions." AEDC-TR-61-8 (AD262714), September 1961.

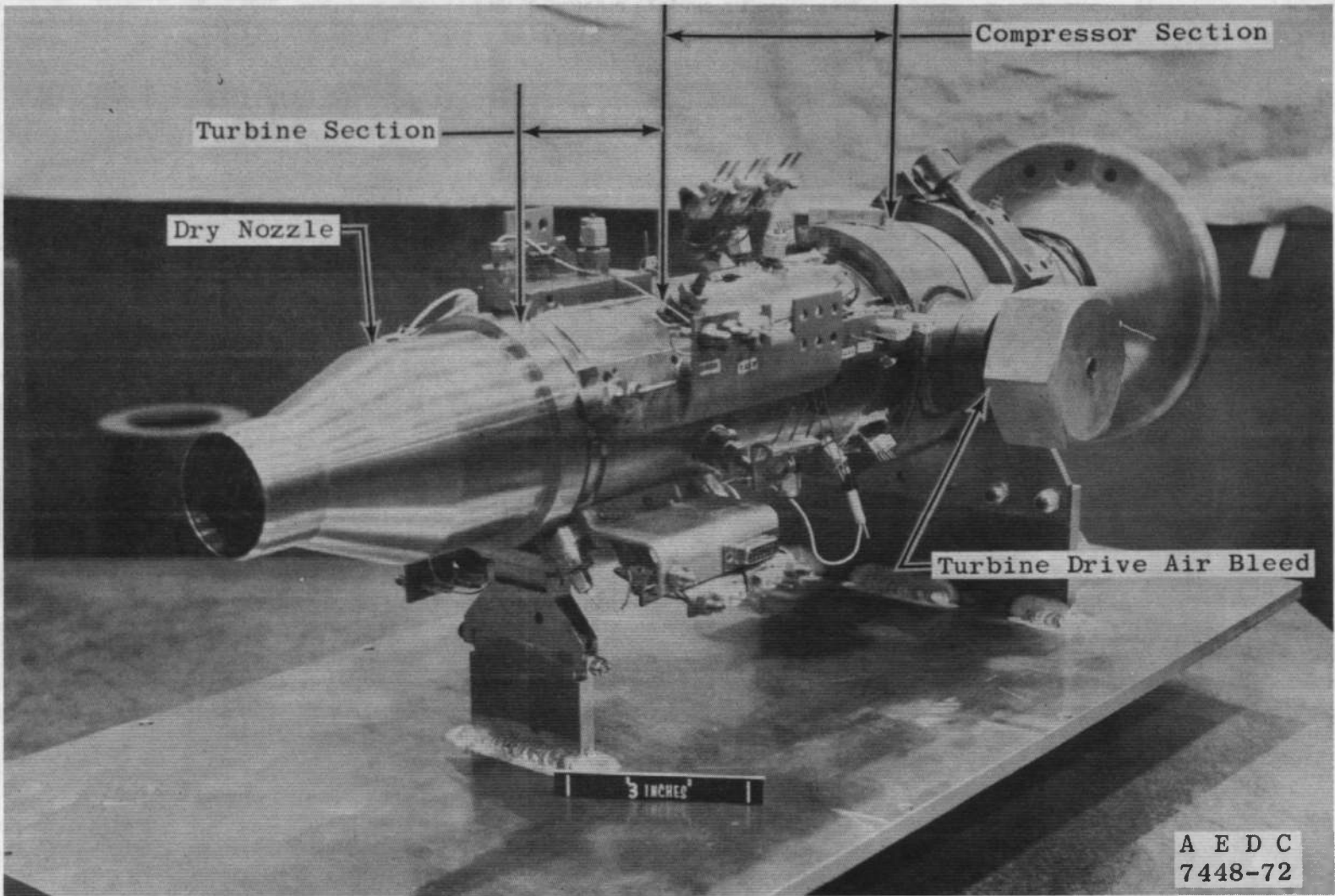
5. Tucker, Maurice. "Approximate Calculation Turbulent Boundary Layer Development in Compressible Flow." NACA-TN-2337, April 1971.
6. Johnson, R. C. "Real-Gas Effects in Critical-Flow-Through Nozzles and Tabulated Thermodynamic Properties." Lewis Research Center, NASA TN-D-2565, January 1965.
7. American Society of Mechanical Engineers. Supplement to Power Test Codes, "Chapter 4: Flow Measurement Part 5—Measurement of Quantity of Materials." ASME, PTC 195, April 1959.

APPENDIXES

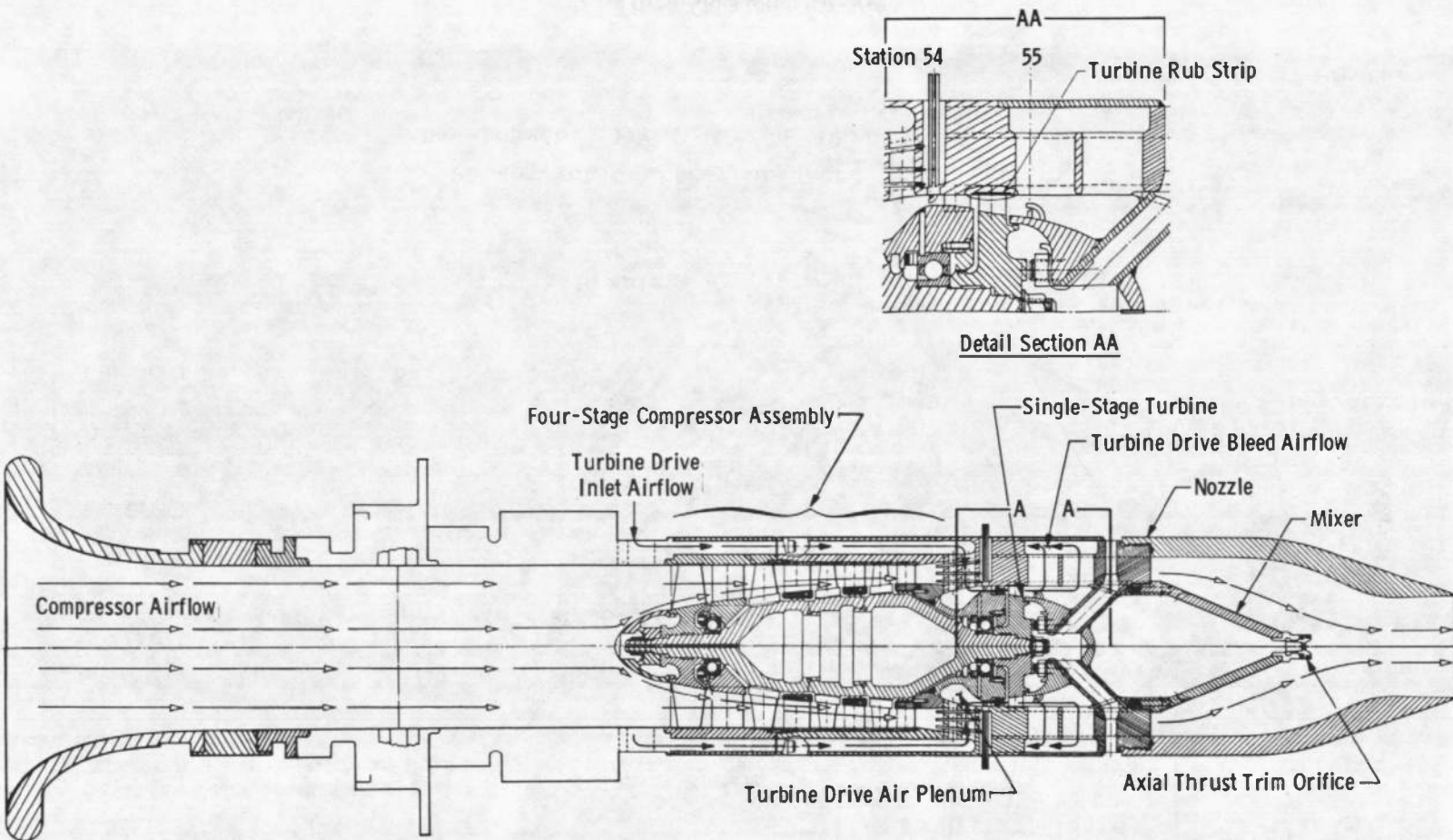
- I. ILLUSTRATIONS**
- II. TABLES**
- III. METHODS OF CALCULATIONS**



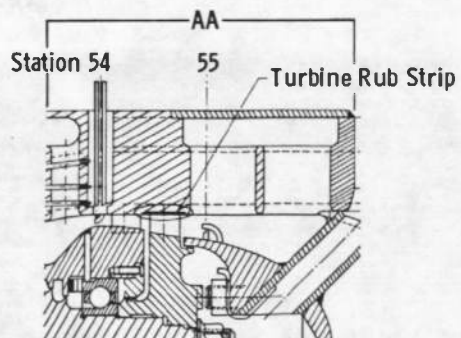
a. Three Quarter Front View
Fig. 1 Engine Propulsion Simulator



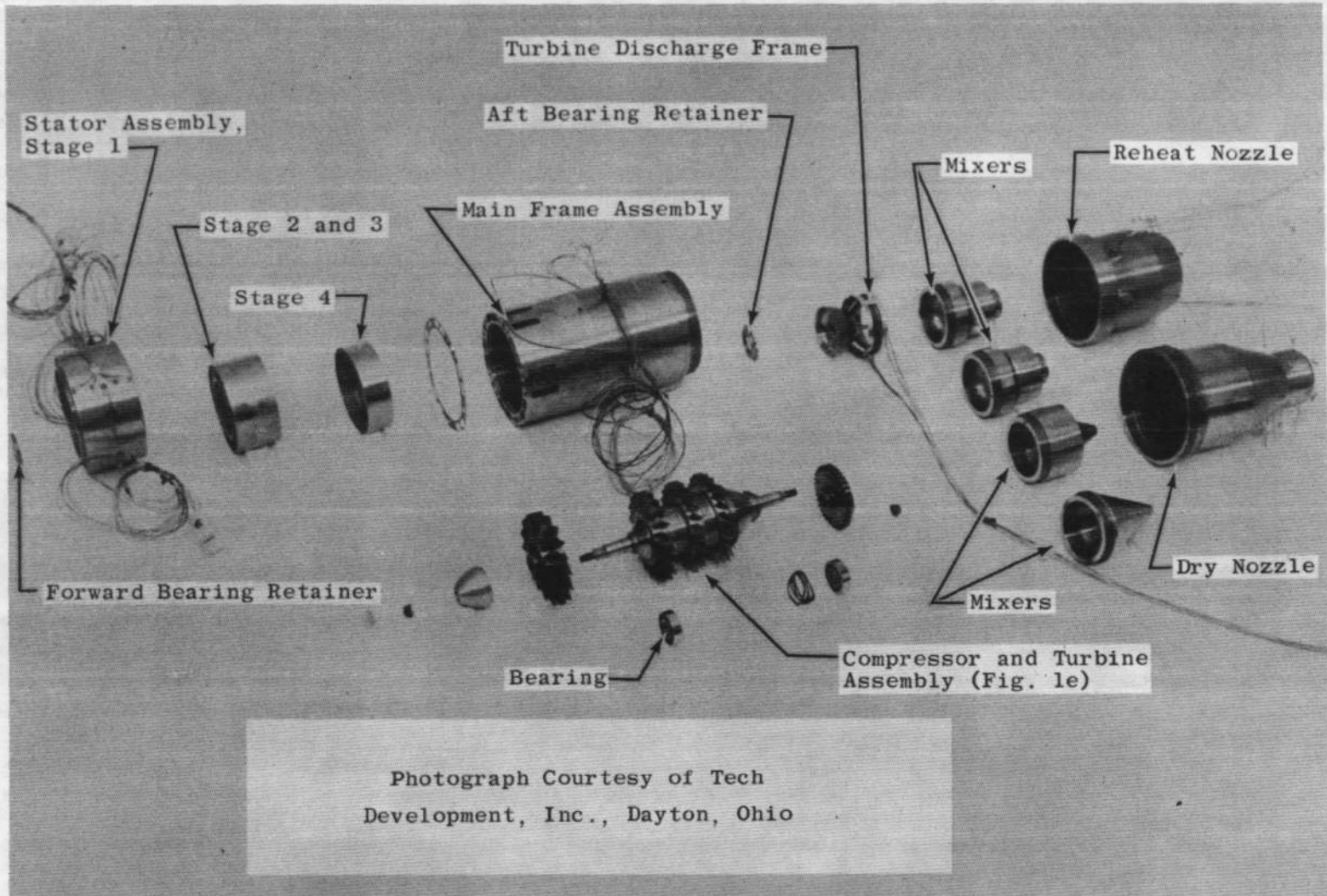
b. Three Quarter Rear View
Fig. 1 Continued



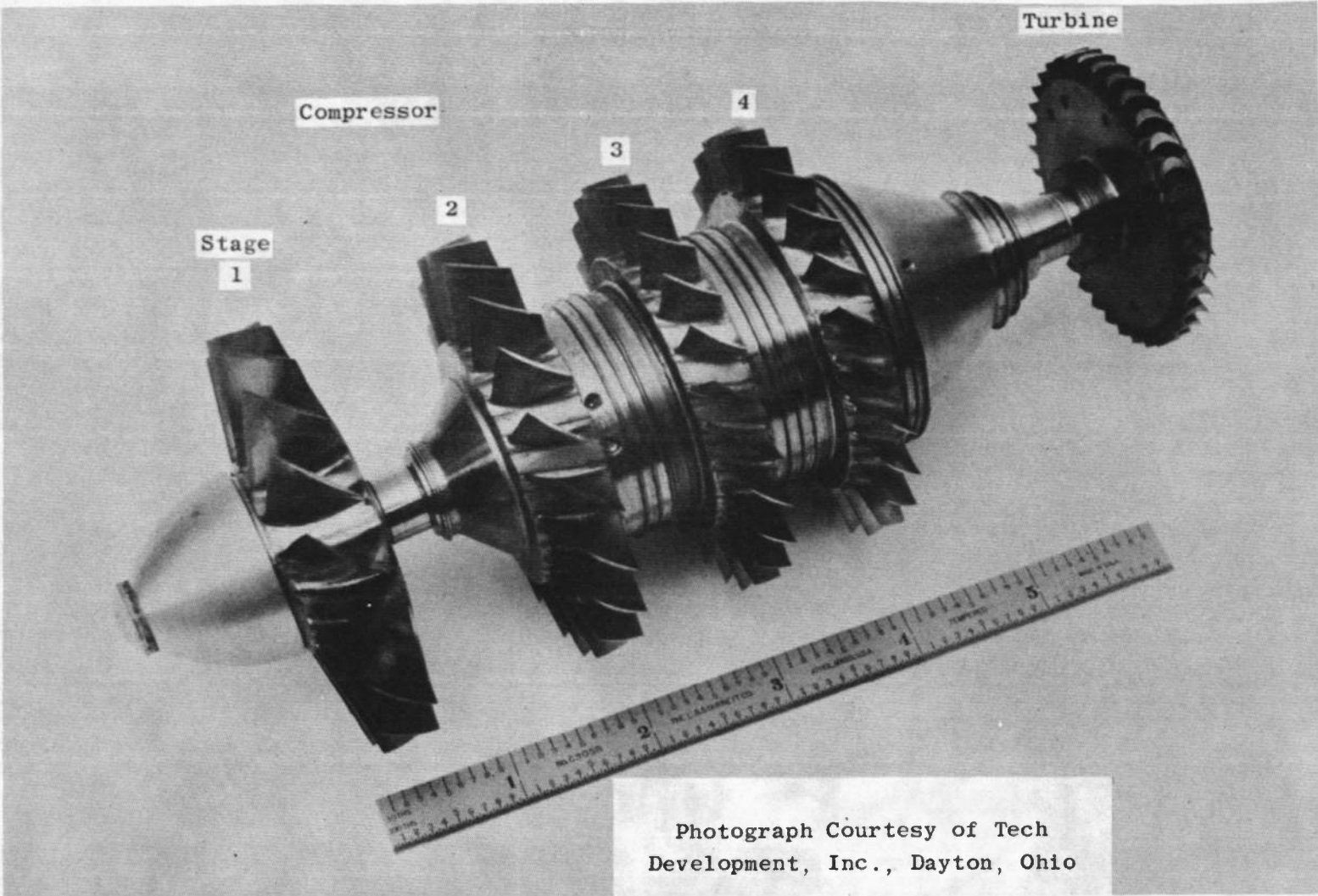
c. Cross-Sectional Schematic
Fig. 1 Continued



Detail Section AA

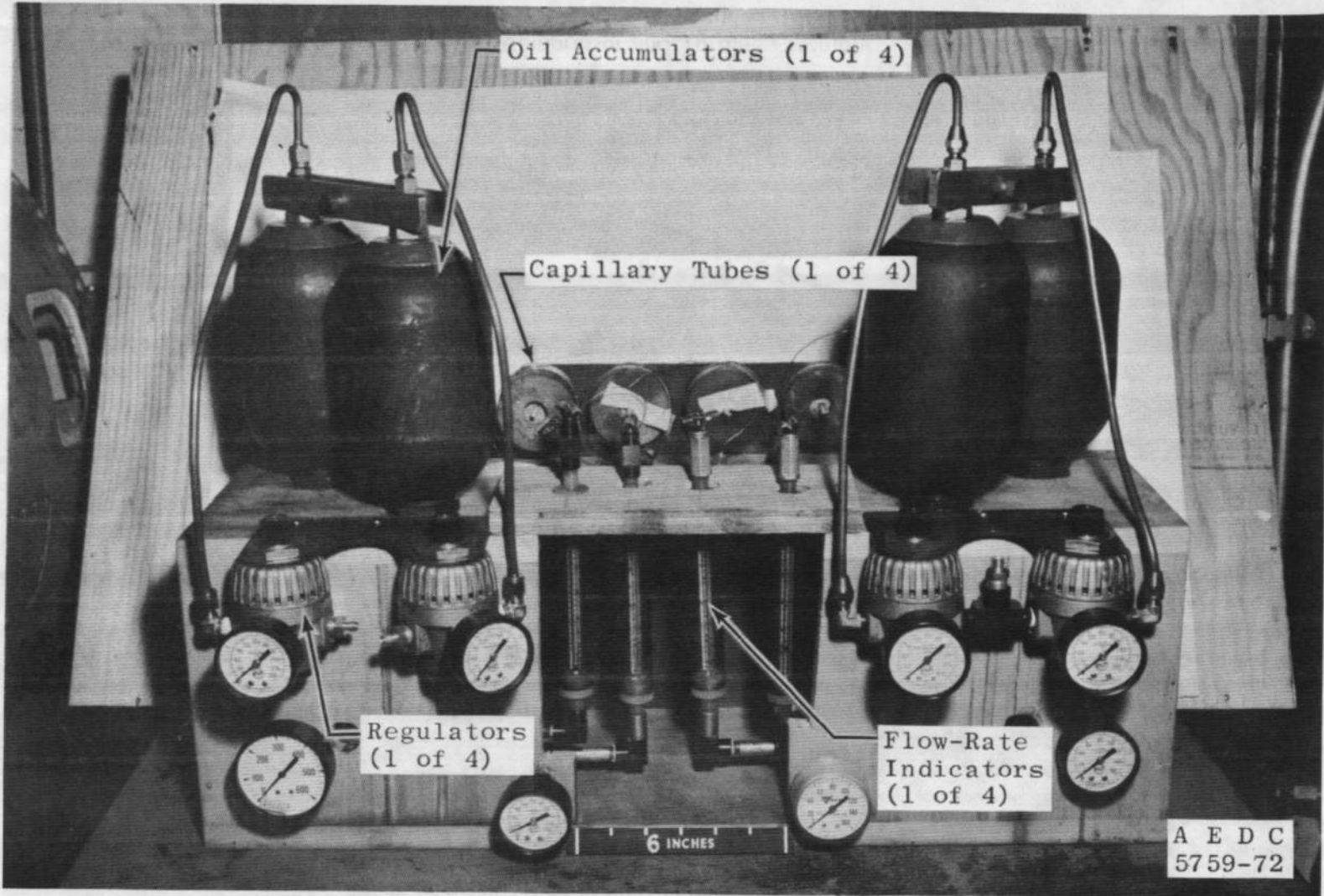


d. Component Layout
Fig. 1 Continued

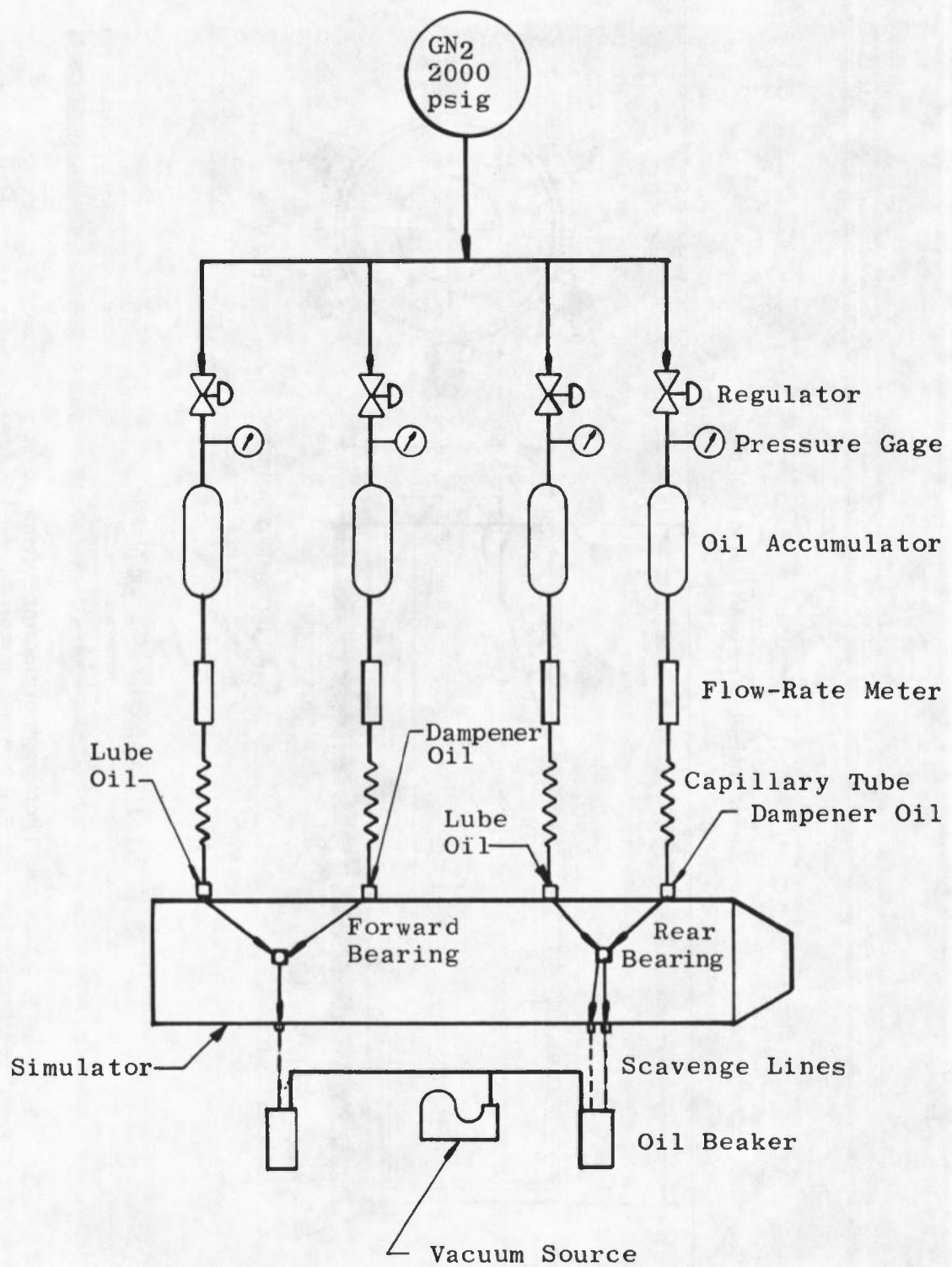


Photograph Courtesy of Tech
Development, Inc., Dayton, Ohio

e. Compressor and Turbine Assembly
Fig. 1 Concluded



a. Photograph of Control System
Fig. 2 Lube Oil System



b. Oil Flow Schematic
Fig. 2 Concluded

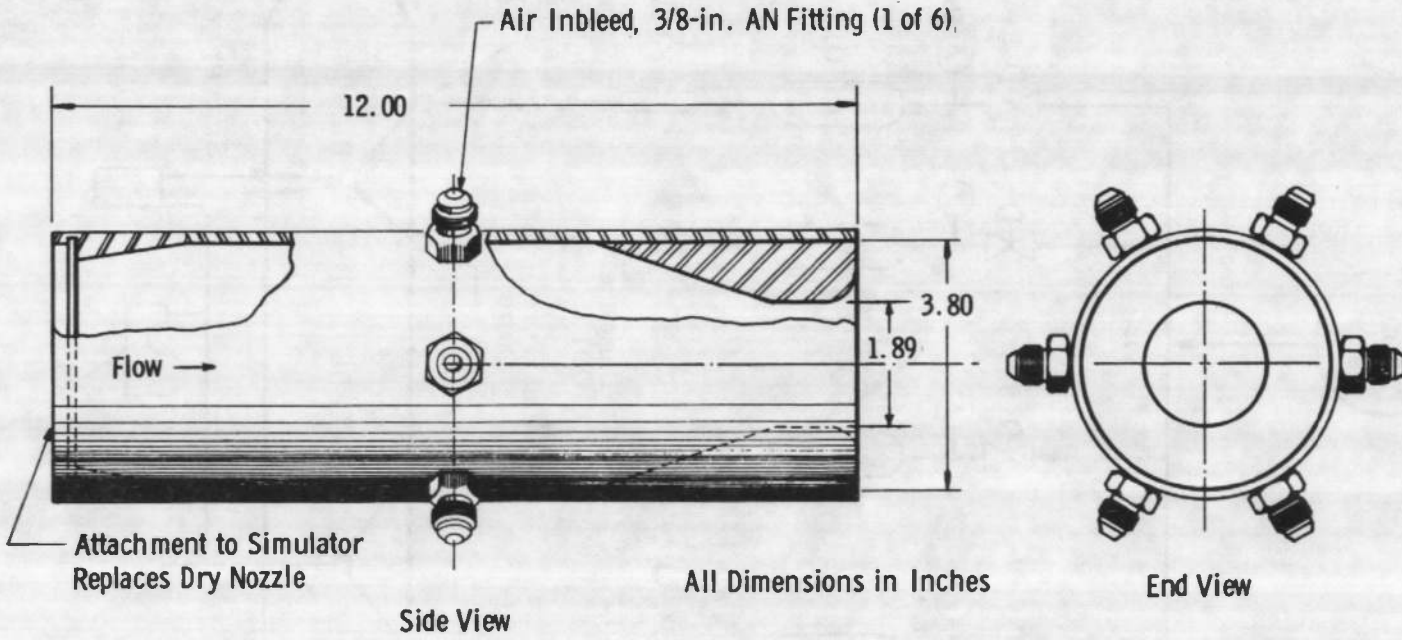
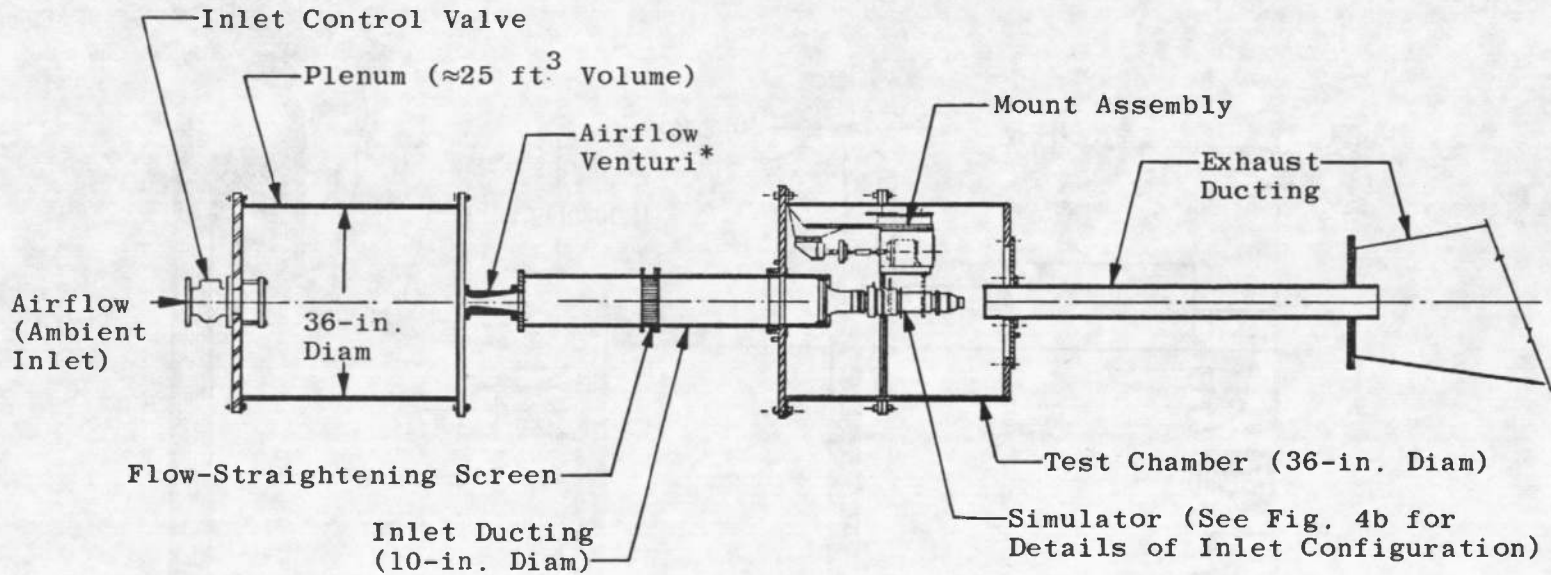


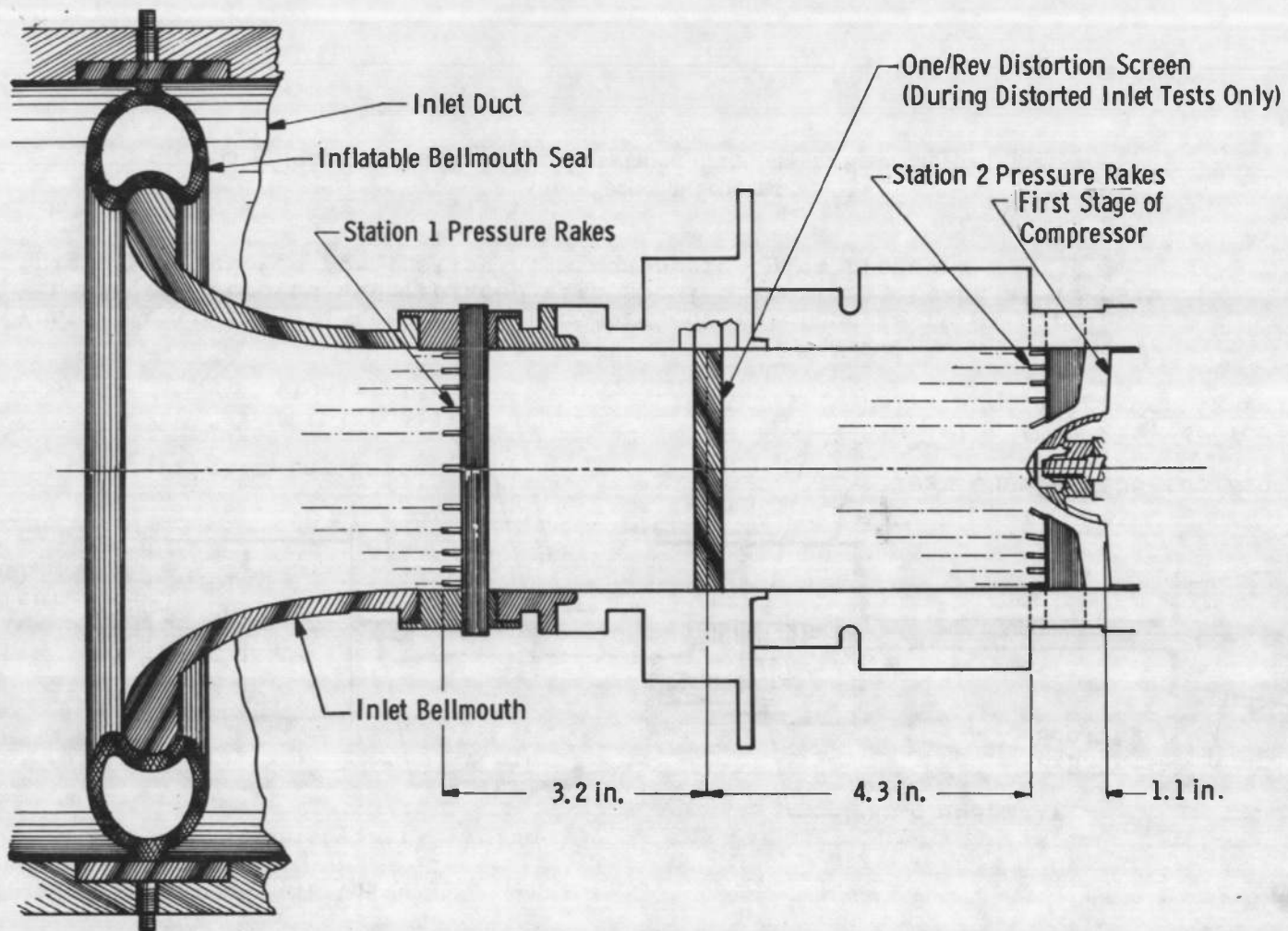
Fig. 3 Compressor Mapping Nozzle



*Venturi used for all testing with compressor inlet pressure of 6 psia.
 Venturi was removed and replaced with spool piece for testing at 12 psia.
 Inlet duct removed for testing at atmospheric inlet pressure.

a. Cross-Sectional Schematic

Fig. 4 Propulsion Simulator Test Installation in Propulsion Research Area (R-2C-4)



b. Detail of Simulator Inlet
Fig. 4 Concluded

Sym

☒	Valve
●	Pressure (P)
X	Temperature (T)
PDS	Supply
PVI	Venturi Inlet
PVT	Venturi Throat
PDM	Drive Manifold
PBM	Bleed Manifold
POU	Upstream Orifice
POD	Downstream Orifice
PSL	Streamline
PDL	Downstream Dump
TDS	Supply
TDV	Venturi
TDM	Drive Manifold
TBM	Bleed Manifold
TBO	Orifice
TDL	Downstream Dump
TDC	Shutoff Valve Skin
TDD	Dump Valve Skin
PED	Exhaust Duct Differential
SVP	Control Valve Position
BVP	Bleed Valve Position

Note: All pressures are wall static.

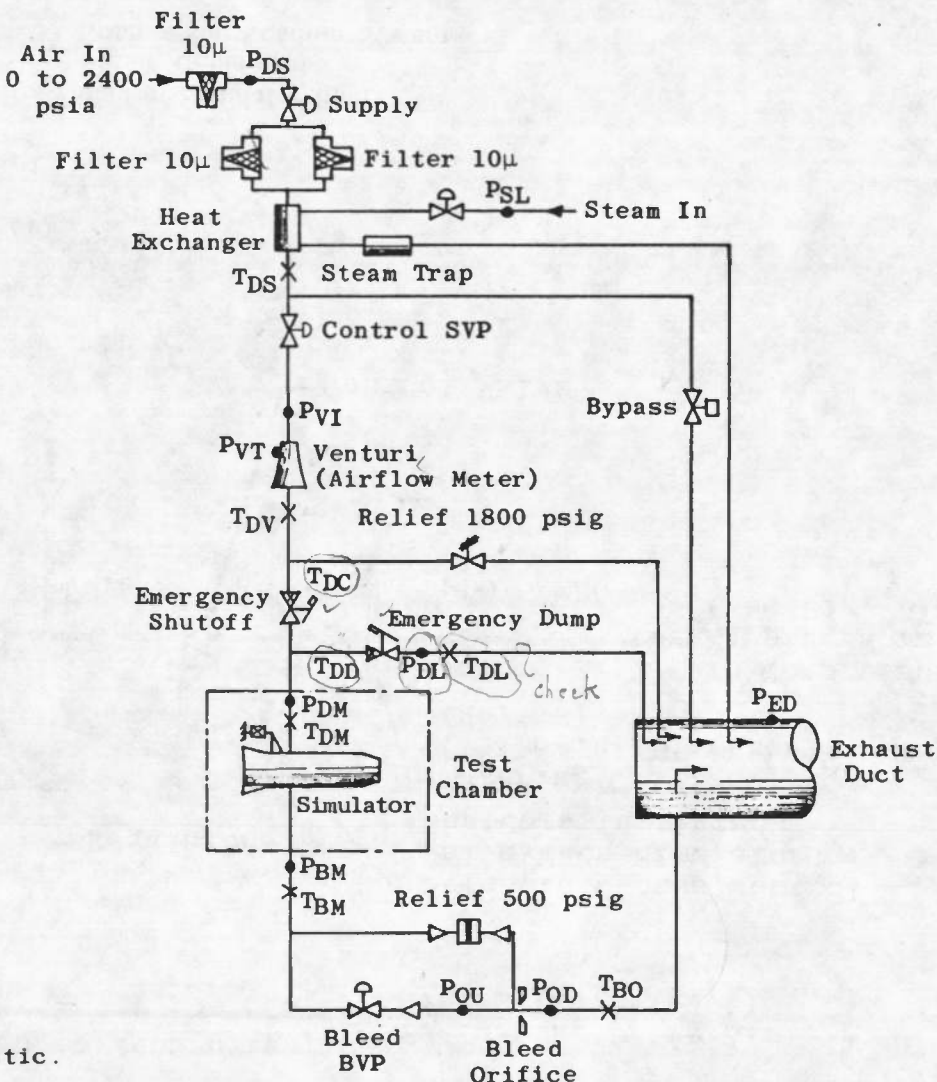


Fig. 5 Schematic of Turbine Drive Air System

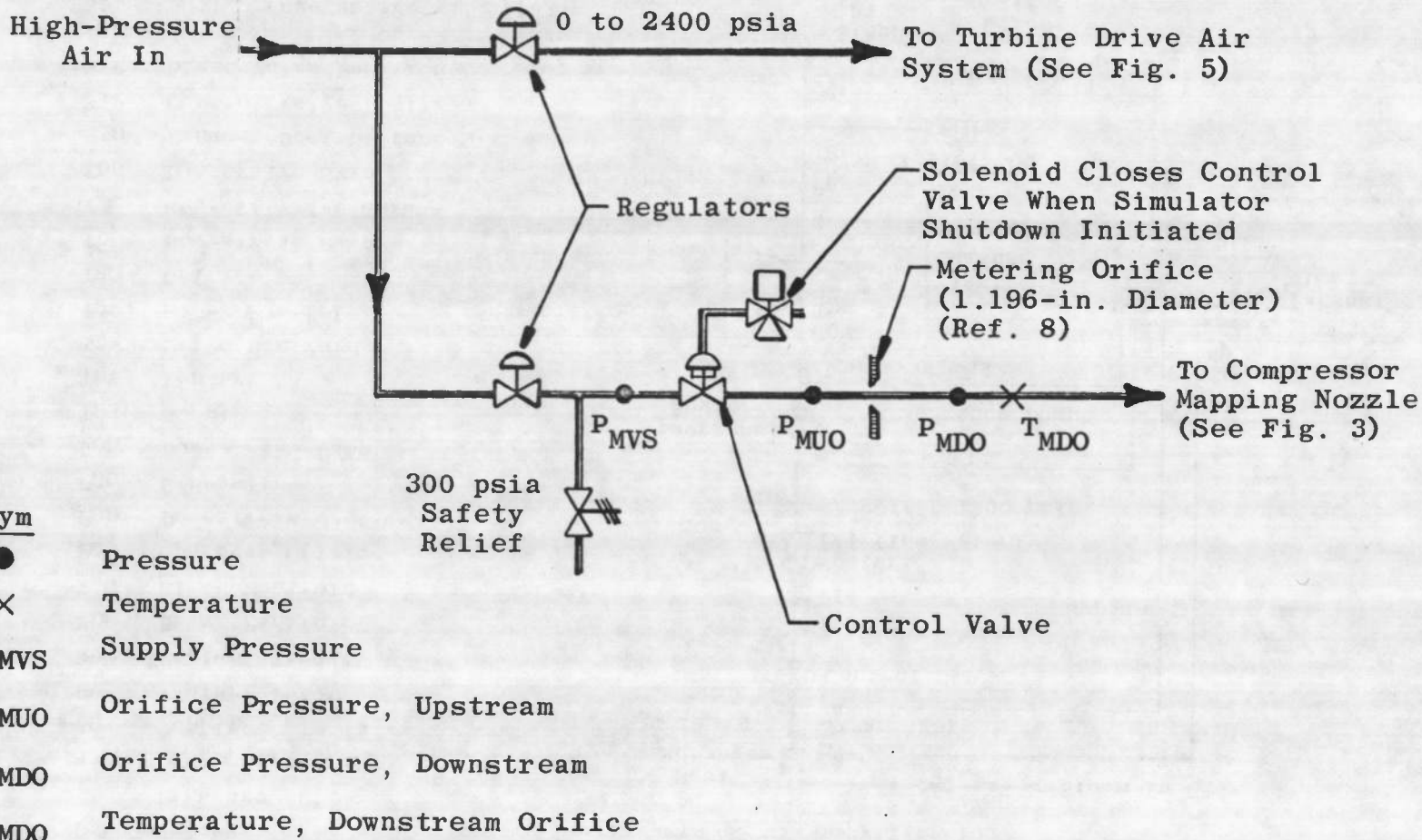


Fig. 6 Compressor Loading System

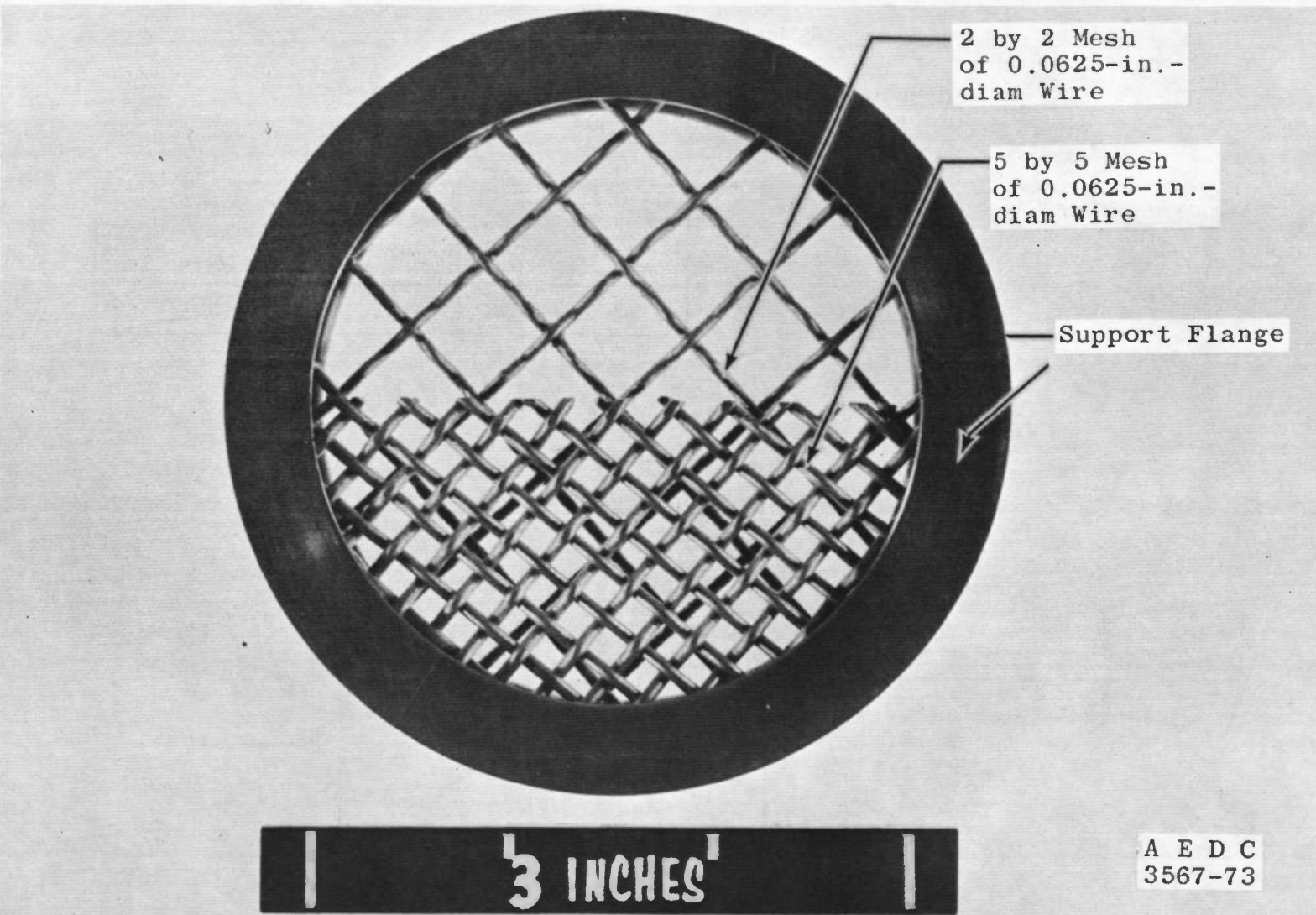
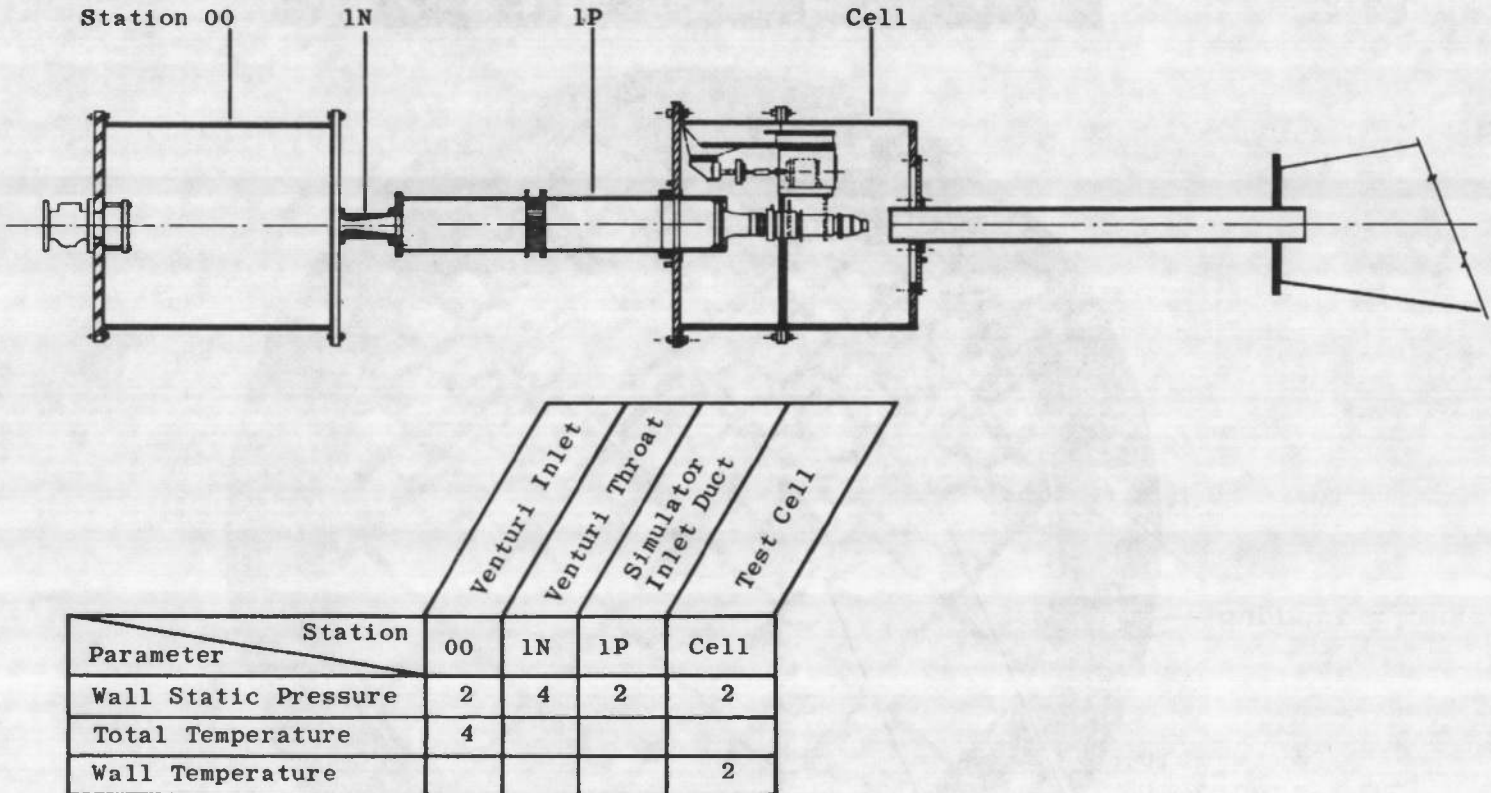


Fig. 7 One/Rev Distortion Screen Assembly



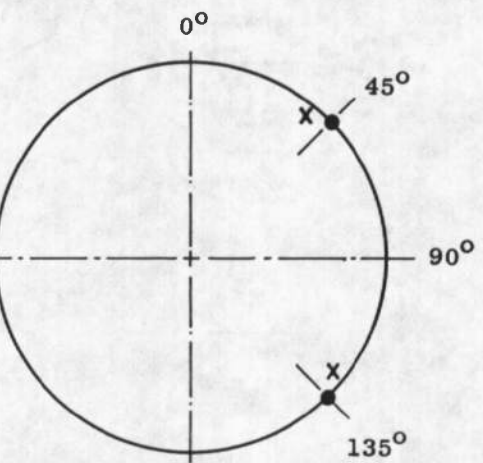
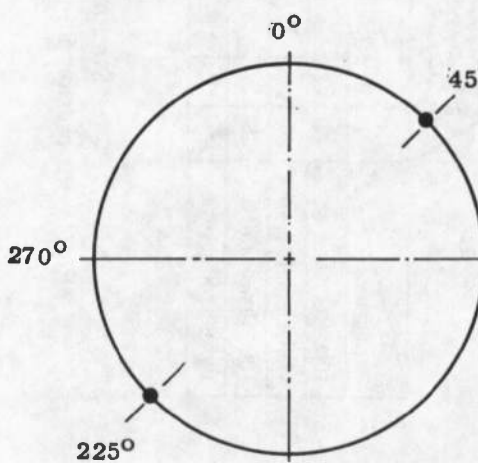
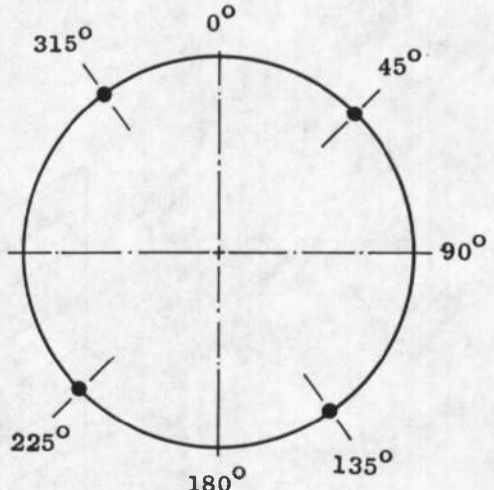
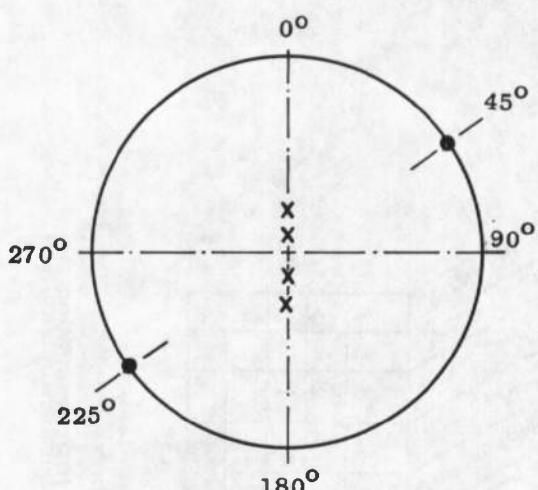
a. Station Location

Fig. 8 Inlet Duct and Test Chamber Instrumentation

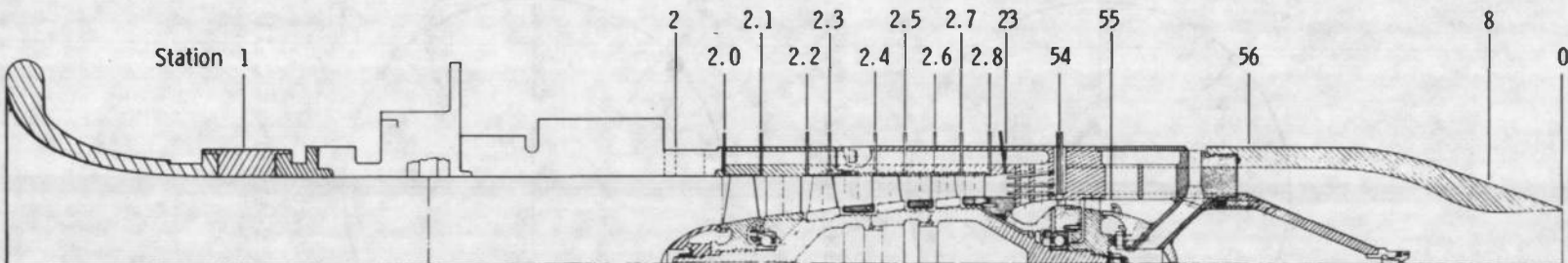
Sym

-
-
- ×

Wall Static Pressure
Total Pressure
Thermocouple, Skin



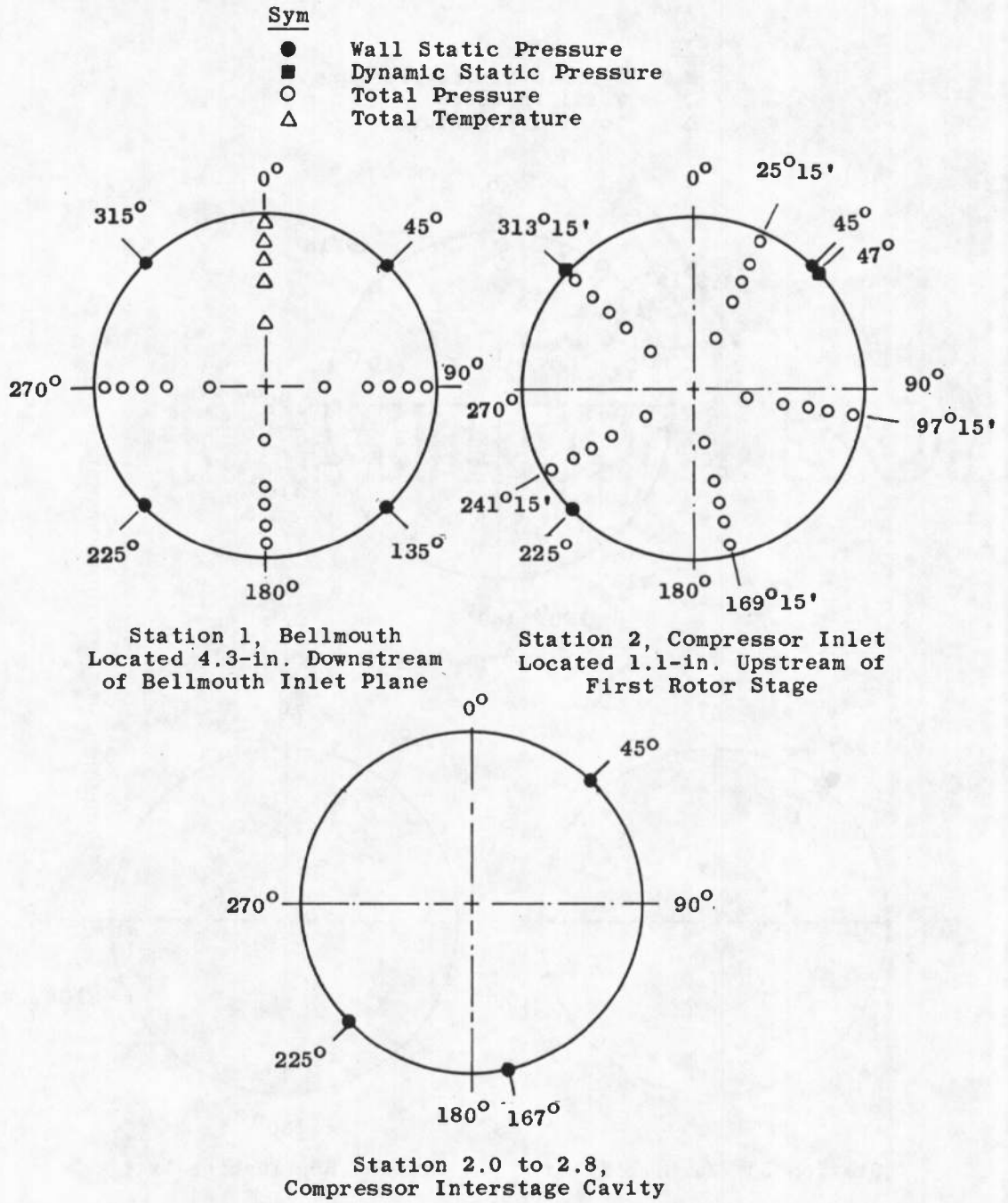
b. Instrumentation Details
Fig. 8 Concluded



Parameter	Station 1	2	2.0	2.8	23	54	55	56	8	0
Bellmouth										
Compressor Inlet										
Compressor Intermediate										
Turbine Discharge										
Turbine Inlet										
Mixer Cavity										
Nozzle Throat										
Nozzle Exit										

a. Station Location

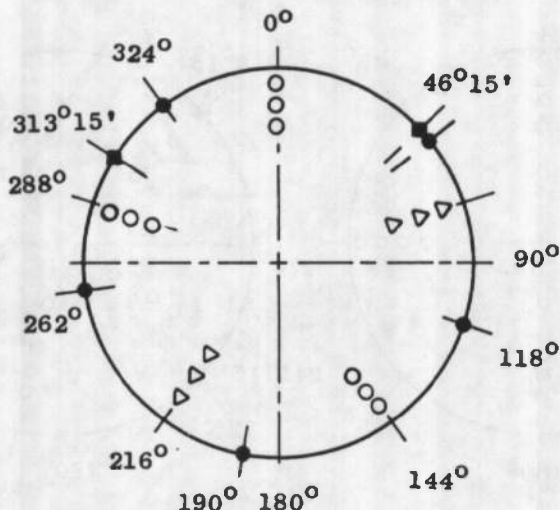
Fig. 9 Propulsion Simulator Instrumentation



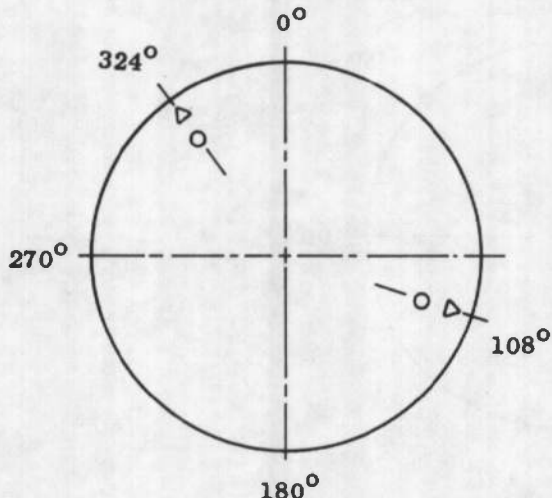
b. Instrumentation Details, Stations 1 to 2.8
Fig. 9 Continued

Sym

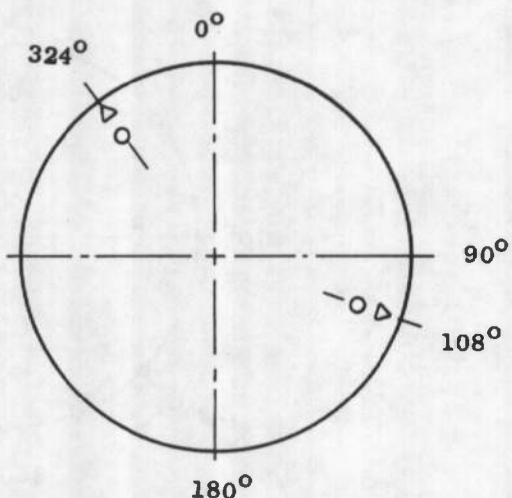
- Dynamic Static Pressure
- Total Pressure
- △ Total Temperature



Station 23, Compressor Discharge



Station 54, Turbine Inlet

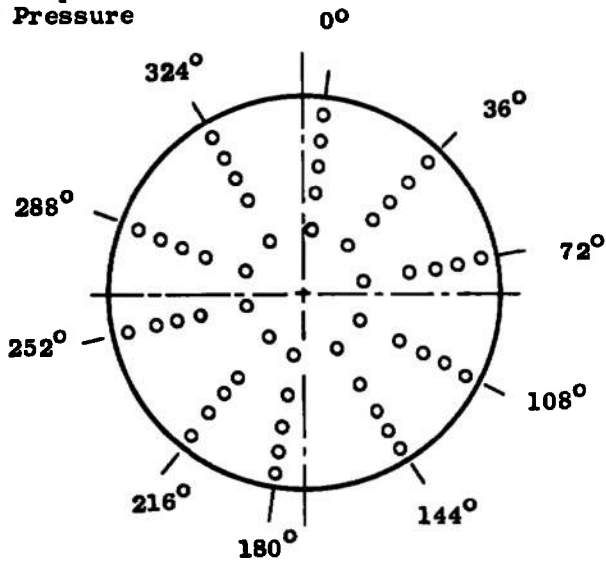


Station 55, Turbine Exit

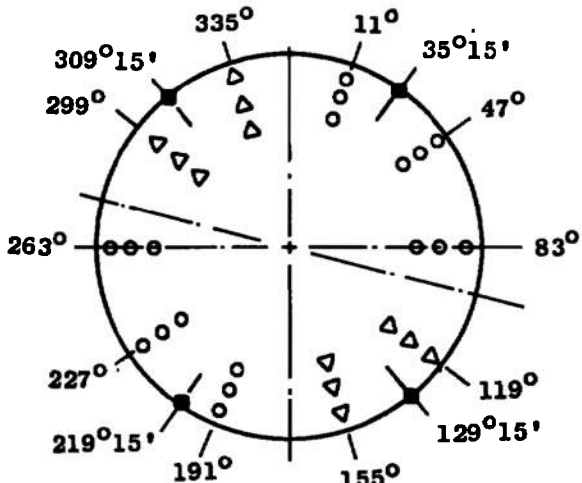
c. Instrumentation Details, Stations 23, 54, and 55
Fig. 9 Continued

Sym

- Dynamic Static Pressure
- △ Total Temperature
- Total Pressure



Station 2, Compressor Inlet



Station 23, Compressor Discharge

d. Effective Instrumentation Location for Stations 2
and 23 obtained by One/Rev Screen Rotated 180 deg
Fig. 9 Concluded

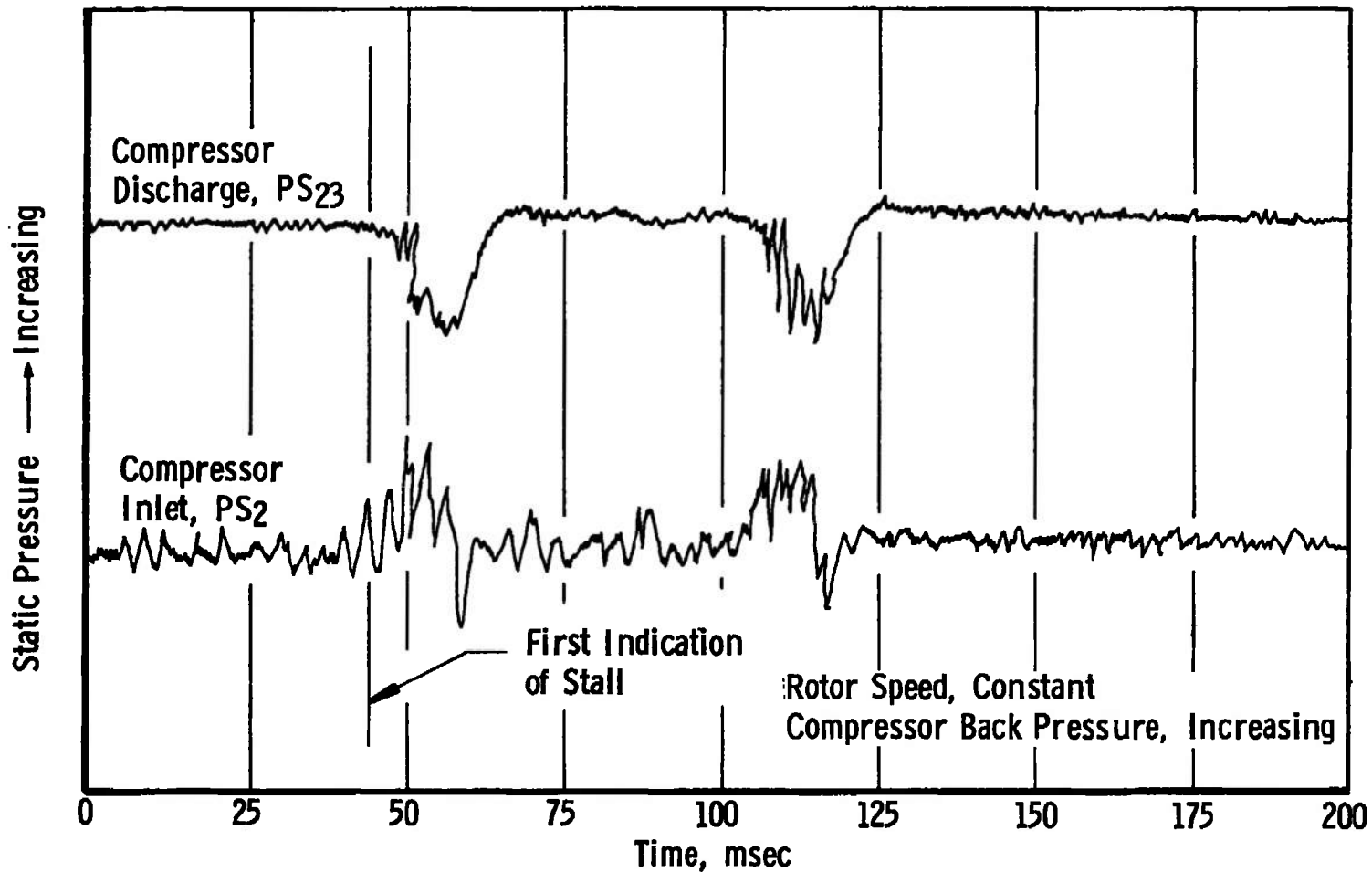
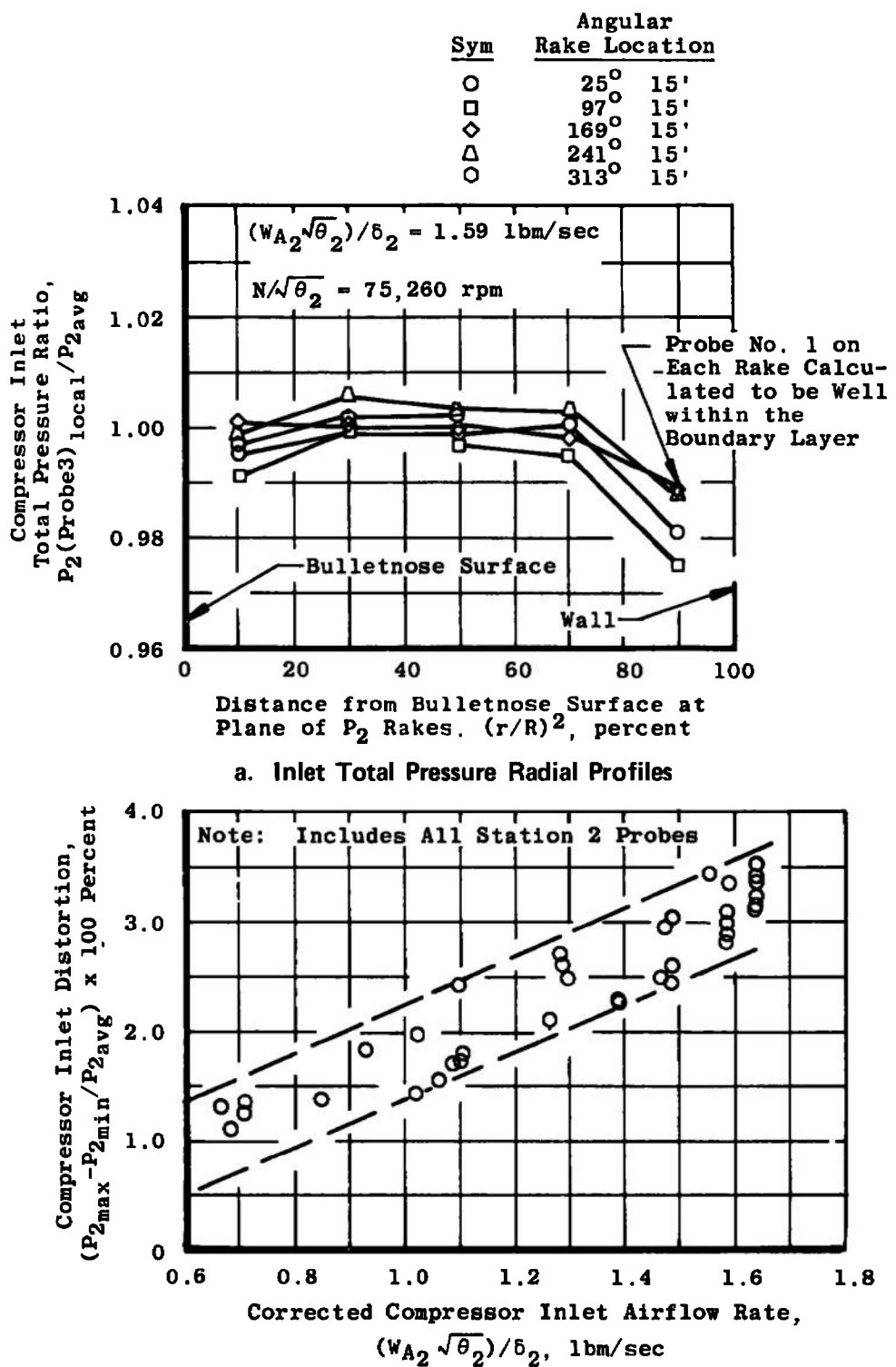
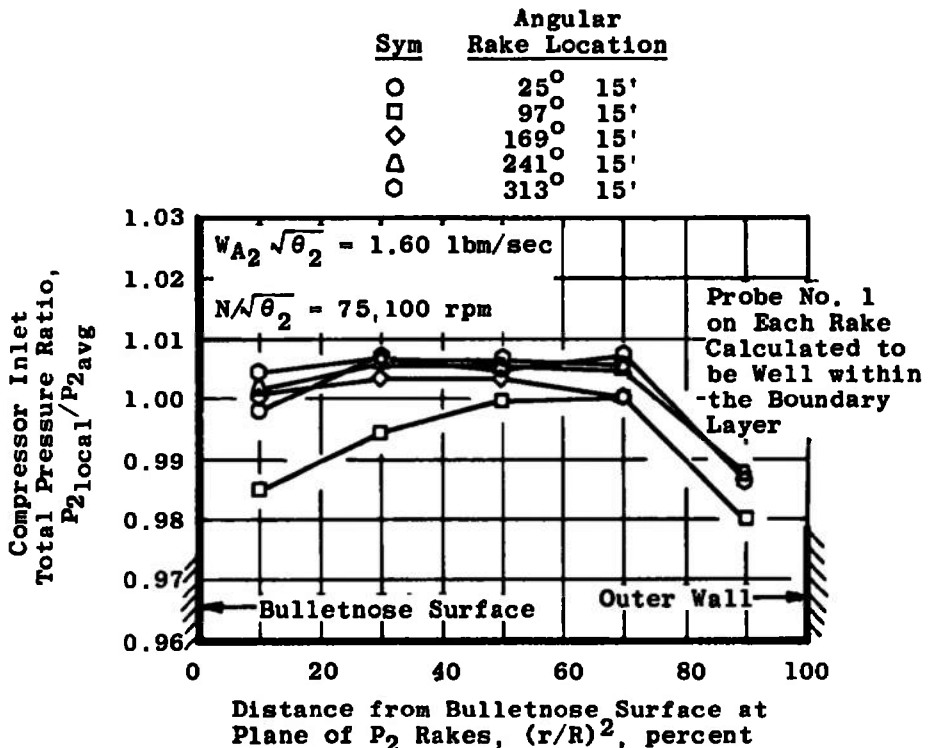


Fig. 10 Typical Transient Pressures during Incipient Compressor Surge

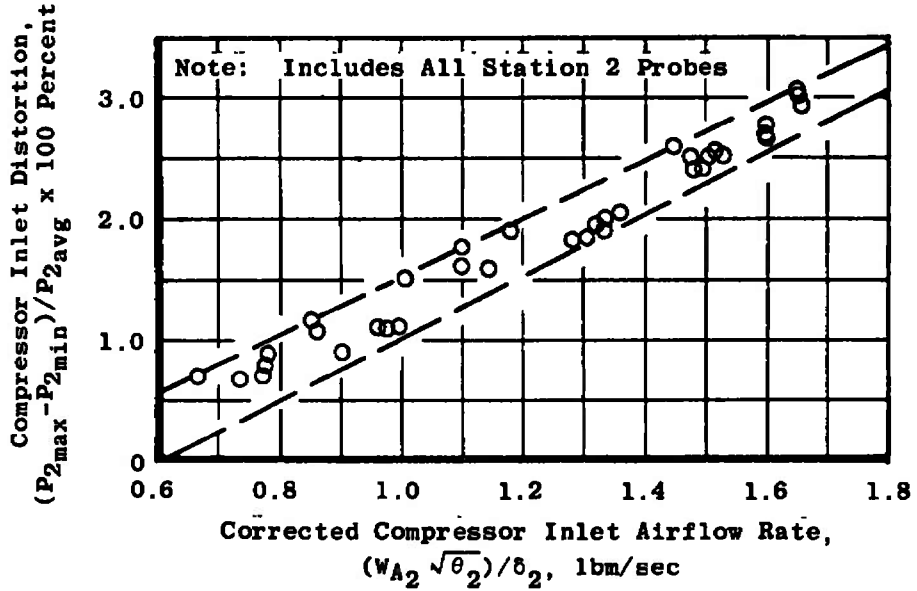


b. Compressor Inlet Distortion as a Function of Corrected Compressor Airflow

Fig. 11 Typical Compressor Uniform Inlet Total Pressure Profile and Distortion at $Re_1 = 0.39$ ($P_1 = 6 \text{ psia}$, $T_2 = 80^\circ \text{F}$)

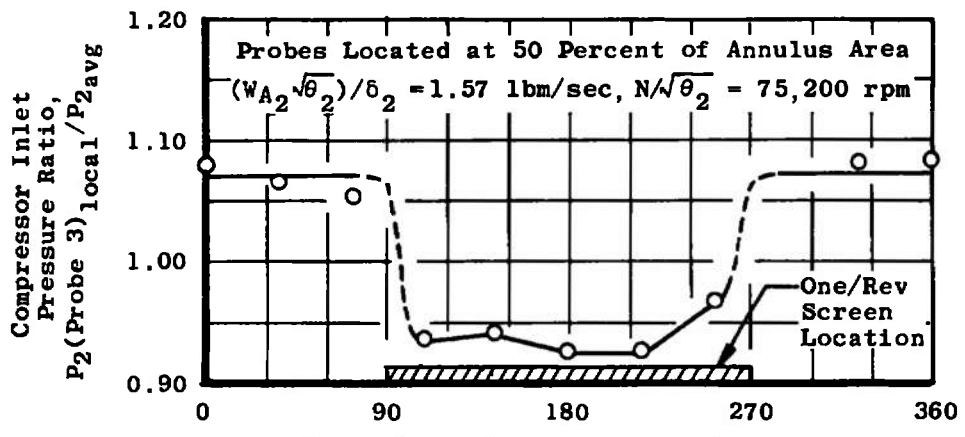


a. Inlet Total Pressure Radial Profiles

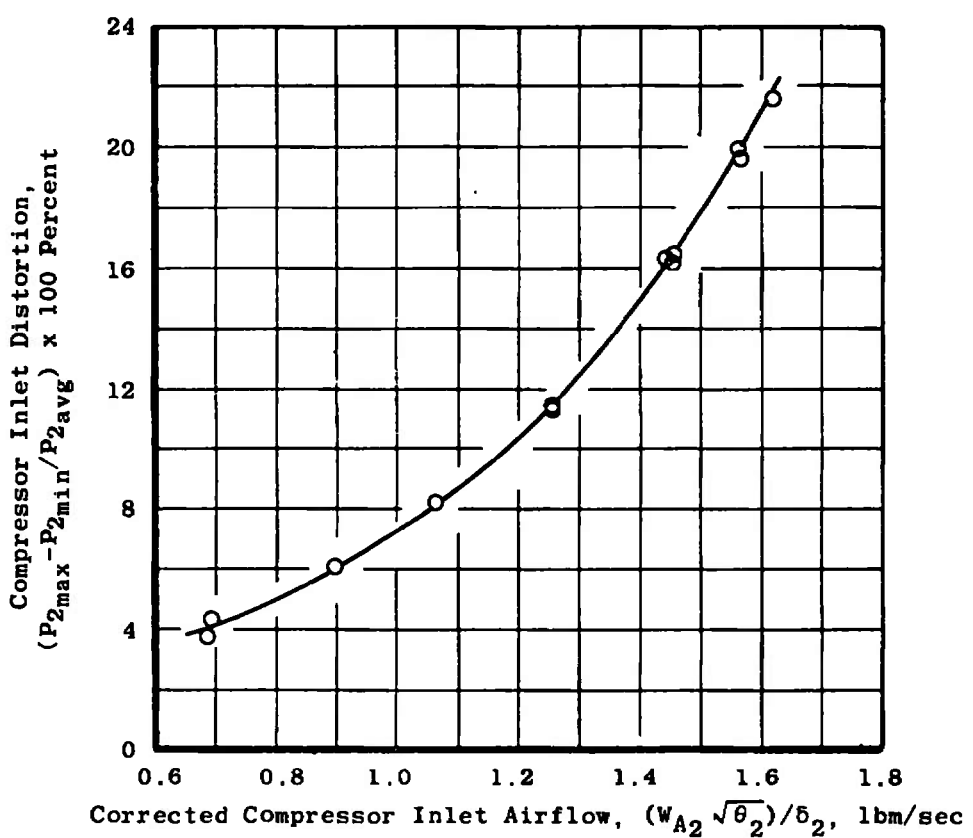


b. Compressor Inlet Distortion as a Function of Corrected Airflow

Fig. 12 Typical Compressor Uniform Inlet Total Pressure Profiles and Distortion at $Re_1 = 0.78$ ($P_2 = 12$ psia, $T_2 = 80^\circ\text{F}$)

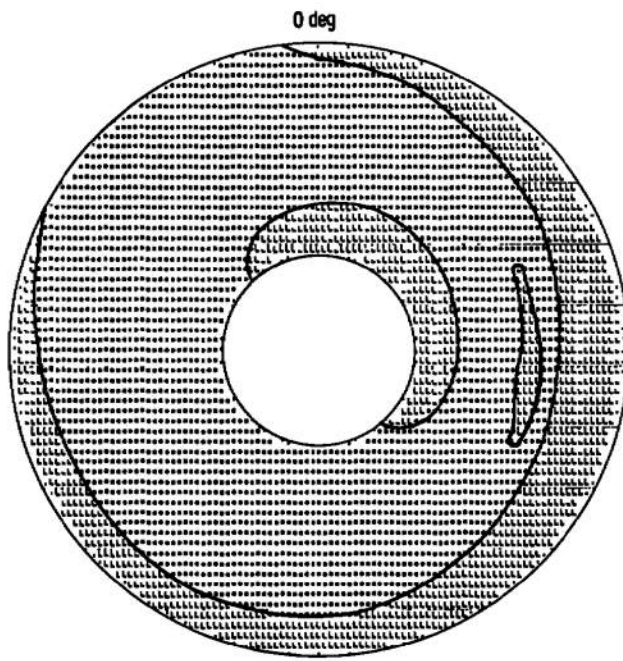


a. Inlet Circumferential Total Pressure Profiles



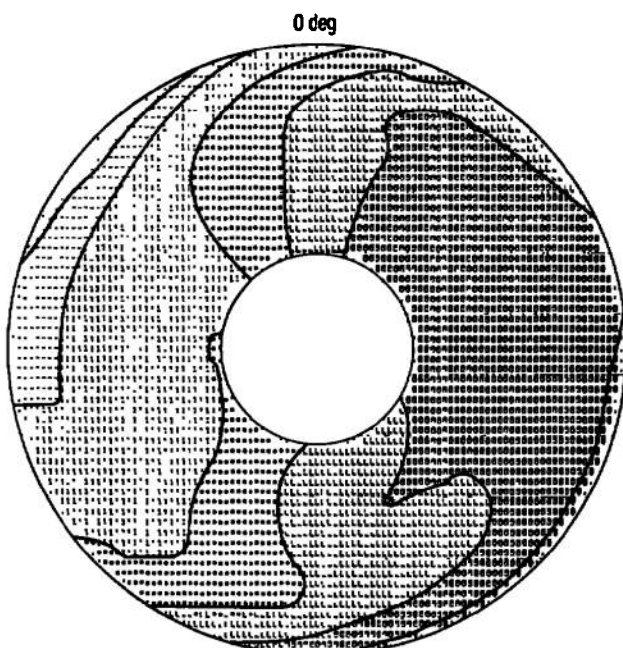
b. Compressor Inlet Distortion as a Function of Corrected Airflow

Fig. 13 Typical Compressor Inlet Circumferential Total Pressure Profiles and Distortion for the One/Rev Screen ($P_2 = 6 \text{ psia}$, $T_2 = 80^\circ\text{F}$)

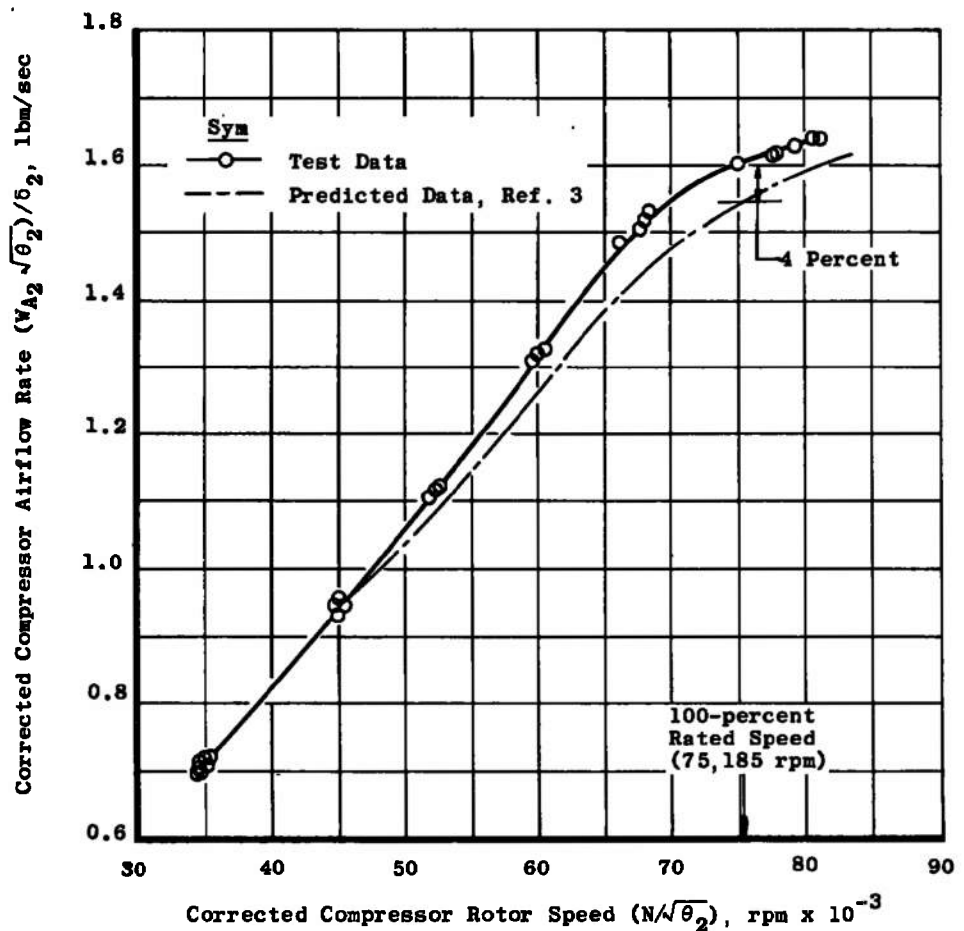

 $N/\sqrt{\theta_2} = 75,328 \text{ rpm}$
 $(WA_2\sqrt{\theta_2})/\delta_2 = 1.598 \text{ lbm/sec}$

$P_{\text{local}}/P_{\text{avg}}$

- 1.15 to 1.20
- 1.10 to 1.15
- 1.05 to 1.10
- 1.00 to 1.05
- 0.95 to 1.00
- 0.90 to 0.95
- 0.85 to 0.90


 $N/\sqrt{\theta_2} = 75,245 \text{ rpm}$
 $(WA_2\sqrt{\theta_2})/\delta_2 = 1.563 \text{ lbm/sec}$

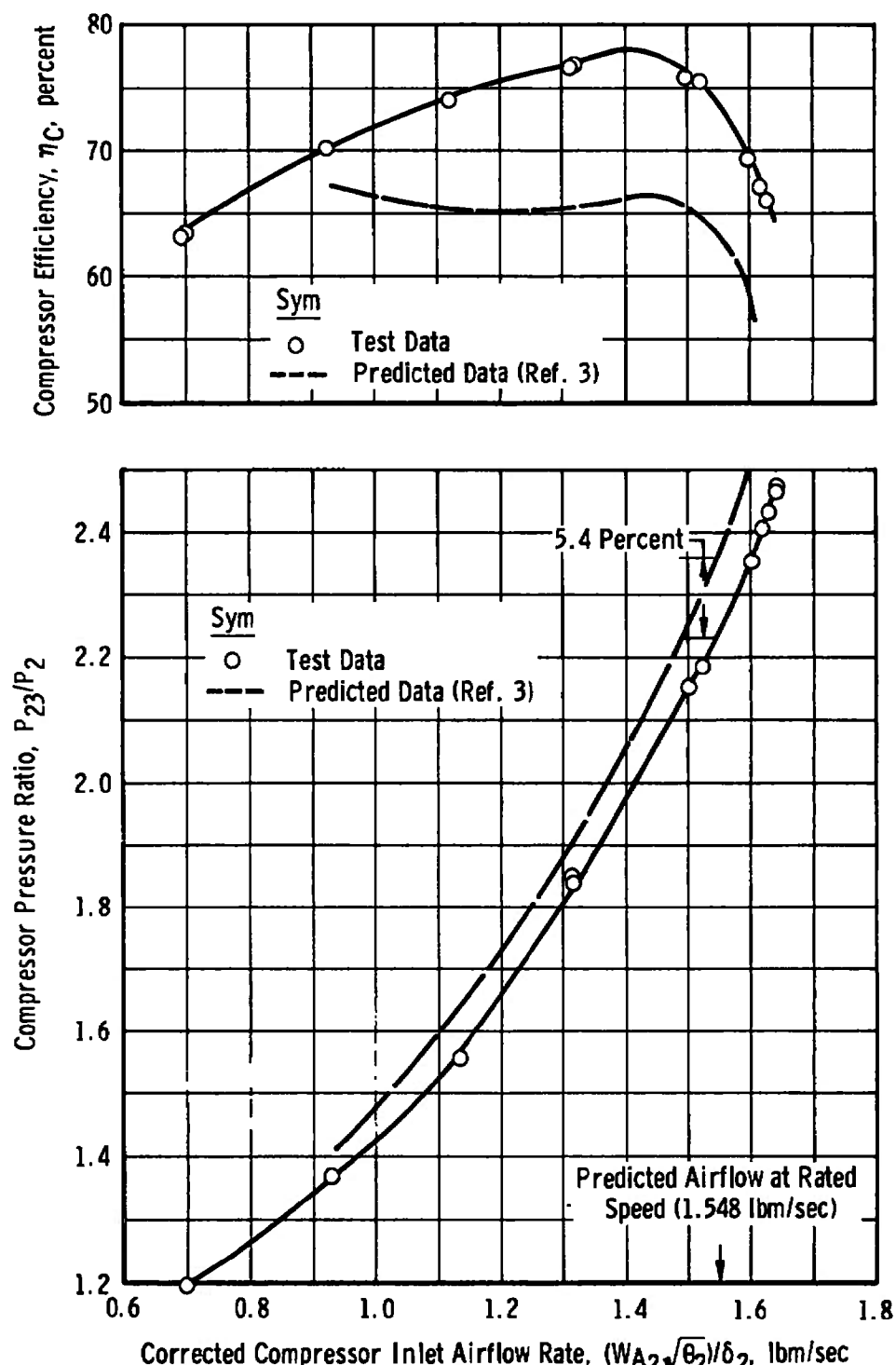
c. Typical Inlet Face Pressure Profiles
Fig. 13 Concluded



a. Variation of Corrected Compressor Inlet Airflow with Corrected Rotot Speed

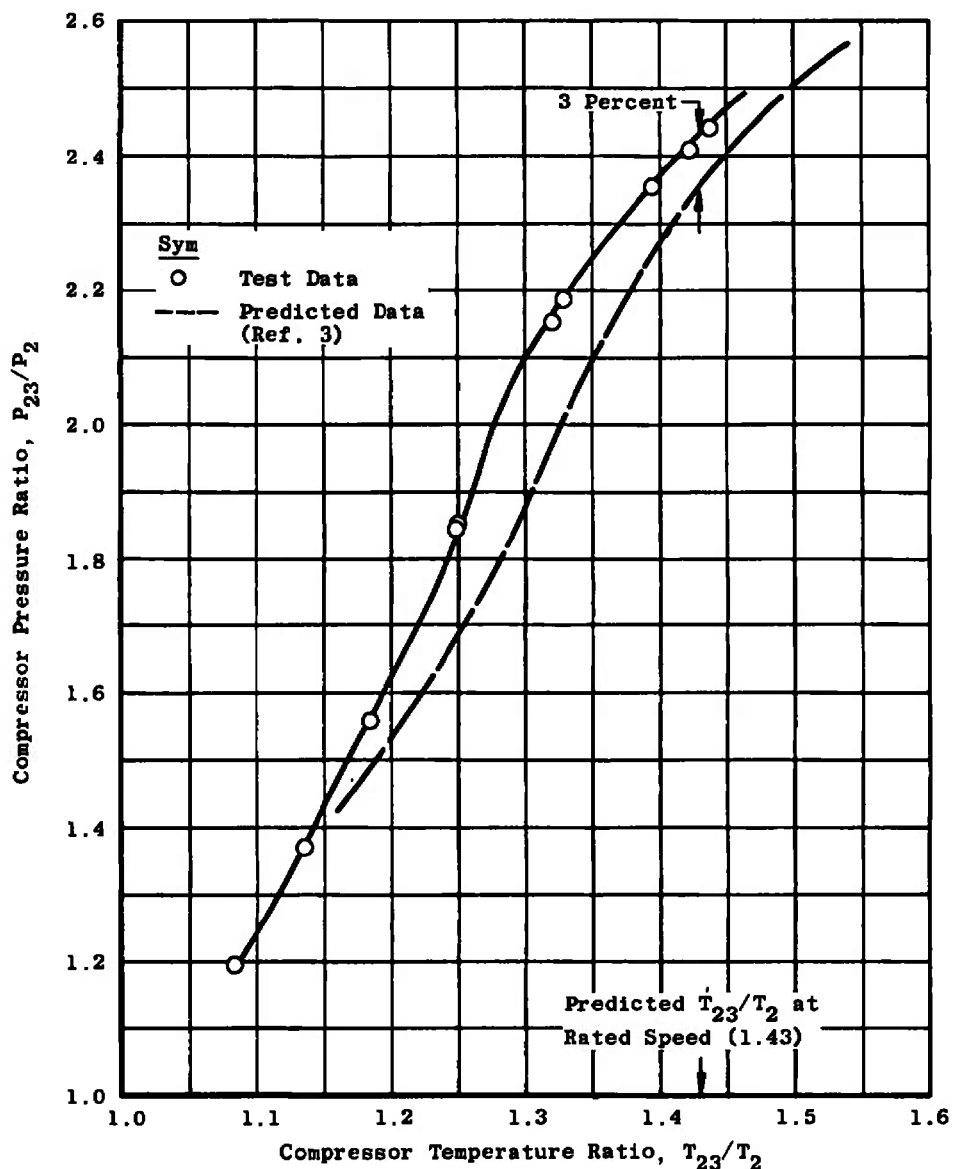
Fig. 14 Compressor Performance at Sea-Level-Static Condition

($A_g = 2.612 \text{ in.}^2$, Uniform Inlet)

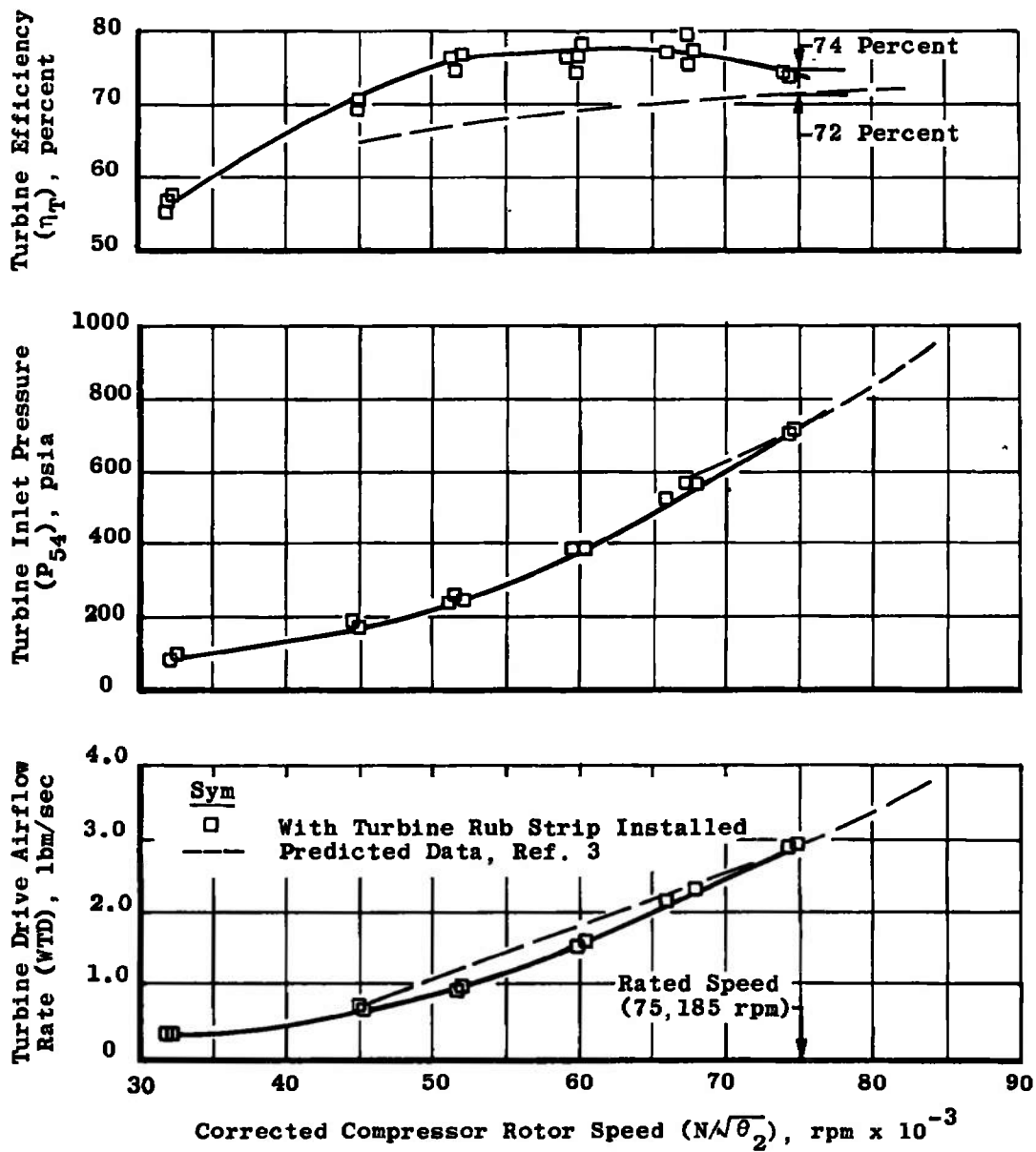


b. Compressor Operating Line and Variation of Compressor Efficiency with Corrected Compressor Inlet Airflow

Fig. 14 Continued

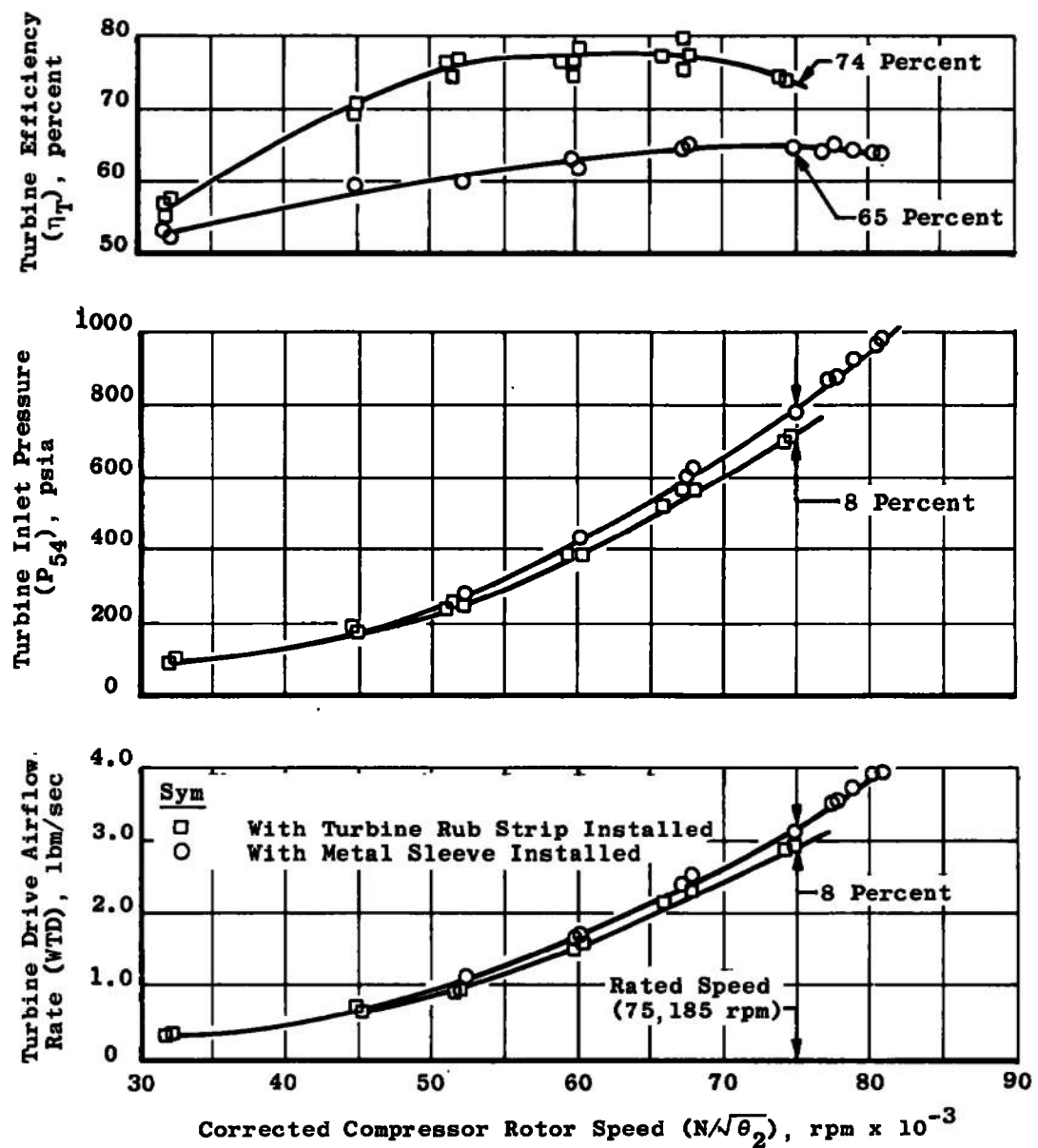


c. Variation of Compressor Pressure Ratio with Compressor Temperature Ratio
 Fig. 14 Concluded



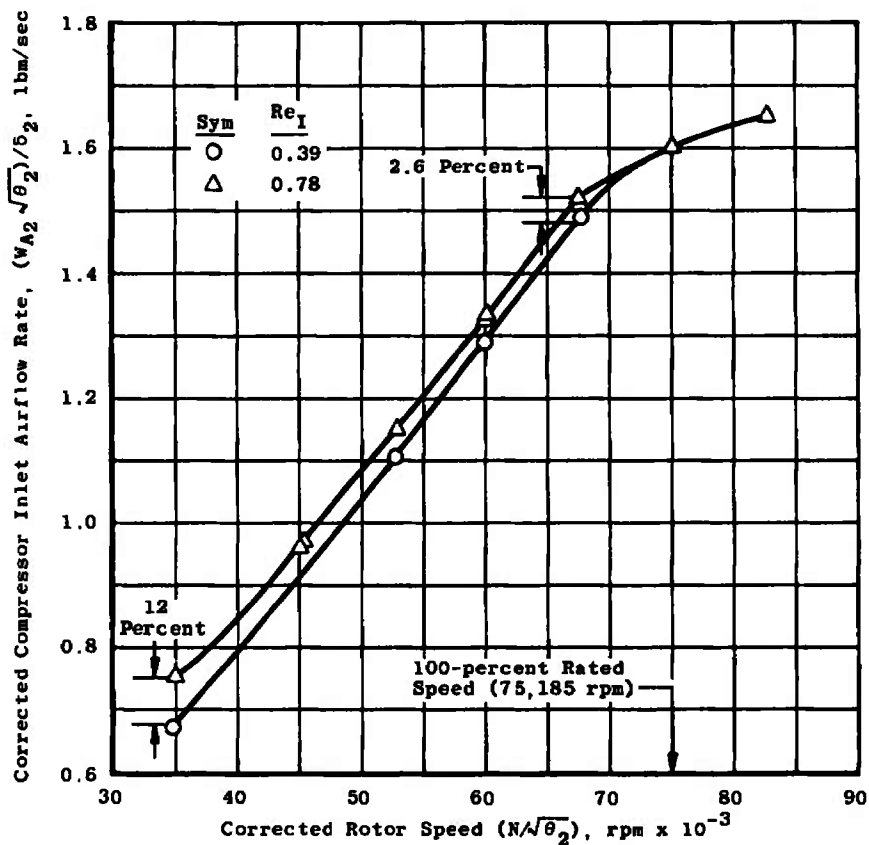
- Comparison of Turbine Performance and Operating Parameters (With Rub Strip Installed) with Predicted Data

Fig. 15 Turbine Performance and Operating Parameters at Sea-Level-Static Conditions ($A_g = 2.612 \text{ in.}^2$, Uniform Inlet)



- b. Comparison of Turbine Performance with Operating Parameters (with Metal Sleeve Installed) with Data Obtained with Rub Strip Installed

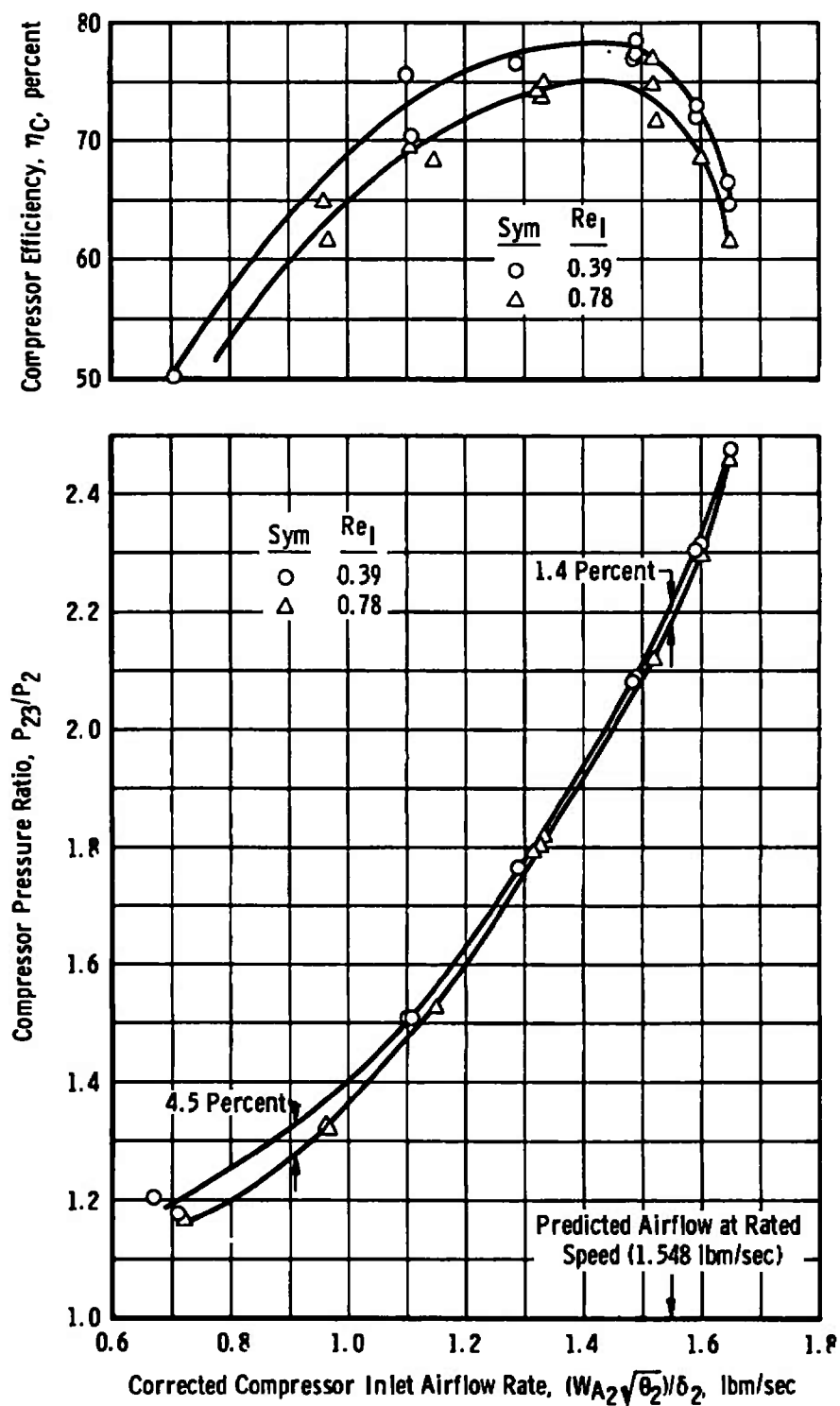
Fig. 15 Concluded



a. Variation of Corrected Compressor Inlet Airflow with Corrected Rotor Speed

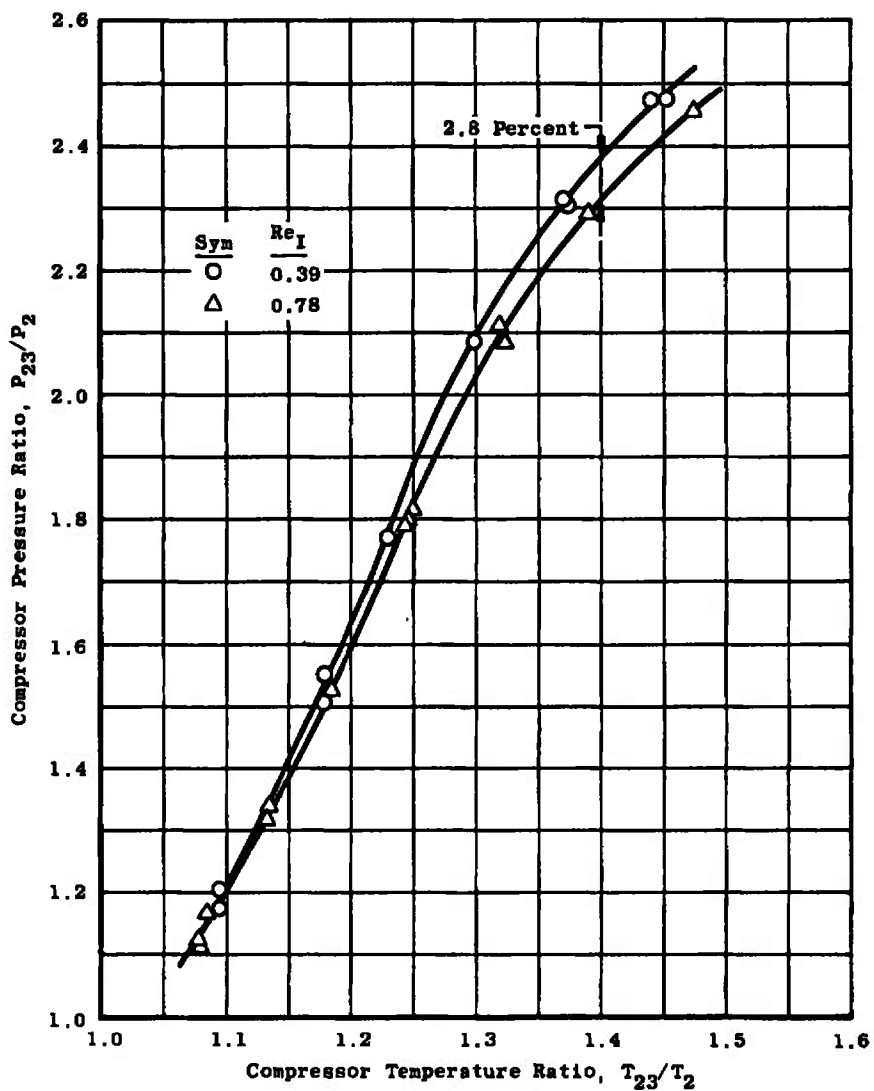
Fig. 16 Effect of Reynolds Number Index on Compressor Performance

$(A_g = 2.80 \text{ in.}^2$, Uniform Inlet)



- b. Compressor Operating Line and Variation of Compressor Efficiency with Corrected Compressor Inlet Airflow

Fig. 16 Continued



c. Variation of Compressor Pressure Ratio with Compressor Temperature Ratio
Fig. 16 Concluded

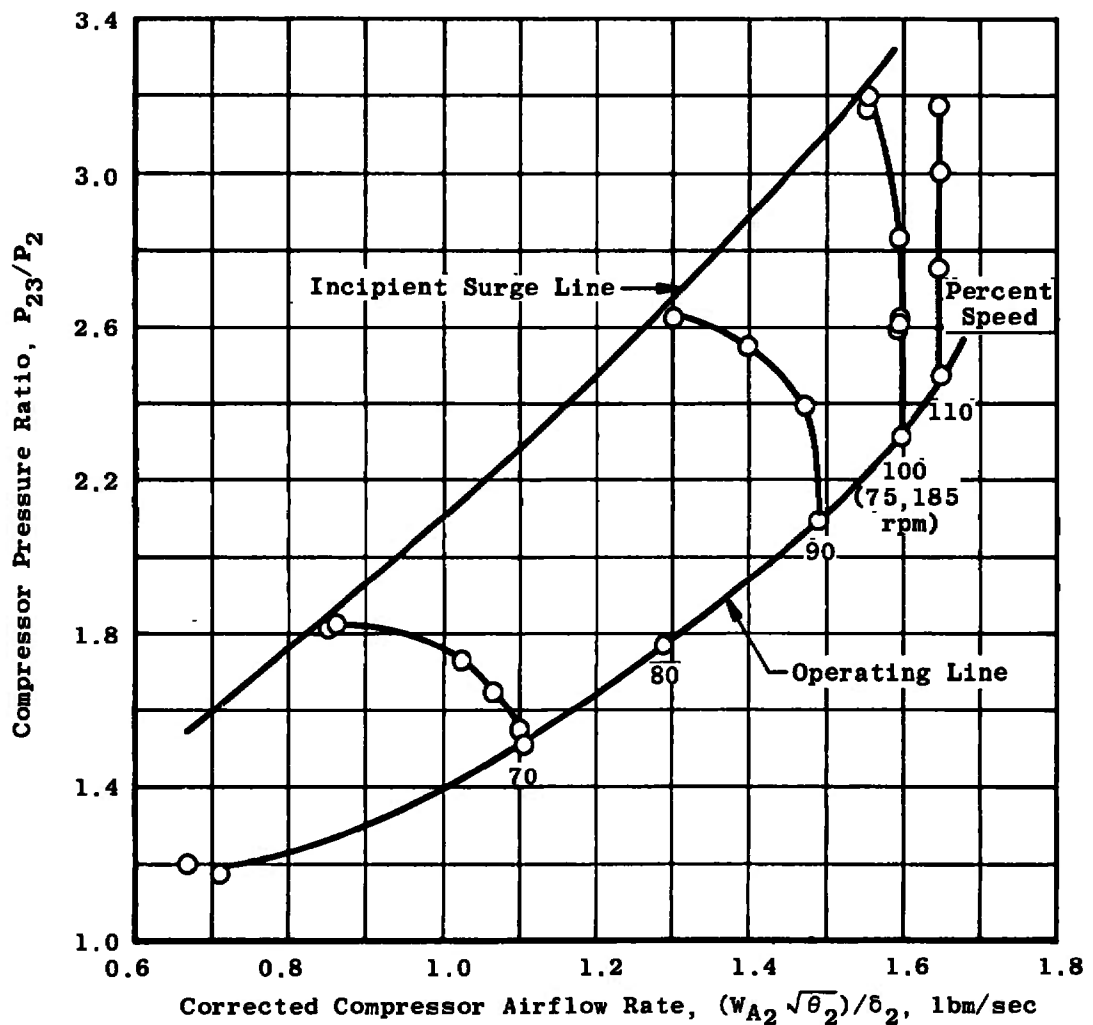


Fig. 17 Compressor Stability Map with Uniform Inlet
 $(Re_1 = 0.39, P_2 = 6 \text{ psia}, T_2 = 80^\circ\text{F}, A_8 = 2.80 \text{ in.}^2)$

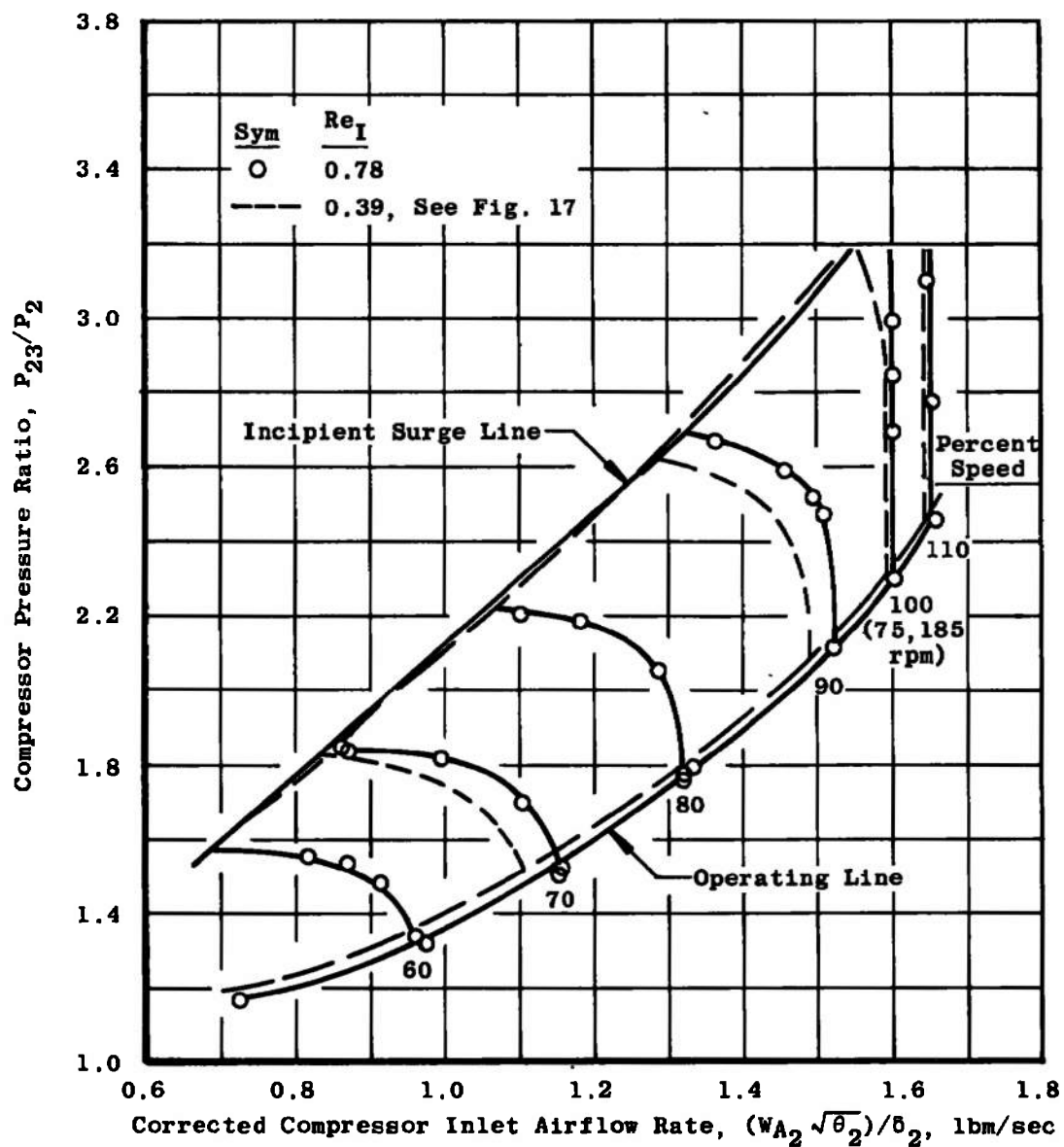
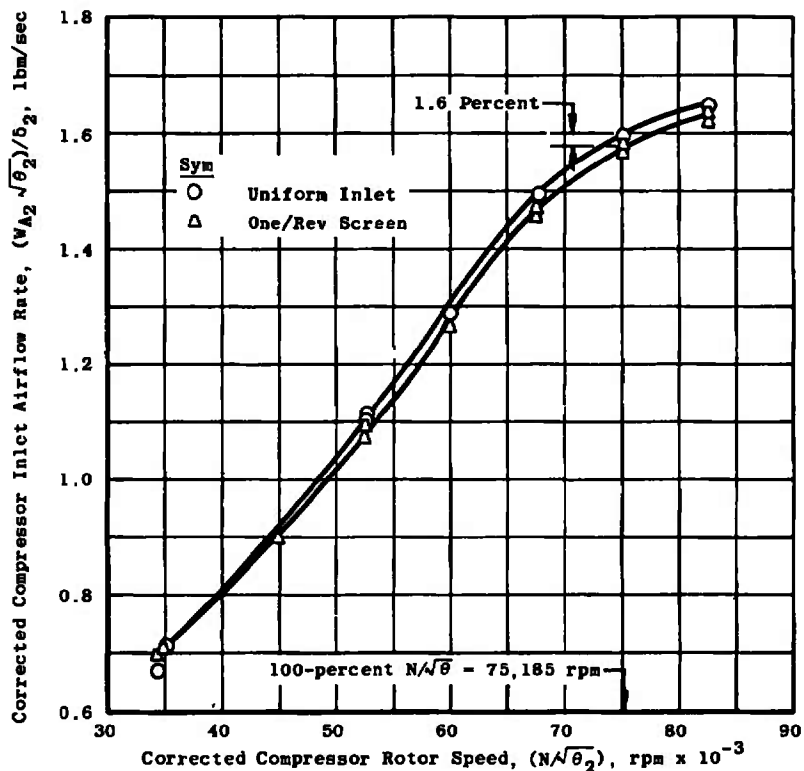


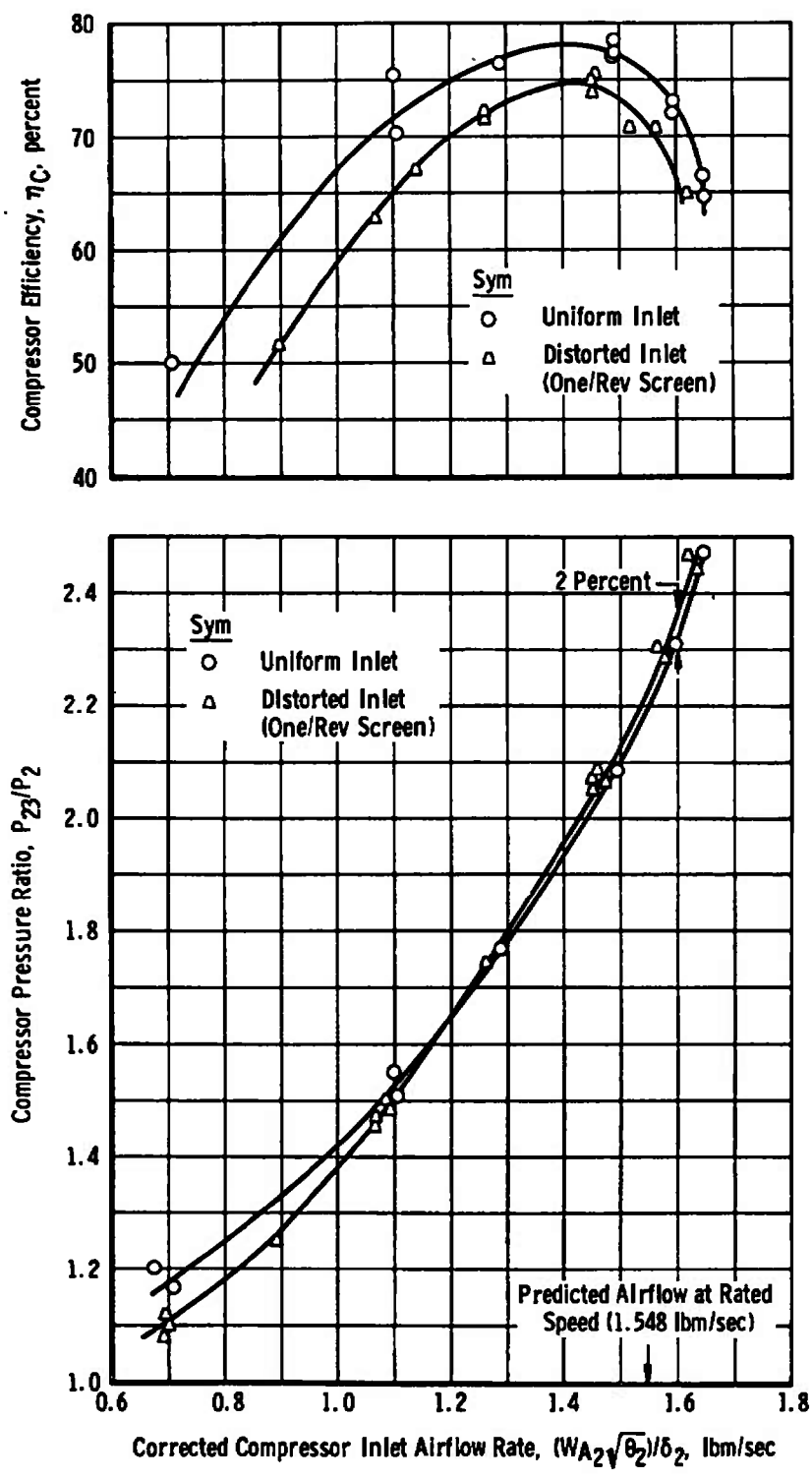
Fig. 18 Effect of Reynolds Number Index on Compressor Operating Map,
($A_B = 2.80$ in.², Uniform Inlet)



a. Variation of Corrected Compressor Inlet Airflow with Corrected Rotor Speed

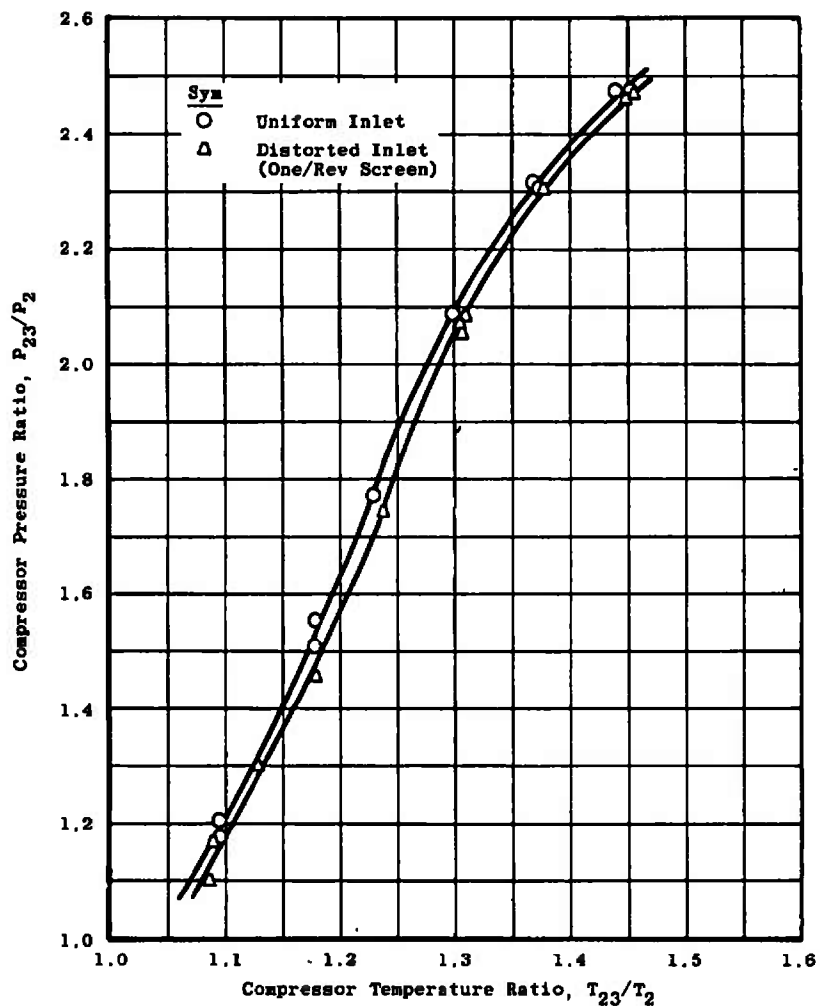
Fig. 19 Effect of Circumferential Inlet Distortion on Compressor Performance

($A_8 = 2.80$ in.², $Re_l = 0.39$, $P_2 = 6$ psia, $T_2 = 80^\circ F$)



b. Compressor Operating Line and Variation of Compressor Efficiency with Corrected Compressor Inlet Airflow

Fig. 19 Continued



c. Variation of Compressor Pressure Ratio with
Compressor Temperature Ratio
Fig. 19 Concluded

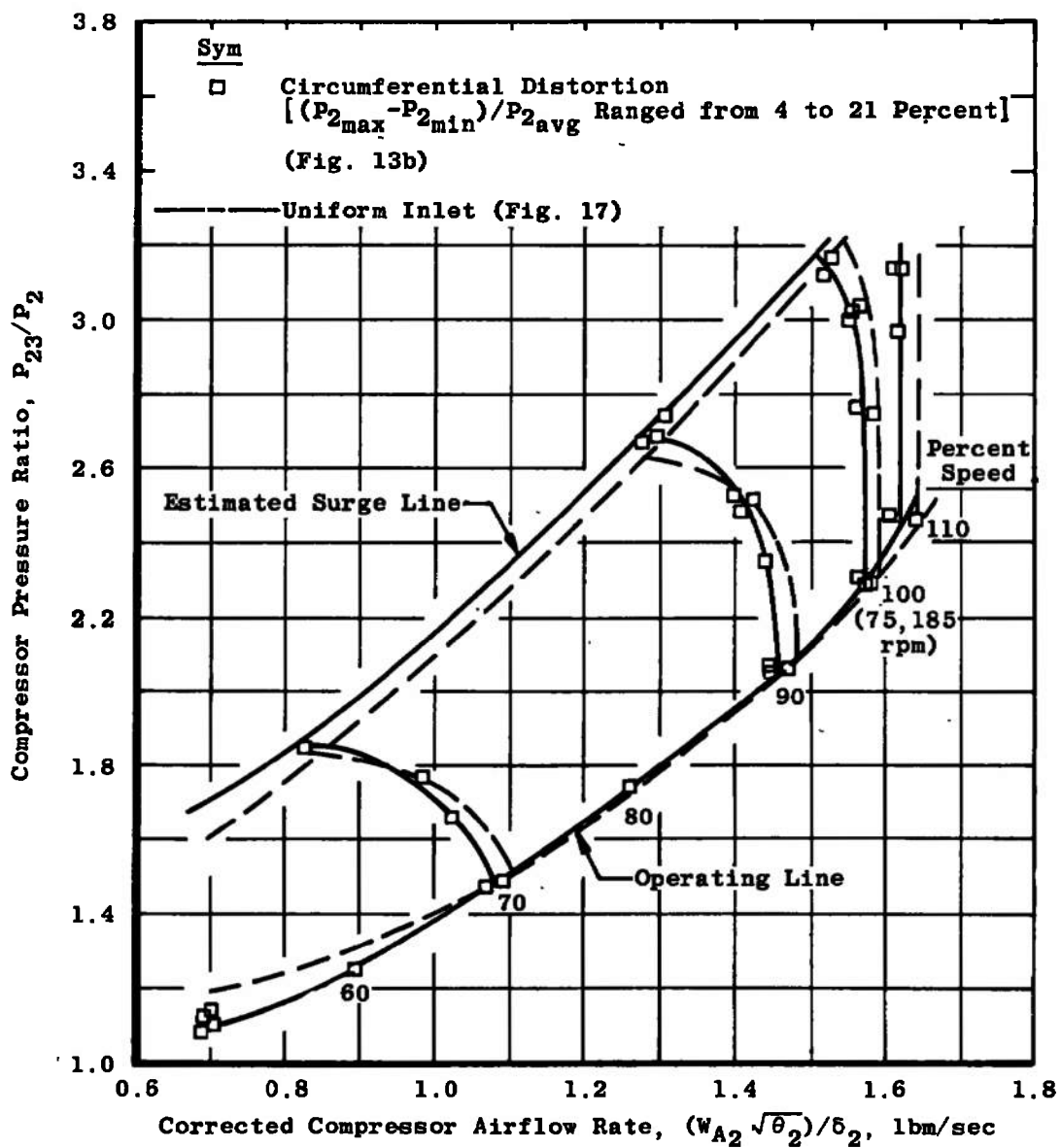
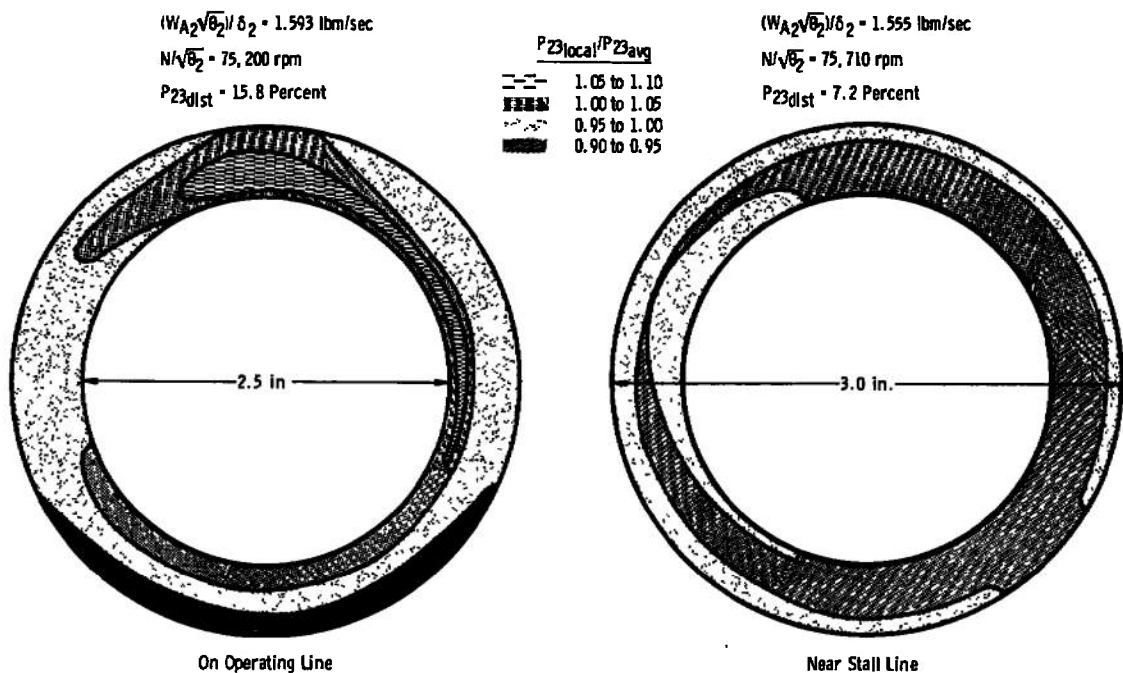
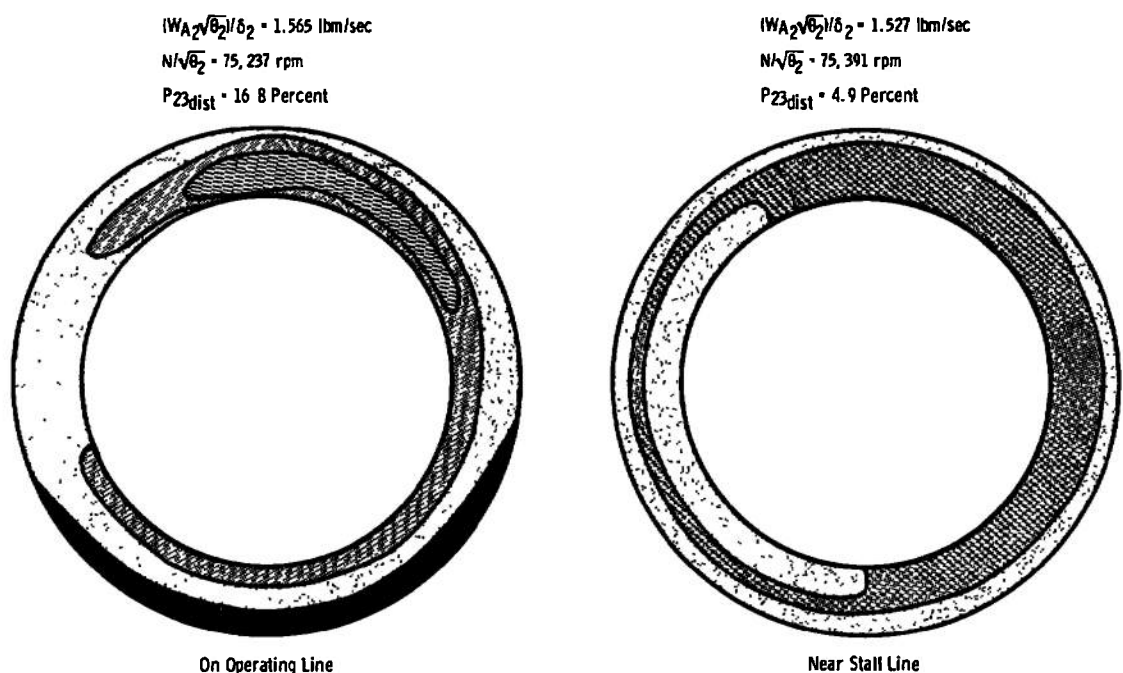


Fig. 20 Effect of Circumferential Inlet Distortion on Compressor Operating Map
 $(A_8 = 2.80 \text{ in.}^2, Re_l = 0.39, P_2 = 6 \text{ psia, } T_2 = 80^\circ\text{F})$



a. Uniform Inlet ($P_{2\text{dist}} \approx 3 \text{ Percent}$)



b. Distorted Inlet (One/Rev Screen) ($P_{2\text{dist}} \approx 19 \text{ Percent}$)

Fig. 21 Typical Compressor Discharge Pressure Profiles ($Re_l = 0.39$, $A_8 = 2.80 \text{ in.}^2$, $P_2 = 6 \text{ psia}$, $T_2 = 80^\circ \text{F}$)

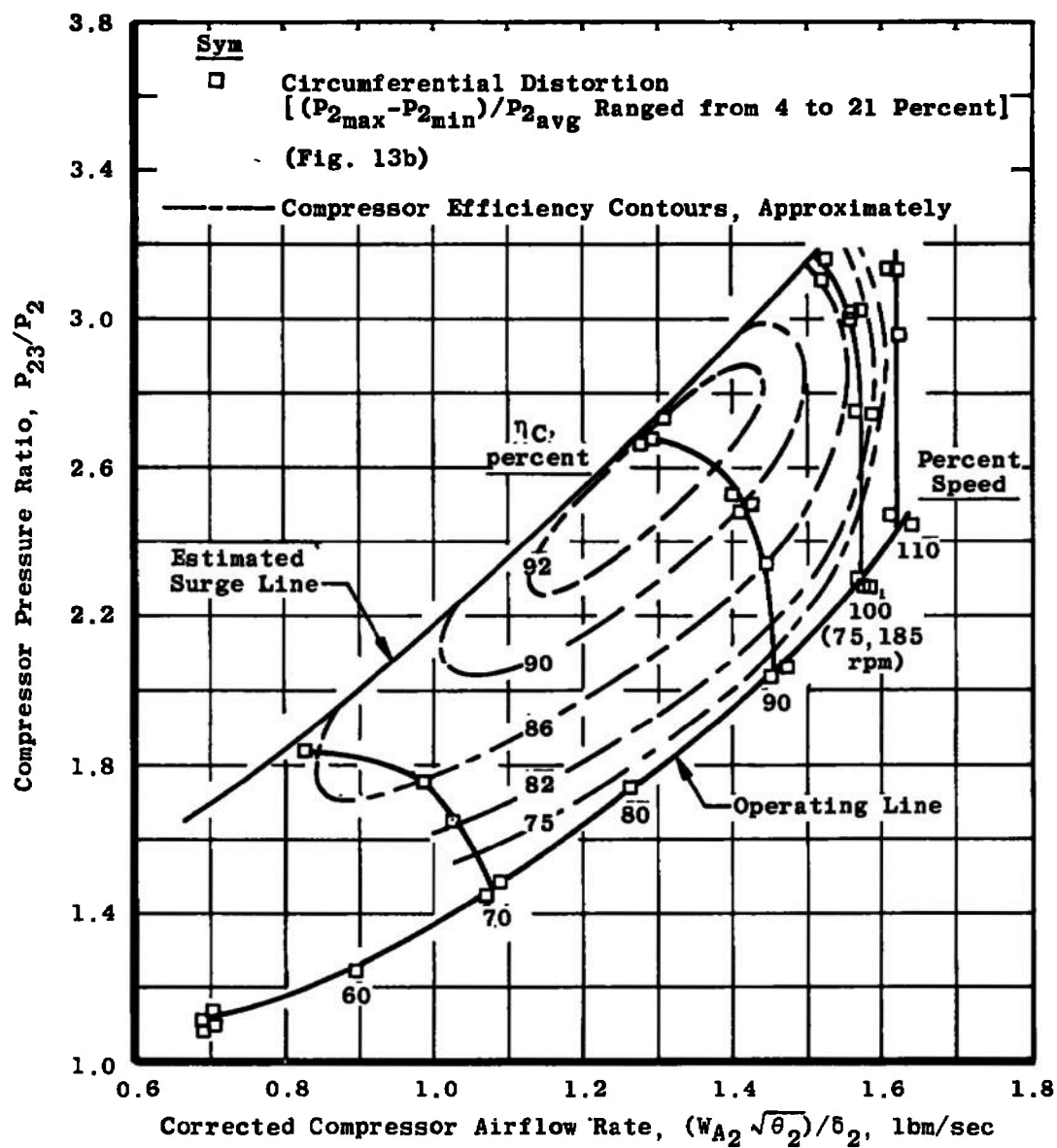


Fig. 22 Compressor Stability Map with Circumferential Inlet Distortion,
 $(A_g = 2.80 \text{ in.}^2, Re_l = 0.39, P_2 = 6 \text{ psia}, T_2 = 80^\circ\text{F})$

TABLE I
STEADY-STATE MEASUREMENT UNCERTAINTY

Parameter Designation	SI STADY-STATE ESTIMATED MEASUREMENT ^a								Type of Measuring Device	Type of Recording Device	Method of System Calibration			
	Precision Index (s)			B is (10)		Uncertainty $t(B + t_{0.5}S)$								
	Percent of Reading	Unit of Measurement	Degrees of Freedom	Percent of Reading	Unit of Measurement	Percent of Reading	Unit of Measurement							
Turbine Drive Venturi Inlet Total Pressure, PVI	---	±0.2 psia	31	---	±0.42 psia	---	±0.82 psia	60 to 200 psia	Bonded Strain-Gage-Type Pressure Transducers	Automatic Multiple Pressure Scanning System onto Sequential Sampling, Millivolt-to-Digital Converter, and Magnetic Tape Storage Data Acquisition System	Resistance Shunt Based on the Standards Laboratory Determination of Transducer Applied Pressure versus Resistance Shunt Equivalent Pressure Relationship			
	±0.1	---		±0.21	---	±0.41	---	200 to 1900 psia						
Turbine Drive Venturi Throat Static Pressure, PVT	---	±0.2 psia	31	---	±0.42 psia	---	±0.82 psia	80 to 200 psia						
	±0.1	---		±0.21	---	±0.41	---	200 to 1000 psia						
Turbine Drive Inlet Manifold Total Pressure, PDM	---	±0.2 psia	31	---	±0.42 psia	---	±0.82 psia	70 to 200 psia						
	±0.1	---		±0.21	---	±0.41	---	200 to 1300 psia						
Turbine Inlet Total Pressure, PS4	---	±0.1 psia	31	---	±0.21 psia	---	±0.41 psia	70 to 200 psia						
	±0.1	---		±0.21	---	±0.41	---	100 to 900 psia						
Turbine Discharge Total Pressure, PS5	±0.1	---	31	±0.21	---	±0.41	---	50 to 430 psia						
Turbine Discharge Plenum Static Pressure, PS56	±0.1	---	31	±0.21	---	±0.41	---	50 to 410 psia						
Turbine Stage Static Pressure, PSTS	±0.1	---	31	±0.21	---	±0.41	---	50 to 360 psia						
Turbine Discharge Frame Cavity Static Pressure, PSTC	±0.1	---	31	±0.21	---	±0.41	---	50 to 100 psia						
Compressor Discharge Total Pressure, (Station 23), P23	±0.1	---	31	±0.21	---	±0.41	---	5.8 to 37 psia						

*Reference: Abernathy, R. B. and Thompson, J. W. "Handbook, Uncertainty in Gas Turbine Measurements." AEDC-TR-73-5 (AD755356), February 1973.

TABLE I (Continued)

Parameter Designation	STANLEY-STATI ESTIMATED MEASUREMENT*								Type of Measuring Device	Type of Recording Device	Method of System Calibration			
	Precision Index (S)			Bias (B)		Uncertainty $\pm(B + k_{0.05}S)$								
	Percent of Reading	Unit of Measurement	Degree of Precision	Percent of Reading	Unit of Measurement	Percent of Reading	Unit of Measurement							
Compressor Flow Venturi Inlet Static Pressure, PS ₀₀	±0.1	---	31	±0.21	---	±0.41	---	5.8 to 14.2 psia	Bonded Strain-Gage-Type Pressure Transducers	Sequential Sampling, Millivolt-to-Digital Converter, and Magnetic Tape Storage Data Acquisition System	Resistance Shunt Based on the Standards Laboratory Determination of Transducer Applied Pressure versus Resistance Shunt Equivalent Pressure Relationship			
Compressor Flow Venturi Throat Static Pressure, PS _{1N}	±0.1	---	31	±0.21	---	±0.41	---	3.1 to 14.2 psia						
Compressor Inlet Plenum Static Pressure, PS _{1P}	±0.1	---	31	±0.21	---	±0.41	---	5.9 to 14.2 psia						
Compressor Flow Bell-mouth Throat Total Pressure (Station 1), P ₁	±0.1	---	31	±0.21	---	±0.41	---	5.8 to 14.2 psia						
Compressor Inlet Total Pressure (Station 2), P ₂	±0.1	---	31	±0.21	---	±0.41	---	5.8 to 14.2 psia						
Compressor Flow Bell-mouth Throat Static Pressure, PS ₁	±0.1	---	31	±0.21	---	±0.41	---	5.0 to 14.2 psia						
Compressor Discharge Static Pressure (Station 23), PS ₂₃	±0.1	---	31	±0.21	---	±0.41	---	5.8 to 32 psia						
Turbine Drive Bleed Manifold Total Pressure, PBM	---	±0.05 psi	31	---	±0.10 psi	---	±0.2 psi	20 to 50 psia						
	±0.1	---		±0.21	---	±0.41	---	50 to 340 psia						
Turbine Drive Bleed Orifice Inlet Total Pressure, POU	---	±0.03 psi	31	---	±0.063 psi	---	±0.123 psi	14 to 30 psia						
	±0.1	---		±0.21	---	±0.41	---	30 to 260 psia						

TABLE I (Continued)

Parameter Designation	STADY-STATE ESTIMATED MEASUREMENT*								Type of Measuring Device	Type of Recording Device	Method of System Calibration
	Precision Index (S)		Bias (B)		Uncertainty $\pm(B + t_{0.5} S)$		Range				
Parameter Designation	Percent of Reading	Unit of Measurement	Degree of Freedom	Percent of Reading	Unit of Measurement	Percent of Reading	Percent of Reading	Unit of Measurement	Type of Measuring Device	Type of Recording Device	Method of System Calibration
Turbine Drive Bleed Orifice Exit Total Pressure, POD	---	$\pm 0.02 \text{ psi}$	31	---	$\pm 0.042 \text{ psi}$	---	$\pm 0.082 \text{ psi}$	14 to 20 psia	Bonded Strain-Gage-Type Pressure Transducers	Sequential Sampling, Millivolt-to-Digital Converter, and Magnetic Tape Storage Data Acquisition System	Resistance Shunt Based on the Standards Laboratory Determination of Transducer Applied Pressure versus Resistance Shunt Equivalent Pressure Relationship
	± 0.1	---		± 0.21	---	± 0.41	---	20 to 200 psia			
Compressor Mapping Orifice Inlet Total Pressure, PMOO	---	$\pm 0.02 \text{ psi}$	31	---	$\pm 0.042 \text{ psi}$	---	$\pm 0.082 \text{ psi}$	5.8 to 20 psia	Bonded Strain-Gage-Type Pressure Transducers	Sequential Sampling, Millivolt-to-Digital Converter, and Magnetic Tape Storage Data Acquisition System	Resistance Shunt Based on the Standards Laboratory Determination of Transducer Applied Pressure versus Resistance Shunt Equivalent Pressure Relationship
	± 0.1	---		± 0.21	---	± 0.41	---	20 to 115 psia			
Compressor Mapping Orifice Exit Total Pressure, PMDO	---	$\pm 0.01 \text{ psi}$	31	---	$\pm 0.021 \text{ psi}$	---	$\pm 0.041 \text{ psi}$	5.8 to 10 psia	Chromel-Alumel Temperature Transducers	Millivolt Substitution Based on the NBS Temperature versus Millivolt Tables	Millivolt Substitution Based on the NBS Temperature versus Millivolt Tables
	± 0.1	---		± 0.21	---	± 0.41	---	10 to 115 psia			
Turbine Inlet Total Temperature, T ₅₄	---	$\pm 0.25^\circ\text{F}$	31	---	$\pm 2.2^\circ\text{F}$	---	$\pm 2.7^\circ\text{F}$	70 to 250°F	Chromel-Alumel Temperature Transducers	Millivolt Substitution Based on the NBS Temperature versus Millivolt Tables	Millivolt Substitution Based on the NBS Temperature versus Millivolt Tables
Turbine Discharge Total Temperature, T ₅₅	---	$\pm 0.25^\circ\text{F}$	31	---	$\pm 2.2^\circ\text{F}$	---	$\pm 2.7^\circ\text{F}$	70 to 150°F			
Compressor Flow Bell-mnuth Throat Total Temperature (Station 1), T ₁	---	$\pm 0.25^\circ\text{F}$	31	---	$\pm 2.2^\circ\text{F}$	---	$\pm 2.7^\circ\text{F}$	70 to 65°F	Iron-Constantan Temperature Transducers	Millivolt Substitution Based on the NBS Temperature versus Millivolt Tables	Millivolt Substitution Based on the NBS Temperature versus Millivolt Tables
Compressor Discharge Total Temperature (Station 23), T ₂₃	---	$\pm 0.25^\circ\text{F}$	31	---	$\pm 2.2^\circ\text{F}$	---	$\pm 2.7^\circ\text{F}$	70 to 360°F			
Forward Bearing Temperature, TB1M	---	$\pm 0.25^\circ\text{F}$	31	---	$\pm 2.2^\circ\text{F}$	---	$\pm 2.7^\circ\text{F}$	100 to 260°F	Iron-Constantan Temperature Transducers	Millivolt Substitution Based on the NBS Temperature versus Millivolt Tables	Millivolt Substitution Based on the NBS Temperature versus Millivolt Tables
Aft Bearing Temperature, TB2M	---	$\pm 0.25^\circ\text{F}$	31	---	$\pm 2.2^\circ\text{F}$	---	$\pm 2.7^\circ\text{F}$	180 to 215°F			
Turbine Drive Inlet Manifold Total Temperature, TDM	---	$\pm 0.25^\circ\text{F}$	31	---	$\pm 2.2^\circ\text{F}$	---	$\pm 2.7^\circ\text{F}$	70 to 250°F	Iron-Constantan Temperature Transducers	Millivolt Substitution Based on the NBS Temperature versus Millivolt Tables	Millivolt Substitution Based on the NBS Temperature versus Millivolt Tables

TABLE I (Concluded)

Parameter Designation	STATIONARY-STATE ESTIMATED MEASUREMENT*								Type of Measuring Device	Type of Recording Device	Method of System Calibration			
	Precision Index (S)			Bias (B)		Uncertainty $t(B + t_{95}S)$								
	Percent of Reading	Unit of Measurement	Degree of Freedom	Percent of Reading	Unit of Measurement	Percent of Reading	Unit of Measurement							
Turbine Drive Bleed Manifold Total Temperature, TBM	---	±0.25°F	31	---	±2.2°F	---	±2.7°F	70 to 150°F	Iron-Constantan Temperature Transducers	Sequential Sampling, Millivolt-to-Digital Converter, and Magnetic Tape Storage Data Acquisition System	Millivolt Substitution Based on the NBS Temperature versus Millivolt Tables			
Turbine Drive Venturi Exit Total Temperature, TDV	---	±0.25°F	31	---	±2.2°F	---	±2.7°F	70 to 250°F						
Turbine Drive Bleed Orifice Total Temperature, TBO	---	±0.25°F	31	---	±2.2°F	---	±2.7°F	70 to 130°F						
Compressor Mapping Orifice Total Temperature, TMDO	---	±0.25°F	31	---	±2.2°F	---	±2.7°F	-22 to 90°F						
Turbine Drive Air Supply Total Temperature, TDS	---	±0.25°F	31	---	±1.8°F	---	±2.3°F	70 to 250°F	Copper-Constantan Temperature Transducers	Frequency-to-Voltage Converter onto Sequential Sampling, Millivolt-to-Digital Converter, and Magnetic Tape Storage Data Acquisition System	Frequency Substitution Based on the Transducer and Transducer-to-Engine Rotor Coupling Characteristics			
Compressor Flow Venturi Inlet Total Temperature, T00	---	±0.25°F	31	---	±1.8°F	---	±2.3°F	70 to 90°F						
Rotor Speed, NC	±0.1	---	31	±0.1	---	±0.3	---	20,000 to 85,000 rpm	Electro-Mechanical Transducers					

APPENDIX III METHOD OF CALCULATION

The general method and equations used to compute the parameters presented in this report are given below. Where applicable, the arithmetic average of the pressures and temperatures were used.

Specific Heats

The specific heats of air at constant pressure were computed from the empirical equation:

$$C_p = (a_1 + b_1 T + c_1 T^2)$$

where a_1 , b_1 , and c_1 are constants based on the specific heats of the constituents of air. The equation was derived from the temperature range shown below:

Temperature Range, °R	<u>a_1</u>	<u>b_1</u>	<u>c_1</u>
400 to 1700	0.2318	0.104×10^{-4}	0.7166×10^{-8}

Enthalpy

The enthalpy of the air was obtained by integrating the empirical specific heat formula.

$$H = \int_{400^\circ R}^T C_p dT$$

Ratio of Specific Heats

The ratio of specific heats was calculated from the expression:

$$\gamma = \frac{C_p}{C_p - \frac{R}{778}}$$

where

$$R = 53.342$$

Calculation of Station 2 Total Pressure

The total pressure at Station 2 (compressor inlet) was calculated in the following manner:

A. Clean Inlet, P_2 rakes installed:

P_2 = arithmetic average of the 25 probes

B. Clean Inlet, P_2 rakes not installed:

$$P_2 = P_1 \left[1 - \left(\frac{P_1 - P_2}{P_1} \right) \right] \text{ clean inlet}$$

where the term $(P_1 - P_2)/P_1$ is a function of corrected compressor rotor speed and is the pressure loss from Station 1 (Bellmouth inlet) to Station 2 determined during tests with P_2 rakes installed (Fig. III-1).

C. Distorted Inlet, P_2 rakes installed:

$$P_2 = (P_{2 \text{ clean}} + P_{2 \text{ screen}})/2$$

where,

$$P_{2 \text{ clean}} = \text{Arithmetic Average of the probes not behind the screen}$$

and

$$P_{2 \text{ screen}} = \text{Arithmetic average of the probes behind the screen}$$

By using this average, the percent pressure loss from Station 1 to Station 2 [$(P_{1 \text{ avg}} - P_2) \times 100\% / P_{1 \text{ avg}}$] was plotted versus N_{R2} for both screen positions. A curve fit was applied, and P_2 was then calculated based on Fig. III-2.

Total Temperature

Total temperature measurements at the bellmouth inlet and at stations inside the simulator were corrected for probe design in the following manner:

$$T = \frac{T_{\text{indicated}}}{\text{Correction Factor}}$$

The following correction factors were provided by the General Electric Co.:

<u>Station</u>		<u>Corrected Factor</u>
1	Bellmouth inlet	0.999
23	Compressor Discharge	1.0024 - (0.0167) M_{23}
54	Turbine Inlet	0.997
55	Turbine discharge	0.997

Mach Number

For Station 23 (Compressor Discharge) where both the static and total pressure were measured, the Mach number was obtained from the equation:

$$M = \left\{ \frac{2}{\gamma - 1} \left[\left(\frac{P_{23}}{PS_{23}} \right)^{\frac{\gamma-1}{\gamma}} - 1 \right] \right\}^{\frac{1}{\gamma}}$$

Simulator Airflows

Compressor inlet airflow was measured with a critical-flow venturi at a compressor inlet pressure of 6 psia ($Re_I = 0.39$) and with a Bellmouth at compressor inlet pressures of 12 psia ($Re_I = 0.78$) and 14.2 psia. Compressor inlet airflow was calculated as follows:

A. Critical-Flow Venturi

For critical flow,

$$W_{A_{1N}} = C_{F_{1N}} PS_{00} A_{1N} C_{t_{1N}} \left(\frac{2}{\gamma + 1} \right)^{\frac{\gamma+1}{2(\gamma-1)}} \sqrt{\frac{2\gamma g}{R T_{00}}}$$

For subcritical flow,

$$W_{A_{1N}} = C_{F_{1N}} \sqrt{\frac{2\gamma g}{R(\gamma-1)}} \frac{PS_{1N} A_{1N} C_{t_{1N}}}{\sqrt{1 - \left(\frac{PS_{1N}}{PS_{00}} \right)^{\frac{\gamma-1}{\gamma}}}} \sqrt{\frac{T_{00}}{T_1}} \left(\frac{PS_{1N}}{PS_{00}} \right)^{\frac{\gamma-1}{\gamma}}$$

where $C_{t_{1N}}$ is the area thermal expansion coefficient calculated from the venturi throat adiabatic wall temperature, $C_{F_{1N}}$ is an empirically determined flow coefficient based on venturi curvature, boundary layer development, and area ratios (Refs. 4 and 5), and $\gamma = \gamma_{oo}$.

B. Bellmouth

$$W_{BM} = C_{F_{BM}} PS_1 A_1 C_{t_1} \frac{\sqrt{\frac{2\gamma g}{R(\gamma-1)}} \sqrt{1 - \left(\frac{PS_1}{P_1} \right)^{\frac{\gamma-1}{\gamma}}}}{\sqrt{T_1} \left(\frac{PS_1}{P_1} \right)^{\frac{\gamma-1}{\gamma}}}$$

Bellmouth Flow Coefficient

The bellmouth flow coefficient was determined (Fig. III-3) by calibrating the bellmouth against venturi measured airflow rate at 6 psia ($Re_l = 0.39$).

Turbine Drive Airflow

Turbine drive airflow was measured with a critical-flow venturi and is calculated as follows:

For critical flow,

$$W_{TD} = C_{F_{DV}} P_{VI} A_{DV} C_t_{DV} \frac{C_{SV}}{C} \sqrt{\frac{\gamma g}{RT_{DV}}} \left(\frac{2}{\gamma + 1} \right)^{\frac{\gamma+1}{2(\gamma-1)}}$$

For subcritical flow,

$$W_{TD} = C_{F_{DV}} P_{VT} C_t_{DV} A_{DV} \frac{C_{SV}}{C} \frac{\sqrt{\frac{2\gamma g}{R(\gamma-1)}} \sqrt{1 - \left(\frac{P_{VT}}{P_{VI}} \right)^{\frac{\gamma-1}{\gamma}}}}{\sqrt{T_{DV}} \left(\frac{P_{VT}}{P_{VI}} \right)^{\frac{\gamma-1}{\gamma}}}$$

where $C_{t_{DV}}$ is the area thermal expansion coefficient calculated from the venturi throat adiabatic wall temperature, $C_{F_{DV}}$ is an empirically determined flow coefficient based on venturi curvature, boundary layer development, and area ratio (Refs. 5 and 6), and $\gamma = \gamma_{DV}$. C_{SV} is a correction to the critical-flow coefficient due to non-real gas effects (Ref. 6).

Mapping Orifice Airflow

The mapping orifice airflow (W_{TMO}) was measured using a standard ASME sharp-edged orifice with flange taps (Ref. 7) and was determined using the following equation:

$$W_{TMO} = 6.3018 C_{DMO} \frac{1}{\sqrt{1 - \beta_{MO}^4}} D_{MO}^2 \left[1 + C_{TE} (T_{MDO} - 540) \right]^2 \times \left[1 - \frac{(P_{MUO} - P_{MDO})}{\gamma P_{MUO}} \left(0.41 + 0.35 \beta_{MO}^4 \right) \right] \sqrt{\frac{P_{MUO} (P_{MUO} - P_{MDO})}{R T_{MDO}}}$$

Turbine Bleed Airflow

The turbine bleed airflow (W_{TB}) was measured using a standard ASME sharp-edged orifice with flange taps (Ref. 7) and was determined using the following equations:

$$W_{TB_E} = 6.3018 C_{D_{BO}} \frac{1}{\sqrt{1 - \beta_{BO}}} D_{BO}^2 \left[1 + C_{TE}(T_{BO} - 540) \right]^2 \\ \times \left[1 - \frac{(P_{OU} - P_{OD})}{\gamma P_{OU}} \left(0.41 + 0.35 \beta_{BO}^4 \right) \right] \sqrt{\frac{P_{OU}(P_{OU} - P_{OD})}{R T_{BO}}}$$

The turbine bleed orifice coefficient ($C_{F_{TB}}$) was determined by calibration of the orifice with the turbine drive air venturi

$$C_{F_{TB}} = 0.008 W_{TB_E} + 0.981$$

$$W_{TB} = C_{F_{TB}} W_{TB_E}$$

Flows at other stations were obtained in the following manner:

Simulator Inlet Airflow

$$W_{A_1} = W_{A_1N} \text{ for venturi installed}$$

$$W_{A_1} = W_{BM} \text{ for venturi removed}$$

Compressor Inlet Airflow

$$W_{A_2} = W_{A_1}$$

Bearing Cooling Airflow

$$W_{AC} = 0.0075 W_{TD} *$$

Compressor Discharge Airflow

$$W_{A_{23}} = W_{A_2} + W_{AC}$$

Turbine Drive Airflow

$$W_{A_{54}} = W_{TD}$$

Turbine Exit Airflow

$$W_{A_{56}} = W_{TD} - W_{TB} - W_{AC}$$

Nozzle Exit Airflow

$$W_{A_8} = W_{A_{56}} + W_{A_{23}} + W_{TMO}$$

*Value from Ref. 4.

Corrected Airflow and Rotor Speeds

The airflows and rotor speeds were corrected to standard sea-level conditions by the following relationships:

$$N_{R2} = \frac{N_C}{\sqrt{\theta_2}}$$

$$W_{A_{2R}} = W_{A_2} \frac{\sqrt{\theta_2}}{\delta_2}$$

where

$$\theta_2 = \frac{T_2(^{\circ}R)}{518.7} \quad \text{and} \quad \delta_2 = \frac{P_2}{14.696}$$

Reynolds Number Index

The Reynolds number index at Station 2 was calculated from the following expression:

$$Re_{I_2} = \frac{\delta_2}{\phi_2 \sqrt{\theta_2}} \quad .^{\circ}F$$

where

$$\phi_2 = 718.2 (\theta_2)^{3/2} / (T_2 + 199.5)$$

Compressor Adiabatic Efficiency

$$\eta_c = \frac{H_{23\text{ isentropic}} - H_2}{H_{23} - H_2}$$

Turbine Adiabatic Efficiency

$$\eta_T = \frac{H_{55} - H_{54}}{H_{55\text{ isentropic}} - H_{54}}$$

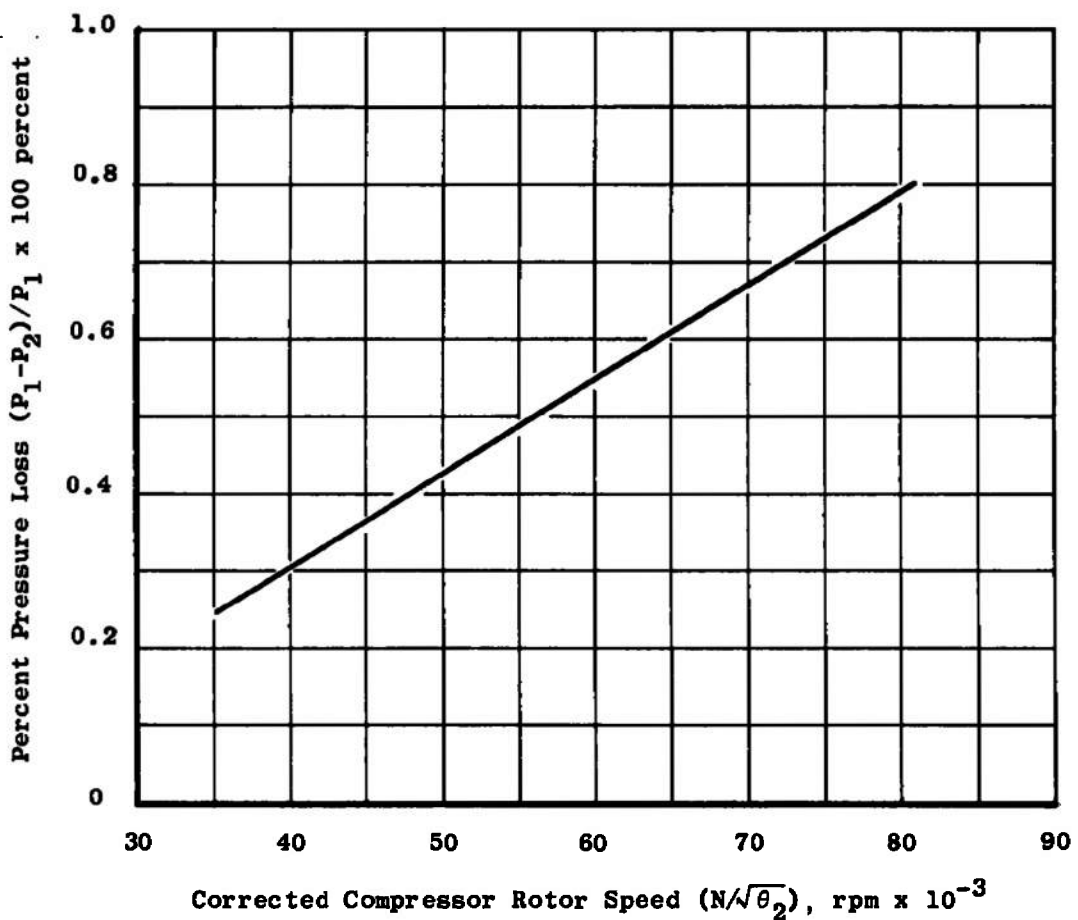


**Fig. III-1 Percent Total Pressure Loss from Simulator Inlet to Compressor Inlet
(Uniform Inlet, $P_2 = 14.2$ psia, $T_2 = 80^\circ\text{F}$)**

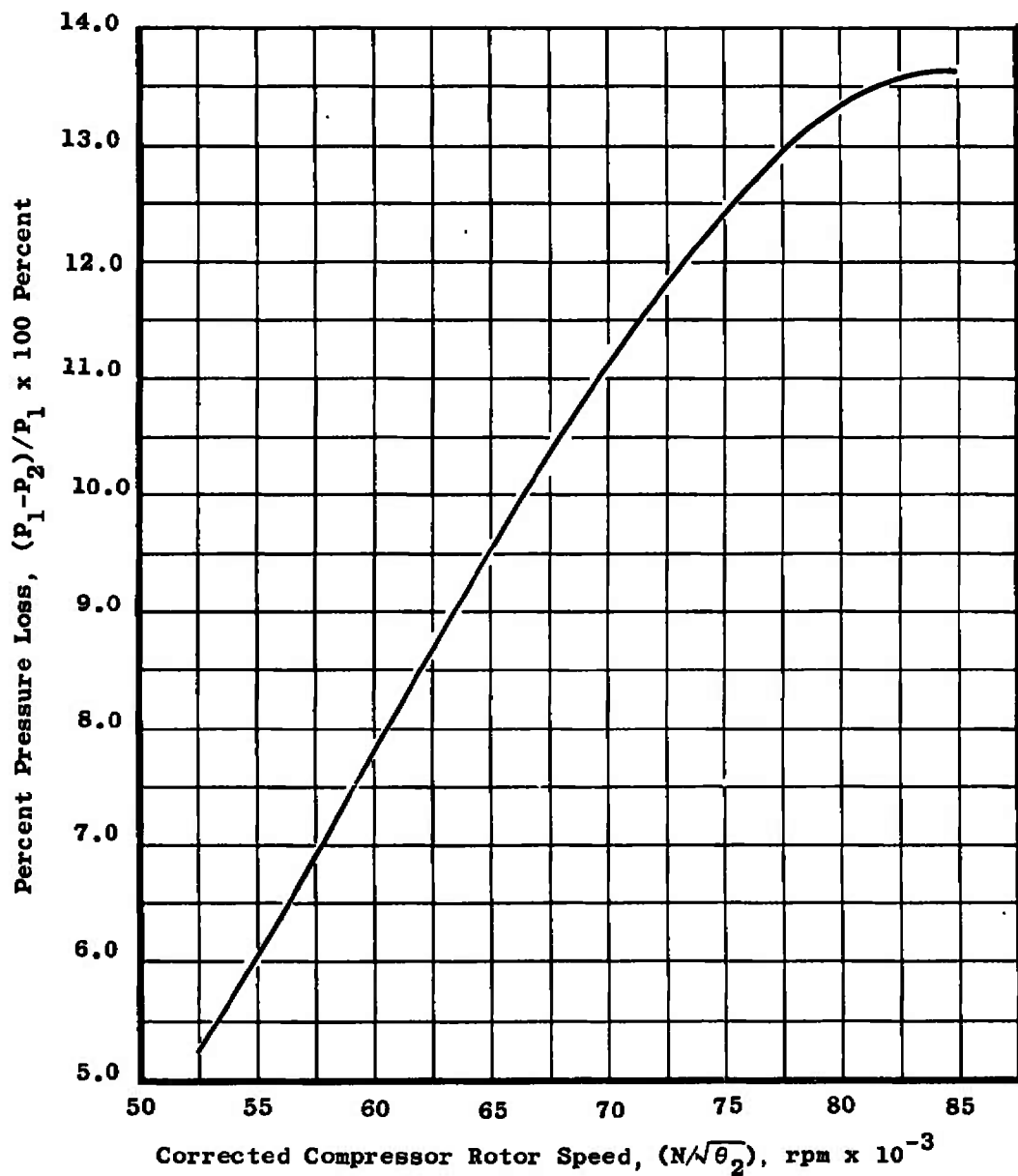


Fig. III-2 Percent Total Pressure Loss from Simulator Inlet to Compressor Inlet
(Distorted Inlet, $P_2 = 6$ psia, $T_2 = 80^\circ\text{F}$)

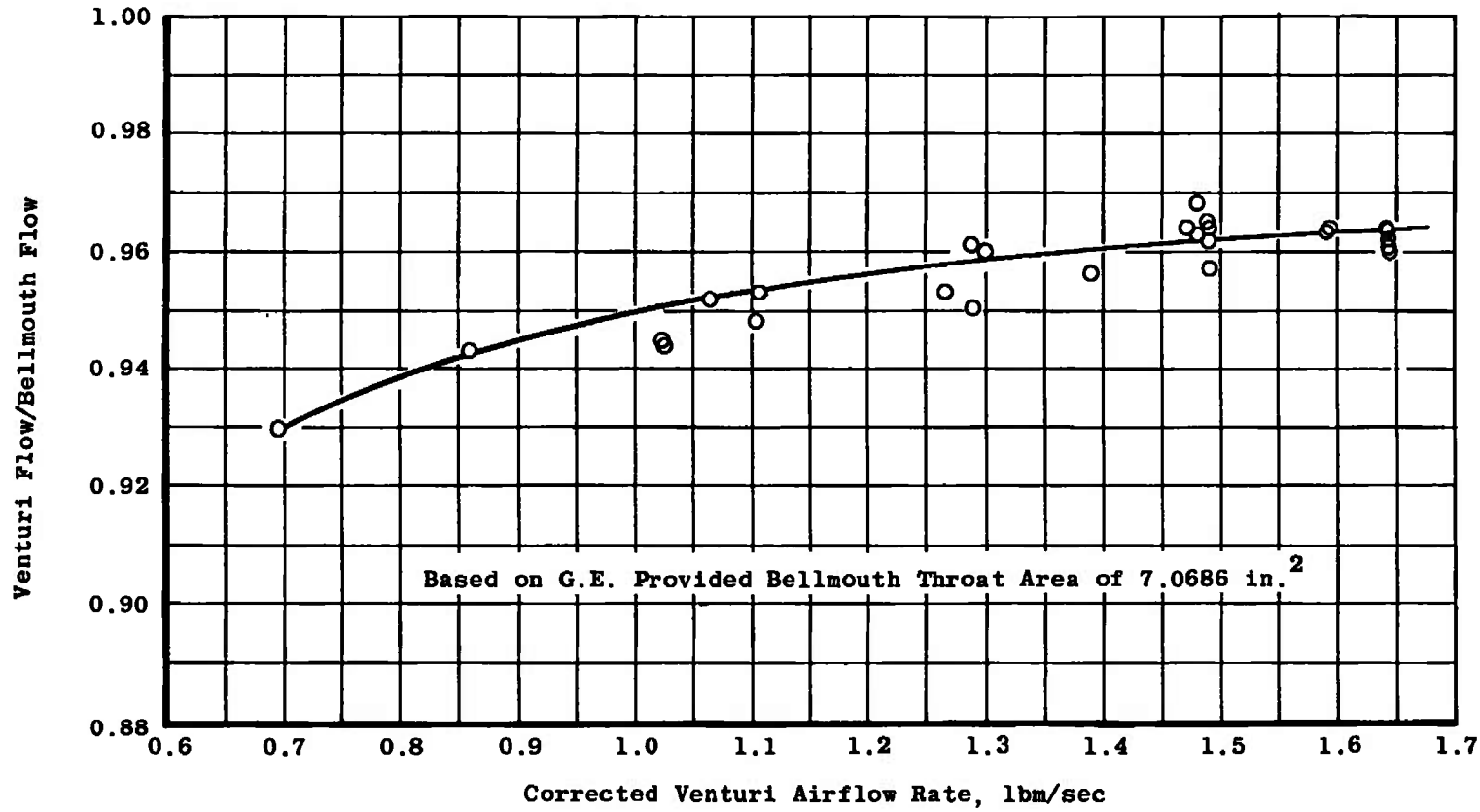


Fig. III-3 Bellmouth Flow Coefficient Variation with Corrected Venturi Airflow Rate, ($Re_l = 0.39$)

UNCLASSIFIED

Security Classification

DOCUMENT CONTROL DATA - R & D

(Security classification of title, body of abstract and indexing annotation must be entered when the overall report is classified)

1. ORIGINATING ACTIVITY (Corporate author) Arnold Engineering Development Center Arnold Air Force Station, Tennessee 37389	2a. REPORT SECURITY CLASSIFICATION UNCLASSIFIED
	2b. GROUP N/A

3. REPORT TITLE COMPONENT PERFORMANCE AND STABILITY CHARACTERISTICS OF AN ENGINE PROPULSION SIMULATOR WITH UNIFORM AND DISTORTED INLET PRESSURE PROFILES AT REYNOLDS NUMBER INDICES OF 0.39, 0.78, and 0.91

4. DESCRIPTIVE NOTES (Type of report and inclusive dates) June 5, 1972--February 10, 1973, Final Report

5. AUTHOR(S) (First name, middle initial, last name) C. R. Darlington, R. M. Brooksbank, and J. O. Brooks, ARO, Inc.
--

6. REPORT DATE March 1974	7a. TOTAL NO. OF PAGES 81	7b. NO. OF REFS 7
-------------------------------------	-------------------------------------	-----------------------------

8a. CONTRACT OR GRANT NO	8b. ORIGINATOR'S REPORT NUMBER(S)
--------------------------	-----------------------------------

b. PROJECT NO	AEDC-TR-73-172
---------------	-----------------------

c. Program Element 63202F	9b. OTHER REPORT NO(S) (Any other numbers that may be assigned this report)
---------------------------	---

d. System 668A	ARO-ETF-TR-73-108
----------------	--------------------------

10. DISTRIBUTION STATEMENT Approved for public release; distribution unlimited.

11. SUPPLEMENTARY NOTES Available in DDC	12. SPONSORING MILITARY ACTIVITY AFAPL/TBP Wright-Patterson Air Force Base Ohio 45433
--	---

13. ABSTRACT An investigation was conducted on an engine propulsion simulator (S/N 001/02) to determine sea-level-static component performance and to determine the compressor performance and stability characteristics with uniform and distorted inlet pressure profiles at Reynolds number indices of 0.39 and 0.78. Steady-state component performance data are presented and are compared with predicted data. The effect of Reynolds number indices and the effect of circumferential inlet distortion on the compressor performance are shown.
--

UNCLASSIFIED

Security Classification

14. KEY WORDS	LINK A		LINK B		LINK C	
	ROLE	WT	ROLE	WT	ROLE	WT
simulator engine inlets distortion Reynolds number performance stability						